CARDIAC OUTPUT MONITORING TECHNIQUES BY PHYSIOLOGIC SIGNAL PROCESSING

By

Guanqun Zhang

A DISSERTATION

Submitted
to Michigan State University
in partial fulfillment of the requirements
for the degree of

DOCTOR OF PHILOSOPHY

Electrical Engineering

2012

ABSTRACT

CARDIAC OUTPUT MONITORING TECHNIQUES BY PHYSIOLOGIC SIGNAL PROCESSING

By

Guanqun Zhang

Continuous cardiac output monitoring is urgently required because of the growth of elderly population and shortage of clinical staff. However, the reliable, less-invasive solution of monitoring cardiac output has not been determined. On the other hand, the measurement of peripheral arterial blood pressure waveform can be conveniently collected. In the dissertation, we proposed novel physiologic waveform analysis techniques which can estimate cardiac output from a peripheral arterial blood pressure waveform. The techniques can overcome the confounding reflection by estimating the cardiac output over multiple cardiac cycles. Validation results have indicated that our method was comparative with other traditional methods at the baseline level and became increasingly superior to others with more challenging cardiac output changes.

We also introduced pulse transit time to overcome the estimation error due to varying arterial compliance. As a direct function of arterial compliance, pulse transit time can reduce the estimation variation and thus improve the accuracy. Two conventional approaches for measuring pulse transit time were compared, and both methods were sensitive to artifact. Therefore, a novel method was developed which can robustly estimate the pulse transit time, with which the accuracy of estimating cardiac output was significantly improved.

A tube-load model with an adaptive transfer function was further proposed. The model can reconstruct the central blood pressure of flow waveforms from the peripheral measurements beat by beat. In this study, the reconstructed central blood pressure waveform is an earlier marker of hypovolemia than the peripheral blood pressure waveform in a simulated hemorrhage experiment. Cardiac output can also be derived from the reconstructed central blood pressure waveform.

In addition, an extended model was proposed for estimating cardiac output from a pulmonary

artery pressure. This extension allows to simultaneously estimate cardiac output and left atrial pressure, which are two important determinants of pulmonary artery pressure. Validation in a large critical/medical population database demonstrated the proof of concept.

The techniques will ultimately be employed for continuous and non-invasive cardiac output monitoring for clinical settings. One potential future direction would be end-diastolic volume and ejection fraction estimation from a peripheral arterial blood pressure waveform.

To my parents, Yaming Zhang and Li Shan

ACKNOWLEDGEMENTS

Though only my name appears on the cover of this dissertation, a great many people have contributed to its production. I owe my gratitude to all those people who have made this dissertation possible and because of whom my graduate experience has been one that I will cherish forever.

I would like to gratefully and sincerely thank Dr. Ramakrishna Mukkamala for his guidance, understanding, patience, and most importantly, his friendship during my graduate studies at Michigan State University. His mentorship was paramount in providing a well rounded experience consistent my long-term career goals. I am highly impressed with his in-depth understanding of research areas, his diligent and enthusiastic working style, his ability to control the multi-disciplinary knowledge and his sincere and friendly attitude with people.

I am also grateful to my dissertation committee members, Dr. Selin Aviyente, Dr. N. Bari Olivier and Dr. Lalita Udpa, for the valuable experience of their courses, experiments and comments on my research. It is my great honor to cooperate with these three outstanding teachers. I would also like to thank many faculty members of MSU who were the instructors for the courses I took. The course works have greatly enriched my knowledge.

I would like to express my special thanks to the colleagues at our PSPML lab, Gokul Swamy, Federico Aletti, Xiaoxiao Chen, Sorour Soltani, Da Xu, Mohsen Moslehpour, Mingwu Gao and Jiankun Liu. Thank you for the collaboration over the last five years.

I also want to thank my friends at Fudan University and Michigan State University. Especially, I would like to thank Jiemei Wang and Dashun Wang. The conversation with them can always provide me insights and inspirations of my research.

Finally, none of this would have been possible without the love and support of my parents, to whom this dissertation is dedicated. I would like to express my heart-felt gratitude to my family.

TABLE OF CONTENTS

LIST OF TABLES

LIST OF FIGURES

Chapter 1

INTRODUCTION

The increasing number of occurrence of cardiovascular diseases requires novel techniques which can effectively and conveniently monitor hemodynamics for patients and clinicians. Nowadays, the continuous measurement of peripheral arterial blood pressure (ABP) has drawn intense attention. Although the invasive catheters are being broadly utilized in clinical practice, the requirement of less-invasive or even non-invasive monitoring techniques is on the rise. Comparing with the routine measurement of ABP, the cardiac output (CO) can introduce more comprehensive information for the diagnose in the therapy and more predictive of patient outcome. However, conventional methods for measuring CO require an experienced operator or an unacceptably high level of invasiveness. Therefore, the application of the CO measurement is limited by the disadvantage.

In our opinion, CO may be continuously and less invasively monitored by physiologic-based mathematical model, which can extract relevant information for the routinely measured ABP waveforms. In this report, several techniques deriving CO from ABP waveforms will be discussed. Those techniques yielded more accurate results and more robust to noises, wave reflection and measurement artifacts. Some techniques have been validated in a series of previous studies, and they are further evaluated for the proof-of-concept. The development of the techniques may ultimately be used in critical care monitoring with invasive ABP catheters and emergency and home monitoring with non-invasive ABP transducers. Successful achievement of these specific aims will lead to an improved understanding of the clinical information embedded in various, routinely measured ABP waveforms.

1.1 Background

1.1.1 Circulation and cardiac output

The cardiovascular system serves to pass and distribute nutrients to the tissues and to remove metabolism substances as well as help stabilize body temperature (Figure 1.1)[77]. In the mammal cardiovascular system, the cardiovascular system consists of a pump (the heart) and a series of connecting and distributing tubes (blood vessels). The cardiovascular system has two division: the systemic circulation, whose blood is pumped from the left ventricle and circulates oxygenated blood to the body tissues; and the pulmonary circulation, whose blood is pumped from the right ventricle and circulates deoxygenated blood to the lungs. Cardiac output (CO), is the volume of blood being pumped from the heart, in the unit of liter per minute. Therefore, CO is equal to the stroke volume (SV, i.e. the volume per beat) multiplied by heart rate (HR).

Arterial blood pressure (ABP), is the pressure of blood exerted on the vessel wall. During each cardiac cycle, the maximum and minimum of ABP are defined as systolic and diastolic pressure, respectively. The driving force of ABP in the circulation is due to the pumping action of the heart. During the circulation, ABP is significantly decreased in arterioles, where accounts for the most resistance in the arterial tree. Therefore, the ABP returning to the heart is negligible comparing with the ABP in major arteries. This hemodynamic phenomenon in the systemic circulation can be mathematically described as the mean of ABP is equal to the produce of CO and total peripheral resistance (TPR).

Today, hemodynamic monitoring techniques enable the measurement and display of blood pressure waveforms. For example, in each year, millions of invasive catheters are inserted in surgery and intensive care patients to monitor the peripheral ABP. Moreover, FDA approved systems have recently been commercialized to non-invasively measure blood pressure in peripheral arteries. With the availability of these systems, the monitoring of ABP condition becomes so simple that patients can utilized them at home. While these systems are continuous and safe enough for clinical use, they are ineffective in the sense that the measured blood pressure levels are imprecise

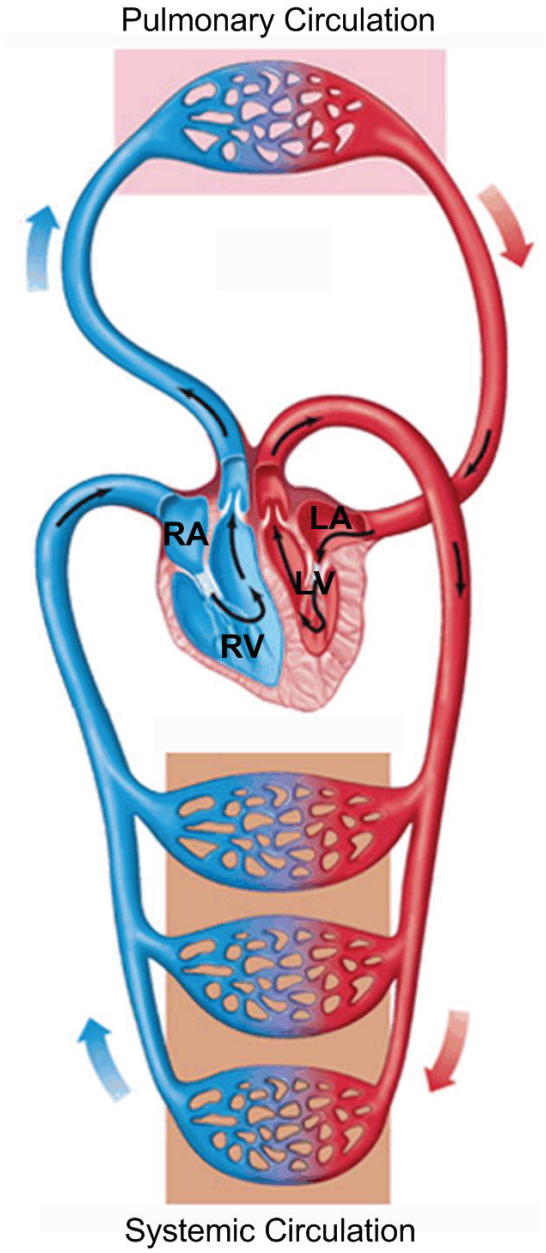

Figure 1.1: The cardiovascular system. For interpretation of the references to color in this and all other figures, the reader is referred to the electronic version of this dissertation.

indicators of circulatory status.

One reason of the ineffectiveness is that ABP levels do not provide an early indicator of a hemodynamic event. For example, at the early stage of hemorrhage, ABP is maintained even while CO is falling due to compensatory physiologic mechanisms (Figure 1.2). While frank hypotension or low blood pressure will eventually occur, it is often too late to intervene at this point. So, it is the CO, which represents the total blood flow rate in the circulation, that would actually give an early enough indication of the need for a life saving intervention.

Another reason is that ABP levels are dependent on multiple physiologic factors and therefore do not permit diagnosis. For example, when the compensatory physiologic mechanisms eventually fail so as to result in hypotension, the root cause could be bacterial blood poisoning, more commonly called sepsis, the inability of the heart to fill or contract, or an internal bleed. With the information of CO, however, the sepsis can be distinguished from cardiac dysfunction and hemorrhage.

The standard CO measurement is the thermodilution (Figure 1.3). This technique involves introducing a catheter into the right atrium, injecting cold saline into the heart, measuring temperature downstream in the pulmonary artery and computing the time-averaged CO based on conservation laws. Although this approach is relatively easy and inexpensive, it is very invasive and it requires an operator to intermittently inject saline. Therefore, this method doesn't permit continuous CO monitoring.

Some other traditional techniques also suffer significant limitations (Table 1.1). For example, the most accurate method is to place a flow probe across the aorta. However, this method is too invasive to be practical.

Therefore, it is relative difficult to directly measure cardiac output. On the other hand, peripheral arterial blood pressure can be reliably obtained by mature techniques. So the problem naturally arises that if CO can be estimated by some mathematical analysis of peripheral arterial blood pressure. This approach is named as pulse contour analysis. A number of investigators have sought techniques to estimate CO from peripheral ABP signals. The earliest technique was

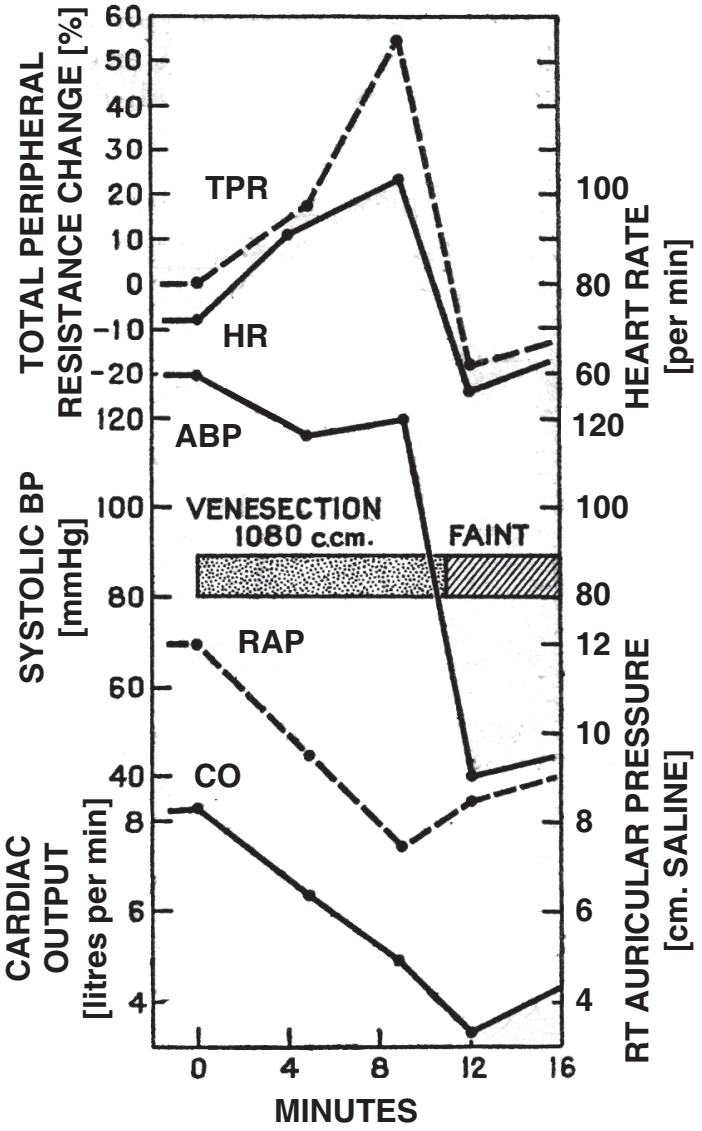

Figure 1.2: Physiologic response in a hemorrhage study.

Table 1.1: Limitations of conventional methods.

Method	Advantages	Disadvantages
aortic flow probe	most accurate, continuous	thoracotomy
doppler ultrasound	non-invasive	expert operator, expensive
oxygen fick	accurate, inexpensive	two catheterizations, operator
thermodilution	inexpensive	pulmonary artery catheterization, inaccurate, operator
thoracic bioimpedance	non-invasive, continuous	inaccurate

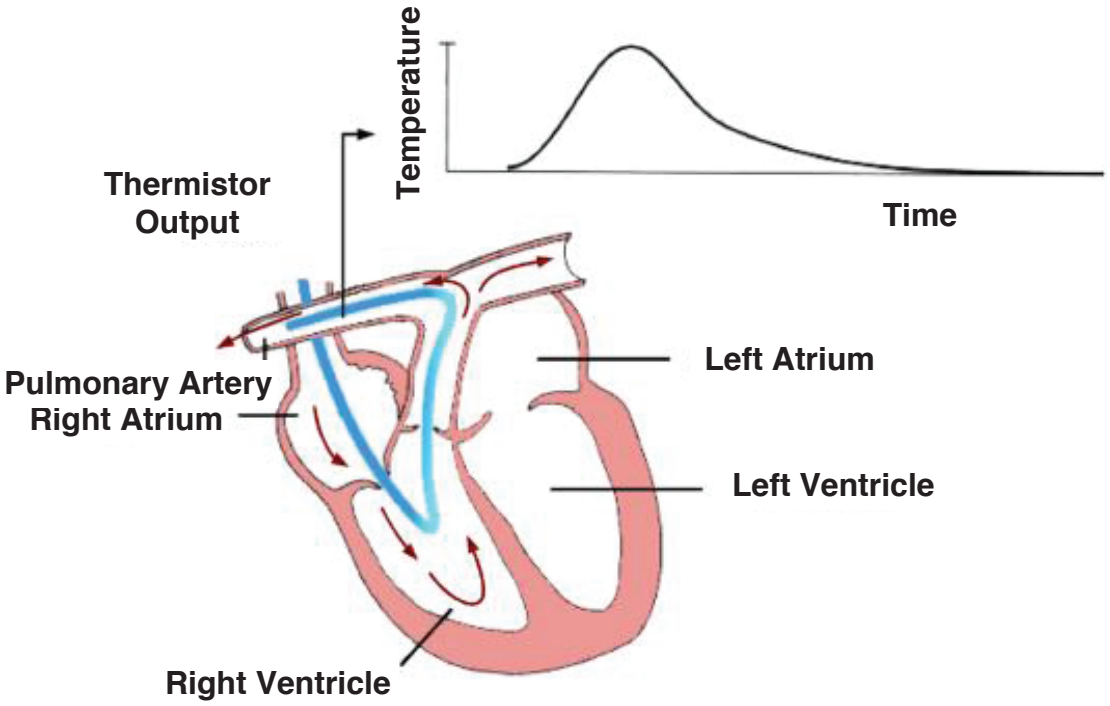

Figure 1.3: Schematic diagram of thermodilution.

based on the observation that central pulse pressure, that is, the systolic minus diastolic pressure in the central aorta, is dependent on SV (Figure 1.4). This technique therefore involves detecting the pulse pressure and multiplying it by the HR to determine CO to within a proportionality constant. In this way, the technique could be utilized to monitor relative changes in cardiac output or absolute cardiac output after a single calibration. However, this simple technique assumes that cardiac ejection occurs instantaneously. In actuality, cardiac ejection occurs in finite time in which a portion of the ejected blood passes through the aorta and into the periphery.

Many years later, an improved technique was proposed that made no assumptions about the cardiac ejection time. This technique models the arterial tree with an RC circuit. It accounts for the compliance of the large arteries and the total peripheral resistance of the small arteries. If CO is considered as the input excitation of the circuit, arterial blood pressure should decay like a pure exponential during each diastolic interval. Further, the time constant of this pressure decay should

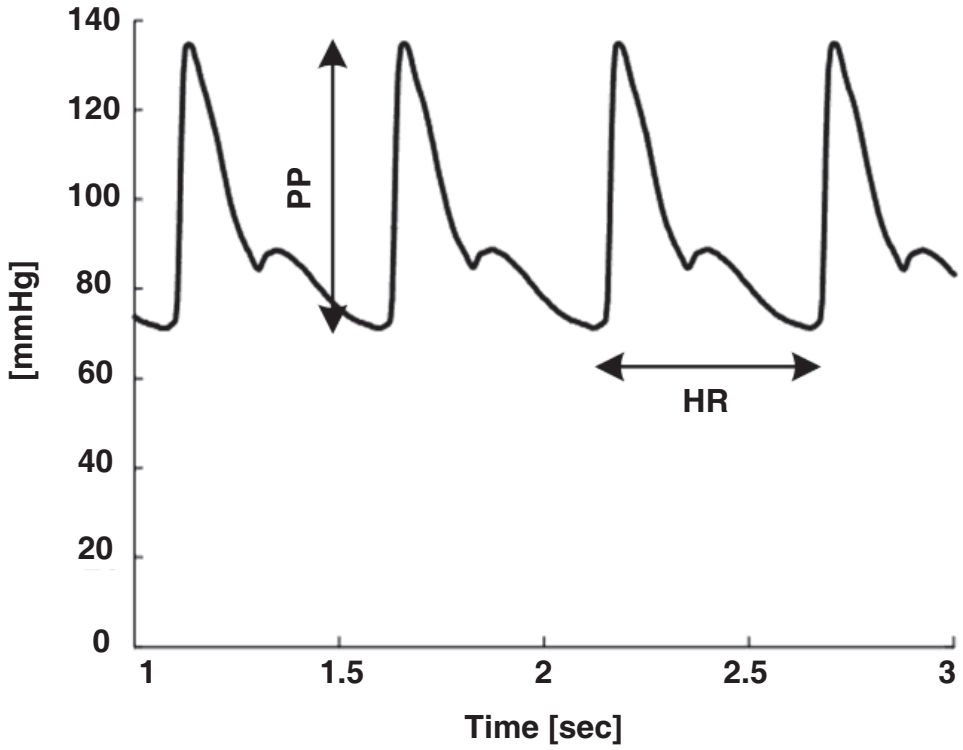

Figure 1.4: Pulse pressure and heart rate.

equal to the product of the total peripheral resistance and the arterial compliance. By assuming constant arterial compliance, the technique fits the exponential, estimates the RC time constant tau and then divides the time-averaged arterial blood pressure to compute proportional cardiac output. This RC circuit technique showed excellent correspondence to the aortic flow probe, as illustrated in figure 1.10.

However, central ABP is not measured for regular patient monitoring. On the other hand, peripheral ABP can be easily collected but its shape is much different from the central pressure, which is due to wave reflection. That is, when the heart ejects blood, a pressure wave is initiated that travels through the arteries. When this wave reaches the level of the arterioles , a significant part of the wave is reflected back towards the heart. As a result, the actual blood pressure waveform at a given arterial site arises as the sum of the forward and backward traveling waves at that site.

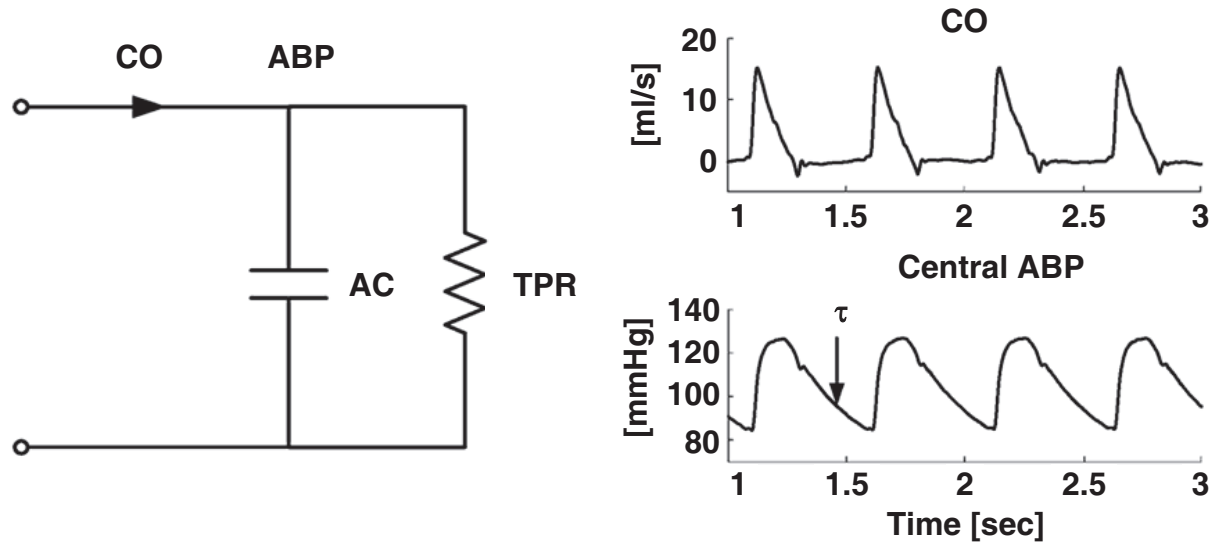

Figure 1.5: Windkessel model for estimating CO from central ABP.

Since wave reflection occurs mainly at the arterioles, there is little time delay between the forward and backward waves in the periphery (Figure 1.6). So the backward wave adds to the forward wave and it increases the peripheral pulse pressure. On the other hand, the forward and backward waves in the central aorta are shifted away from each other. For this reason, pulse pressure becomes much amplified with increasing distance from the heart. And the exponential becomes less apparent. Further, the magnitude of the backward wave relative to the forward wave increases with total peripheral resistance. As a result, peripheral pulse pressure increases with vasoconstriction and decreases with vasodilation.

We found that the wave reflection ceases to be a major factor over long time scales. Figure 1.7 shows two blood pressure signals measured at the same time but at different sites in the arterial tree. Note that the signal variations are different within a beat, since the wave reflections differs between the two measurement sites. However, if we zoom out to see the signal envelopes, they are more similar. These beat-to-beat variations are always present and due to, for example, breathing and compensatory physiologic mechanisms. Therefore, we proposed several techniques which can estimate CO from peripheral ABP over long time scales.

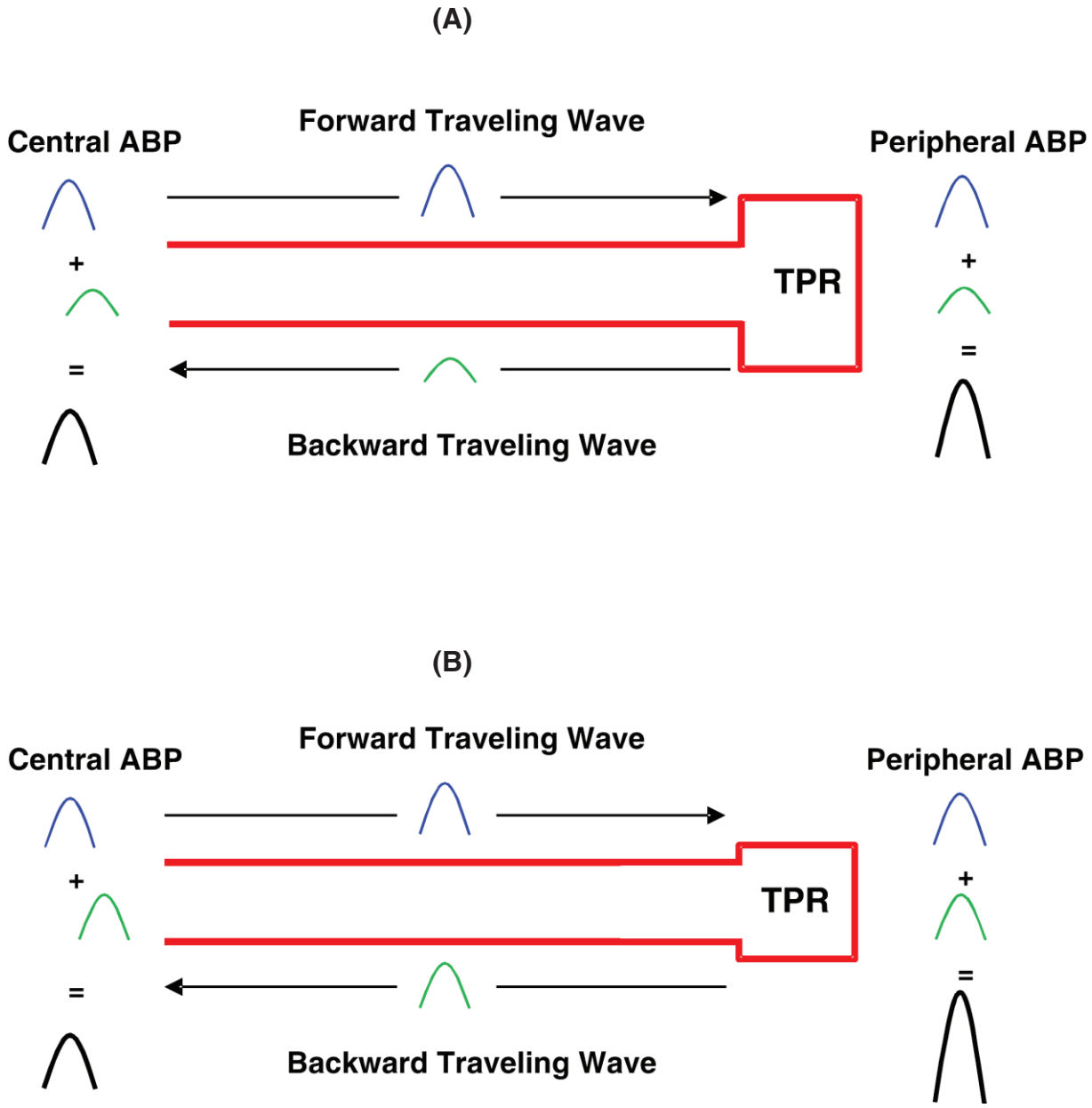

Figure 1.6: Wave reflection and amplification.

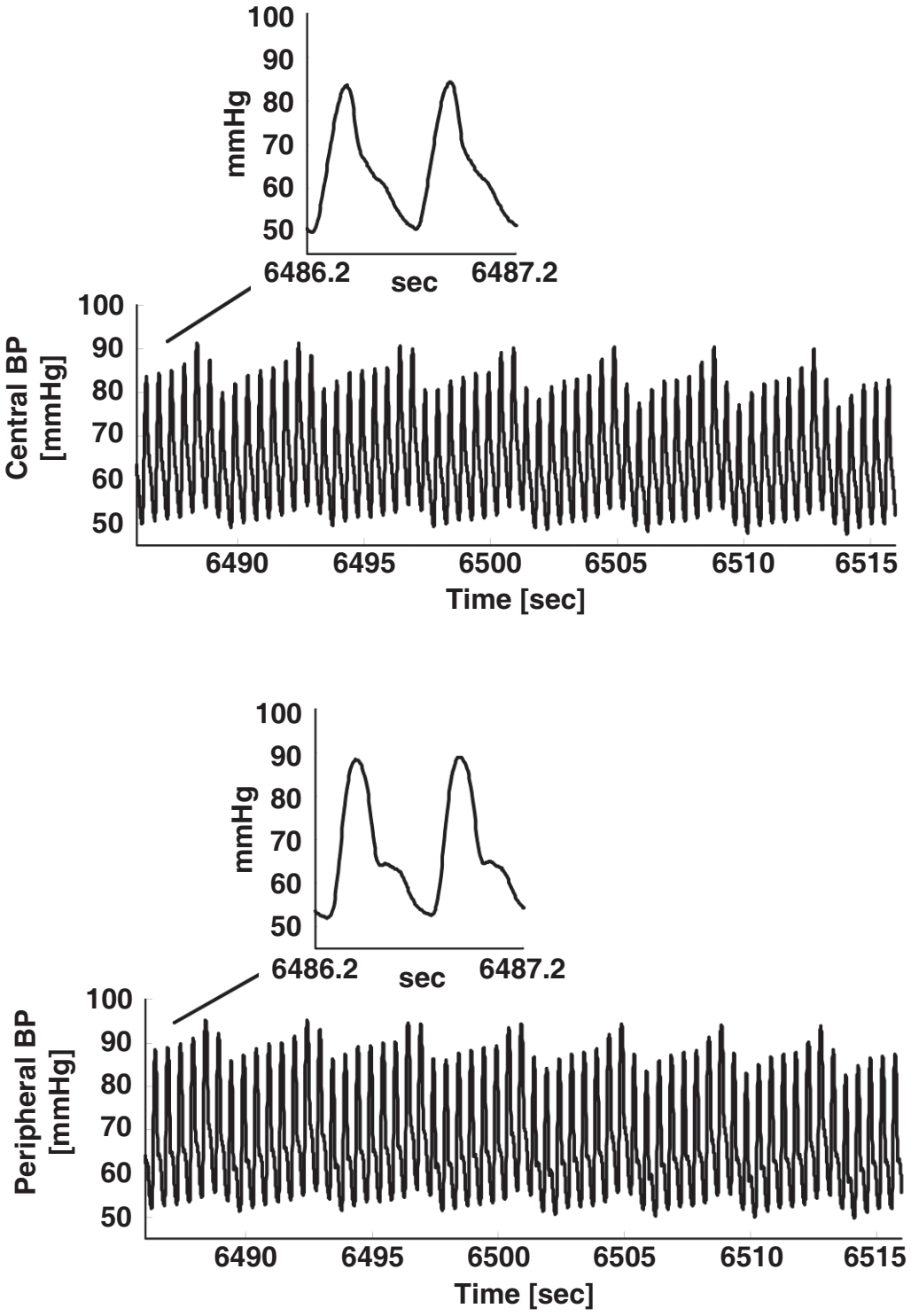

Figure 1.7: Two pressure waveforms simultaneously measured at two different positions.

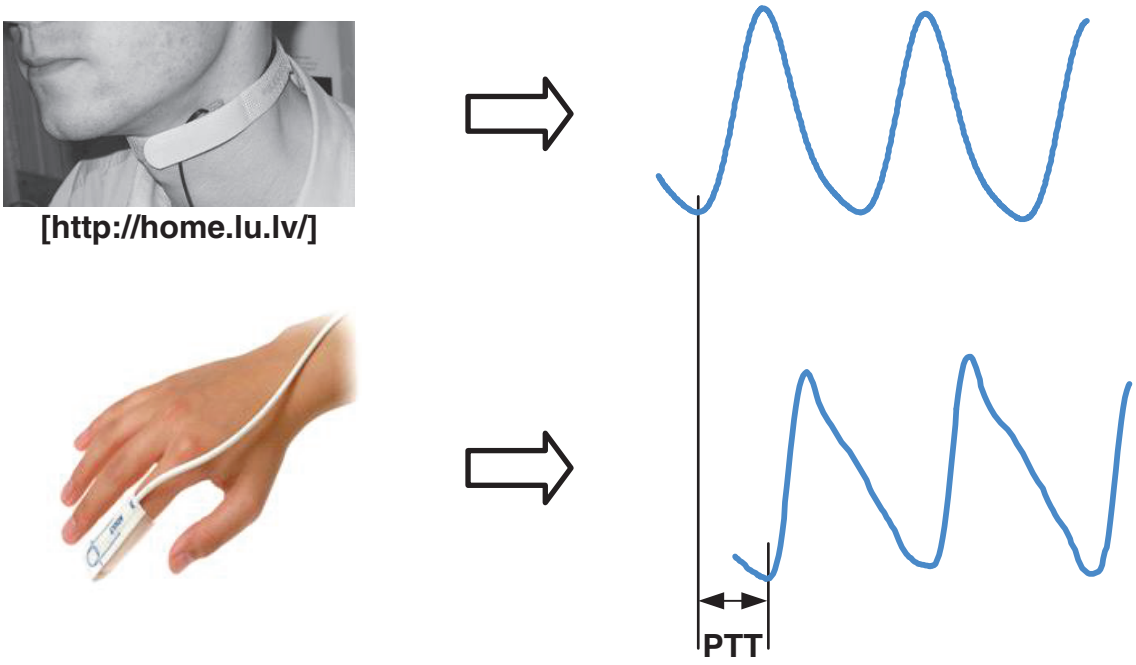

Figure 1.8: Measurement of PTT.

1.1.2 Pulse wave velocity, pulse transit time and pulse arrival time

Pulse wave velocity (PWV) is the speed of energy wave transmission in the arteries. According to the Bramwell-Hill equation, PWV varies inversely with the square root of arterial compliance (AC) [11]. Indeed, PWV increases as the arteries stiffen with aging and disease [43, 56]. PWV is now the most important index of arterial stiffness for two reasons [60]. Firstly, it is an independent predictor of all-cause mortality and cardiovascular events in hypertensive and other patients [60, 109]. Secondly, while direct measurement of AC involves nontrivial tracking of changes in vessel area and ABP, PWV is easier to measure [10, 60].

PWV is most easily determined as the ratio of the distance and pulse transit time (PTT) between central and peripheral arterial sites. PTT is estimated by measuring typically ABP waveforms at the two sites with non-invasive, handheld tonometers or Doppler ultrasound probes and then detecting the foot-to-foot time delay between the waveforms (Figure 1.8). This regional PWV measurement technique is used by most clinicians [60] and commercial systems [96].

A simpler method measures the time delay between the R-wave of an ECG waveform and

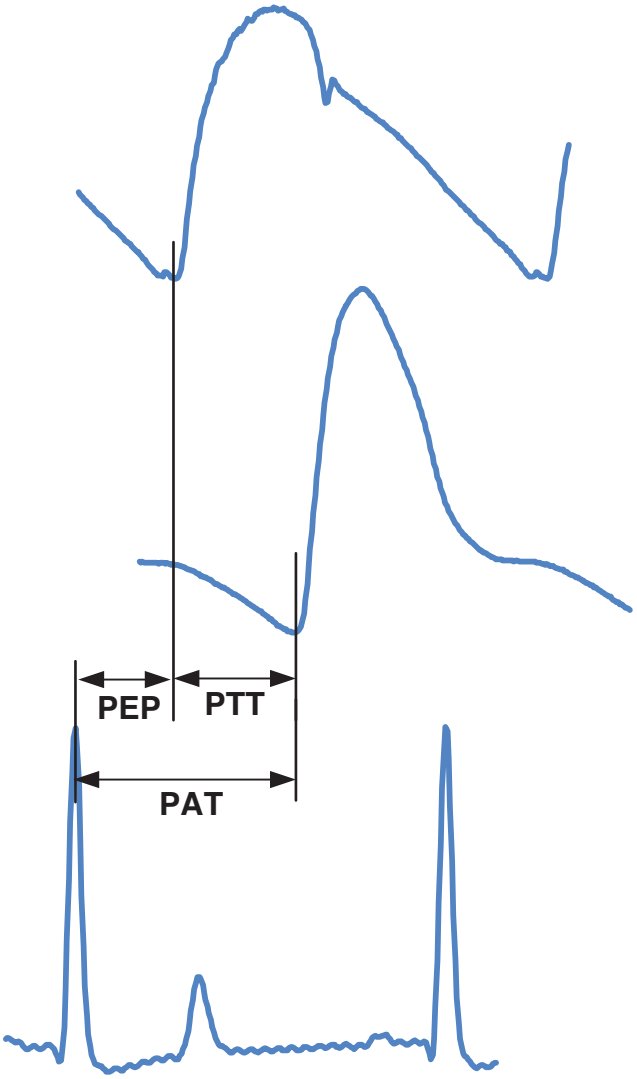

Figure 1.9: Measurement of PAT.

the distal arterial waveform foot has captured great interest [1, 37, 48, 62, 70, 113]. This time delay is called pulse arrival time (PAT) and it has captured great interest recently. PAT is equal to the sum of PTT and the pre-ejection period (PEP), where PEP is determined by the ventricular electro-mechanical delay and isovolumic contraction phase (Figure 1.9).

1.2 Arterial system modeling

Mathematical modeling of arterial hemodynamics has been longstanding. Two basic modeling approaches have been employed: forward modeling and inverse modeling. Forward modeling concerns building a model based on physical principles to predict data (i.e., estimating data from physical models with known parameters). This approach is useful for testing our understanding of the physiology underlying arterial hemodynamics. On the other hand, inverse modeling concerns building a model from observed data (e.g., estimating model parameters by fitting measured waveforms). Although less developed than its forward modeling counterpart, this approach is becoming more and more important by virtue of its ability to permit individualized monitoring of arterial hemodynamics.

The available models may be divided into two classes: lumped-parameter models and distributed-parameter models. The most popular lumped-parameter model is the "Windkessel" model proposed by Frank [91]. It analogizes the arterial system as a capacitor connected in parallel with a resistor. The capacitor represents the large artery compliance, whereas the resistor represents the total peripheral resistance. This 2-parameter Windkessel model can be extended to include additional circuit elements in order to improve accuracy [98]. Because Windkessel models are so simple, they are highly suitable for parameter estimation purposes. That is, Windkessel models are characterized by only a few parameters, which can be readily estimated from the limited arterial waveforms typically available in practice. However, lumped-parameter models assume infinite pulse wave velocity and therefore cannot reproduce wave propagation and reflection phenomena that are essential in shaping these waveforms.

By contrast, distributed-parameter models can reproduce wave propagation and reflection phenomena through finite pulse wave velocity. Most often, distributed-parameter models represent the arterial system using a one-dimensional simplification of the Navier-Stokes equation. These models usually account for both geometrical and mechanical properties of the arteries explicitly as model parameters. Detailed distributed-parameter models have been built that account for multi-level branching, elastic and geometric tapering, and arterial terminations [3, 4, 44, 86, 95, 110, 117].

These comprehensive models can provide great accuracy. However, the models cannot be readily applied for parameter estimation purposes, because they are characterized by an excessive number of model parameters that makes it virtually impossible to obtain unique parameter estimates from limited arterial waveforms.

Less accurate, yet mathematically tractable, distributed-parameter models have also been developed. These models usually consist of multiple tubes with terminal loads in parallel. Often times, the model comprises two such tubes and loads ("T-tube" model). The tube represents the wave propagation path in the large conduit arteries, whereas the load signifies the wave reflection site (e.g., arterial bed distal to a peripheral artery). The tube can be elastically and/or geometrically tapered or uniform as well as lossy (i.e., exhibits energy dissipation) or lossless, while the load can be non-parametric (i.e., characterized without a model structure through a generic frequency response) or parametric. It turns out that the simplest of these models, the uniform, lossless tube with parametric load, is almost as accurate as the most complicated of the models. Indeed, this model, which will henceforth be referred to simply as the tube-load model, is often able to fit arterial pressure and flow waveforms remarkably well despite being characterized by only a few parameters. Consequently, the tube-load model carries advantages of both Windkessel and comprehensive distributed-parameter models and therefore permits an attractive platform for improved monitoring of arterial hemodynamics.

1.2.1 Windkessel model

Over a century ago, Frank first suggested that SV could be measured from ABP waveforms [91]. Shortly thereafter, Erlanger et al. introduced the first analysis technique for doing so [34]. They observed that pulse pressure (PP, i.e., systolic pressure minus diastolic pressure) in the aorta was positively correlated to SV. Thus, their technique simply involved detecting PP from the central ABP waveform to monitor relative change in SV for each beat or CO via PP·HR. However, a major assumption of this PP technique is that cardiac ejection occurs instantly when, in actuality, it occurs over finite time in which a portion of the ejected blood passes through the aorta and into

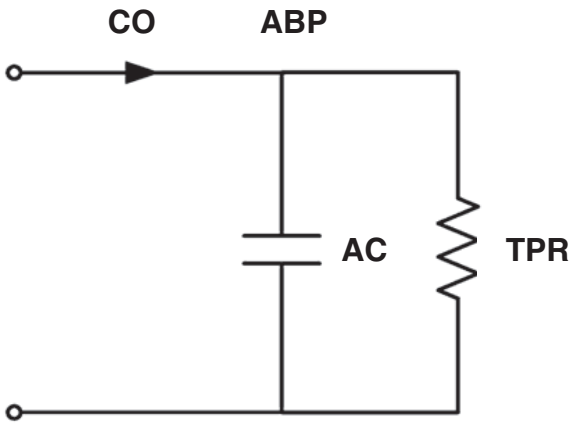

Figure 1.10: The Windkessel model which characterizes the arterial tree.

the periphery. Amongst the many ensuing studies, Bourgeois et al. performed perhaps the most compelling [9]. These investigators developed a more intricate central ABP waveform analysis technique that made no assumptions about the cardiac ejection time. They specifically represented the arterial tree with a Windkessel model accounting for the lumped compliance of the large arteries (AC) and the TPR of the small arteries (Figure 1.10). According to this model, central ABP should decay like a pure exponential during each diastolic interval with a time constant (τ) equal to the product of TPR and AC.

1.2.2 Tube-load model

1.2.2.1 Model description

Figure 1.11(A) illustrates the tube-load model. This model represents the arterial system as a parallel connection of m uniform, lossless tubes with parametric loads. The meaning of the tubes and loads depend on perspective. From the perspective of the central (ascending) aorta, a tube represents the wave propagation path through a segment of the aorta, whereas the load represents an effective reflection site due to the entire arterial network distal to the segment. For example, for the

T-tube model in which m is equal to two, the two effective reflection sites correspond to the head-end and body-end arterial beds. The flow through the body-end tube represents the descending aortic flow, whereas the flow through the head-end tube represents the difference between central and descending aortic flows. From the perspective of a peripheral artery, on the other hand, a tube represents the wave propagation path from the central aorta to the peripheral artery, whereas the load represents the reflection site due to the arterial bed distal to the peripheral artery. In this case, m is equal to the number of peripheral arteries. The flow at the proximal end of a tube is not measurable. It represents the component of central aortic flow that reaches a peripheral artery. However, the sum of the flows at the proximal end of all tubes corresponds to the total central aortic flow.

The i^{th} tube is of length d_i and has constant characteristic impedance $Z_{ci} = \sqrt{l_i/c_i}$, where l_i and c_i are the large artery inertance and compliance, respectively. Pressure and flow waves propagate with constant time delay $T_i = \sqrt{l_i \cdot c_i}$ from one end of the tube to the other. Note that this time delay corresponds to pulse transit time and that its governing equation arises from the Bramwell-Hill equation [11]. The mean value of the waves is constant throughout the tube.

The i^{th} load has frequency-dependent impedance $Z_{Li}(j\omega)$, where j is the imaginary number and ω is the frequency, that is characterized by a pole-zero structure. Figure 1.11(B) shows three types of commonly used loads along with the specific form of their $Z_{Li}(j\omega)$. The Type I and Type II loads are 3-parameter Windkessel models. These models account for the resistance R and compliance C of the effective load or peripheral resistance and compliance (depending on perspective) while matching the tube impedance at infinite frequency per arterial input impedance studies [72, 73]. The Type III load is a generic pole-zero model. A principal advantage of this type of model is that it allows a flexible system order rather than being fixed to first-order as with its Type I and Type II counterparts. The disadvantage is that it has no physiologic meaning. As a result, its coefficients are neither dependent on each other nor constrained as they are with the Type I and Type II loads. For any load, the wave reflection coefficient at the i^{th} load is given by the following relationship involving tube and load impedances:

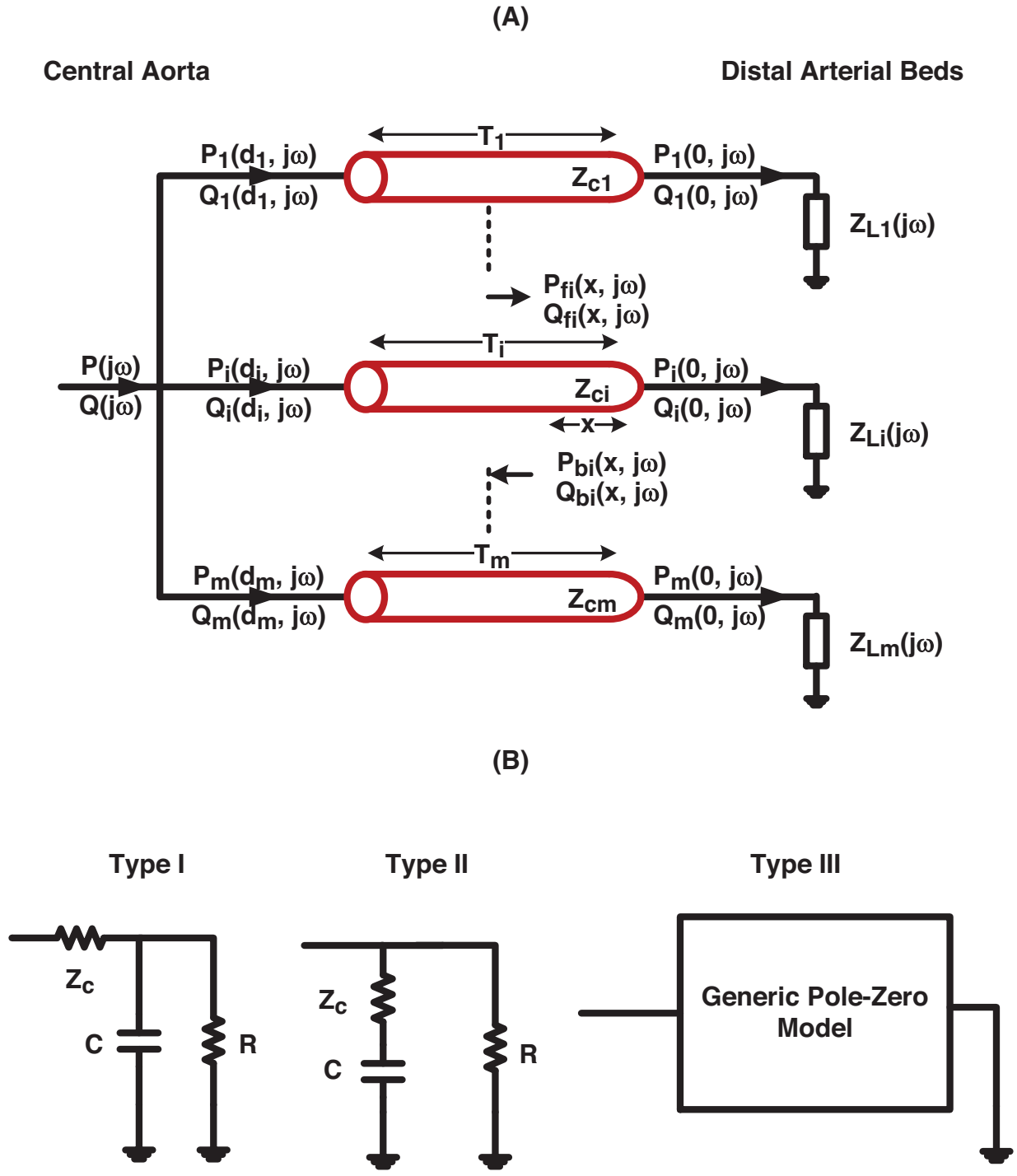

Figure 1.11: (A) The tube-load model with arbitrary load. (B) Three types of commonly used loads.

$$\Gamma_i(j\omega) = \frac{Z_{Li}(j\omega) - Z_{ci}}{Z_{Li}(j\omega) + Z_{ci}}. \tag{1.1}$$

Qualitatively, pressure and flow waves propagate in the forward direction (proximal to distal tube ends) along a tube without distortion and are proportional to each other. These waves are reflected in the opposite direction at the load due to the impedance mismatch ($Z_{ci} \neq Z_{Li}(j\omega)$). The resulting backward pressure and flow waves likewise propagate along the tube without distortion and are proportional to each other but have opposite sign. The actual arterial pressure and flow waveforms at any point on the tube then arise as the sum of the forward and backward propagating waves shifted in time to account for their wave propagation time to the point of interest.

Quantitatively, pressure and flow waves on a tube are related through its characteristic impedance as follows:

$$Q_{fi}(x, j\omega) = \frac{P_{fi}(x, j\omega)}{Z_{ci}}, Q_{bi}(x, j\omega) = \frac{P_{bi}(x, j\omega)}{Z_{ci}}. \tag{1.2}$$

Here, $P_{fi}(x, j\omega)$ and $P_{bi}(x, j\omega)$ are forward and backward propagating pressure waves in the frequency-domain at a point x on the i^{th} tube, and $Q_{fi}(x, j\omega)$ and $Q_{bi}(x, j\omega)$ are the corresponding flow waves at the same point. Note that the forward waves actually represent the sum of all waves propagating from the proximal to distal tube ends (i.e., the incident wave from the heart and the backward waves re-reflected at the heart), while the backward waves may be interpreted analogously. Also, note that $x = 0$ and $x = d_i$ correspond to the distal and proximal ends of the tube, respectively.

The forward and backward waves at a distal tube end are related to each other through the wave reflection coefficient as follows:

$$P_{bi}(0, j\omega) = \Gamma_i(j\omega) \cdot P_{fi}(0, j\omega). \tag{1.3}$$

The forward and backward waves at any point on a tube may be expressed in terms of the corresponding waves at the distal tube end as follows:

$$P_{fi}(x, j\omega) = P_{fi}(0, j\omega)e^{j\omega T_i \cdot x/d_i}$$
$$P_{bi}(x, j\omega) = P_{bi}(0, j\omega)e^{-j\omega T_i \cdot x/d_i}, \tag{1.4}$$

where the exponential term is the frequency-domain time-shifting operator.

By combining equations (1.1) to (1.3), the actual arterial pressure and flow waveforms at any point on a tube may then be expressed in terms of the forward and backward waves as follows:

$$\begin{aligned} P_i(x, j\omega) &= P_{fi}(x, j\omega) + P_{bi}(x, j\omega) \\ &= P_{fi}(0, j\omega) \cdot [e^{j\omega T_i \cdot x/d_i} + \Gamma_i(j\omega)e^{-j\omega T_i \cdot x/d_i}] \\ Q_i(x, j\omega) &= Q_{fi}(x, j\omega) + Q_{bi}(x, j\omega) \\ &= \frac{P_{fi}(0, j\omega)}{Z_{ci}} \cdot [e^{j\omega T_i \cdot x/d_i} - \Gamma_i(j\omega)e^{-j\omega T_i \cdot x/d_i}], \end{aligned} \tag{1.5}$$

where $P_i(x, j\omega)$ and $Q_i(x, j\omega)$ are the arterial pressure and flow waveforms in the frequency-domain at point x on the i^{th} tube.

Due to the parallel connection of the model, the central aortic pressure waveform is identical to the arterial pressure waveforms at each proximal tube end, whereas the central aortic flow waveform is the sum of all flow waveforms at the proximal tube ends as follows:

$$\begin{aligned} P(j\omega) &= P_i(d_i, j\omega) = P_{fi}(0, j\omega) \cdot [e^{j\omega T_i} + \Gamma_i(j\omega)e^{-j\omega T_i}] \\ Q(j\omega) &= \sum_{i=1}^{m} Q(d_i, j\omega) = \sum_{i=1}^{m} \frac{P_{fi}(0, j\omega)}{Z_{ci}} \cdot [e^{j\omega T_i} - \Gamma_i(j\omega)e^{-j\omega T_i}], \end{aligned} \tag{1.6}$$

where $P(j\omega)$ and $Q(j\omega)$ are the central aortic pressure and flow waveforms in the frequency-domain.

Finally, equations (1.5) and (1.6) may be given explicitly in terms of the tube-load model parameters by substituting a $\Gamma(j\omega)$ from figure 1.11(B) into these equations.

1.2.2.2 Assumptions and validity

Assumptions of the tube-load model include: (a) wave propagation without energy loss in large conduit arteries, (b) a load characterized by a few parameters, and (c) non-interacting reflections occurring at distal sites only by virtue of neglecting elastic and geometric tapering and multi-level branching. Assumption (a) is quite valid. Friction in the large conduit arteries is indeed negligible, because resistance is inversely proportional to the fourth power of the vessel radius. Pressure loss in the descending aorta, for example, has been shown to be trivial [15]. Assumption (b) is justifiable based on empirical data. That is, while the actual load is certainly complicated with many parameters needed for its representation, the arterial input impedance computed with the tube-load model has been shown to match that determined with standard non-parametric Fourier analysis [13, 14]. Note, however, that an even simpler purely real load may not be supported by empirical data [15]. Assumption (c) is the least tenable but can be defended to some extent. The arterial terminations do often constitute the dominant reflection sites for two reasons. First, they pose the greatest impedance mismatch, as the radius of the arterioles is much smaller than that of proximal arteries [77]. Second, vessel tapering tends to be offset by vessel branching in the forward direction so as to achieve relative impedance matching [73]. In addition, the tube-load model has been shown to fit experimental waveforms almost as well as an exponentially tapered version of the model [36]. On the other hand, backward waves should experience strong re-reflections as they return to the heart due to necessarily significant impedance mismatches in the backward direction [73]. Further, the multiple reflected waves that return from distal sites actually interact in the aorta due to multi-level branching.

In short, the tube-load model has a physiologic foundation but does ignore aspects of actual arterial hemodynamics. Despite its simplicity, it is able to fit experimental arterial pressure and flow waveforms remarkably well. Figure 1.12 illustrates major waveform phenomena that the model can predict. This ability to fit experimental data provides further validation of the tube-load model and suggests that it may be phenomenological in addition to physiological.

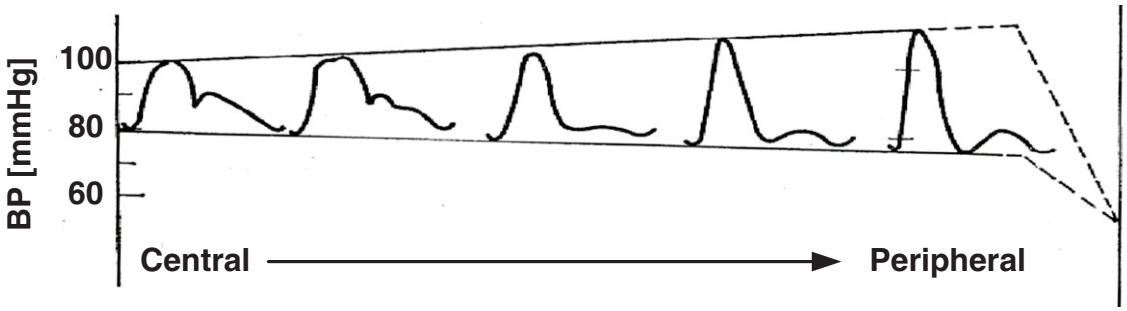

Figure 1.12: Experimental arterial pressure with increasing distance from the heart.

1.2.2.3 Parameter estimation

Most often, estimating the tube-load model parameters is accomplished by casting the governing equations into a transfer function. The transfer function relating a pair of arterial pressure and/or flow waveforms at any points on a tube may be obtained based on equation (1.5). For example, using the T-tube model with Type II load, the transfer function relating the central aortic pressure waveform to the central aortic flow waveform is given as follows:

$$Q_i(d_i, j\omega) = H_i(j\omega) \cdot P(j\omega) = \frac{1}{Z_{ci}} \frac{e^{j\omega T_i} - \Gamma_i(j\omega)e^{-j\omega T_i}}{e^{j\omega T_i} + \Gamma_i(j\omega)e^{-j\omega T_i}} \cdot P(j\omega) \quad i = 1,2. \tag{1.7}$$

As another example, using the Type I load, the transfer function relating the central aortic pressure waveform to a peripheral arterial pressure waveform is given as follows:

$$\begin{aligned} P_i(0, j\omega) &= \frac{1 + \Gamma_i(j\omega)}{e^{j\omega T_i} + \Gamma_i(j\omega)e^{-j\omega T_i}} \cdot P(j\omega) \\ &= \frac{j\omega + \dfrac{1}{R_i C_i} + \dfrac{1}{Z_{ci} C_i}}{(j\omega + \dfrac{1}{R_i C_i} + \dfrac{1}{2Z_{ci} C_i})e^{j\omega T_i} + \dfrac{1}{2Z_{ci} C_i} e^{-j\omega T_i}} \cdot P(j\omega). \end{aligned} \tag{1.8}$$

The former transfer function is defined by the eight unknown parameters of the T-tube model. However, while the latter transfer function includes all four unknown model parameters of a single tube and load, only three aggregate parameters are actually observable (T_i, $R_i C_i$ and $Z_{ci} C_i$). Thus,

all four parameters cannot be estimated, but identification of the transfer function is simplified to a three-parameter problem.

Estimation of the observable model parameters is accomplished in two steps. First, arterial pressure and flow waveforms corresponding to the input and output of the transfer function of interest are measured. Then, the parameters are estimated by finding the transfer function, which when applied to the measured input, optimally fits the measured output. Alternatively, in some instances, the parameters of the transfer function may be optimally estimated using a priori physiologic knowledge. The advantage of this alternative is to reduce the burden on the required waveform measurements. In either case, parameter estimation is usually performed in the time-domain by converting the transfer function into a recursive difference equation, and the optimality is typically established in the least squares sense.

The step of estimating the tube-load model parameters is actually quite challenging. First, the transfer functions are not simply linear in distinct parameters. For example, as can be ascertained from equations (1.7) and (1.8), the transfer functions are nonlinear in the T_i (pulse transit time) parameter. Second, the parameter values have numerical constraints. For instance, the characteristic impedance should be smaller than the peripheral resistance, and all parameters must be positive and not exceed physiologic bounds. For these two reasons, straightforward parameter estimation techniques with analytical solutions are generally not applicable. The parameters are instead typically estimated via numerical search in which the needed global optimum cannot be guaranteed. Use of brute force methods that search over a discretized grid in multi-dimensional parameter space increases the likelihood of identifying the global optimum at the expense of substantial computational time. On the other hand, use of available local search methods such as the steepest descent method, conjugate gradient method, Newton's method and its Levenberg-Marquardt modification, and simplex method (possibly with penalty factors for keeping the parameters within physiologic bounds) [58] require little computational time, but the global optimum is seldom found without an initial guess that resides near the global optimum. This problem is often mitigated by employing multiple, initial guesses and then choosing the solution that represents the optimum amongst the

multiple solutions of the local search method. However, the computational time will obviously increase with the number of initial guesses. Another practical issue is that the upper physiologic bounds on the parameters are often unclear. However, the challenge of parameter estimation can be alleviated to some degree by direct measurement of one or more parameters, especially pulse transit time and load resistance [14, 17, 40, 105]. Despite these challenges, asymptotic variance analysis has shown that the confidence intervals on the parameters estimates can be tight [40].

1.3 Organization

In this report, we will review the contribution of novel techniques for CO monitoring from a peripheral arterial blood pressure waveform. Chapter 2 discusses the proposed long time interval analysis (LTIA) and applies the technique to a large, ICU human dataset (MIMIC II) and a human lower body negative pressure (LBNP) experiment. Our technique was superior to other conventional methods when the change in CO became challenging. In the study, we found that the varying AC introduced estimation errors. Therefore, we introduced the pulse transit time to eliminate the influence of arterial compliance, as discussed in Chapter 3. Comparing with pulse transit time, pulse arrival time gains popularity since it is even easier to measure. However, it is not adequate to be a surrogate in replacing with pulse transit time. Therefore, we can only recommend pulse transit time for monitoring arterial compliance changes. Conventional detection of pulse transit time is sensitive to artifact, so we applied a black-box model which can robustly estimate pulse transit time from blood pressure waveforms. Pulse transit time estimated in this approach was employed to correct AC, which was validated both in an animal study and the LBNP experiment. In Chapter 4, a novel technique of short time interval analysis was proposed to monitor the cardiac output variation which permits beat-by-beat monitoring. The accuracy was also improved by the pulse transit time correction. Further, we added an additional term to the LTIA method, which can estimate CO from a pulmonary artery pressure. In the end, future direction is discussed in Chapter 6.

Chapter 2

CARDIAC OUTPUT MONITORING FROM PERIPHERAL ARTERIAL BLOOD PRESSURE BY LONG TIME INTERVAL ANALYSIS

2.1 Introduction

The acute shortage of clinical personnel [35], declining pulmonary artery catheter usage [112], and recent success of goal-directed therapy [64, 81] collectively indicate the urgent need for an accurate, continuous (i.e., automated), and minimally invasive cardiac output (CO) monitoring technique. A potential practical approach for intensive care unit (ICU) patients is to track CO by mathematical analysis of an arterial blood pressure (ABP) waveform obtained with an existing radial artery line. Indeed, various "pulse contour analysis" techniques have been suggested in the literature ([69] and references therein), and a few such techniques are now commercially offered [26, 31]. The assessment of these techniques in patients has been the subject of a number of recent articles published in this journal [6, 7, 19, 33, 76] and others. However, the relative accuracy of the techniques has yet to be conclusively established [79].

2.2 The technique

We too have previously proposed a mathematical analysis technique to estimates relative CO changes from an ABP waveform measured at any arterial site including the radial artery (Figure 2.1)[69]. Unlike all other techniques, the technique analyzes the slow, beat-to-beat changes in the waveform wherein confounding arterial wave reflections cease to be a major factor in an attempt to maximize accuracy. More specifically, first, the ABP response to a single heart beat ($h(t)$) is estimated by analyzing the waveform over many beats. Then, the Windkessel time constant (τ), which is equal to the product of the total peripheral resistance (TPR) and the approximately constant arterial compliance (AC), is determined by fitting an exponential to the tail end of this

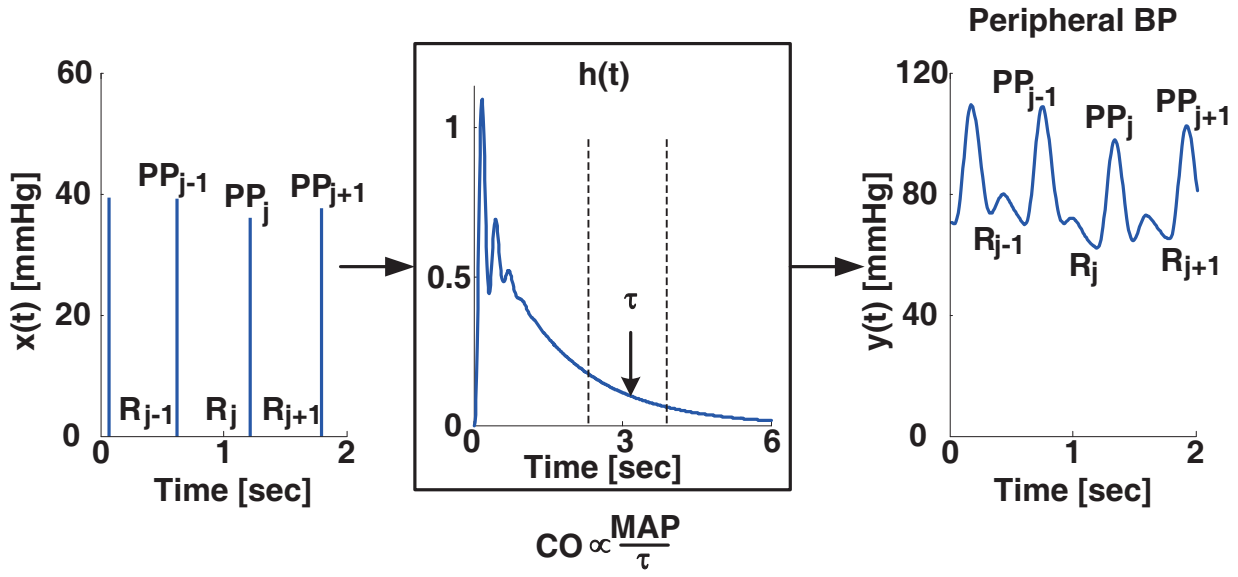

Figure 2.1: Continuous and minimally invasive technique for estimating relative cardiac output (CO) change by unique long time interval analysis (LTIA) of an arterial blood pressure (ABP) waveform obtained with an existing radial artery line.

response once the faster wave reflections vanish. Finally, CO is computed to within a 1/AC scale factor by dividing mean ABP (MAP) with τ. (Figure reffig:MIMIC-LTIA caption for further details.) We have verified this "long time interval analysis" (LTIA) technique against reference CO measurements from animals and humans during various physiologic conditions [69, 59, 87]. However, as recommended in a recent editorial in this journal [19], the technique has yet to be assessed in a significant ICU patient population.

Recently, Sun et al. used their "MIMIC II" database, which includes radial ABP waveforms and thermodilution CO measurements from a substantial number of ICU patients, to compare eight published pulse contour analysis techniques [103]. These investigators found that pulse pressure times heart rate normalized by the sum of systolic and diastolic pressures (PP $\cdot$ HR/(SP+DP)), as proposed by Liljestrand et al. [57], was most accurate in tracking changes in the reference thermodilution CO measurements. They concluded that their electronic database could represent a useful standard for testing pulse contour analysis techniques, with the PP $\cdot$ HR/(SP+DP) technique serving as a benchmark for comparison, and invited others to assess their own techniques by

making the database readily and freely available.

We assessed the LTIA technique using the MIMIC II database. In this way, we were able to demonstrate the relative accuracy of the technique while testing it in a significant ICU patient population. We describe the retrospective data analysis below.

2.3 Experiment 1: validation in the MIMIC II database

2.3.1 Materials and analysis

We studied all pairs of radial ABP waveforms and reference thermodilution CO measurements in the MIMIC II database that did not meet any pre-defined exclusion criteria. We applied the LTIA, PP·HR/(SP+DP), and other previous techniques to the ABP waveforms. Since all of these techniques estimate CO to within a patient specific scale factor (i.e., K·CO or "proportional CO"), we calibrated each technique (i.e., determined K for each technique) by scaling its proportional CO estimates to a single value yielded by thermodilution per patient. We then assessed the accuracy of each technique based on the magnitude of the differences between its calibrated CO estimates and the thermodilution CO measurements ("CO errors"). Finally, we compared the accuracy of the techniques via statistical tests of their CO error magnitudes.

The MIMIC (Multiparameter Intelligent Monitoring in Intensive Care) II database is described in detail elsewhere[103, 90]. Briefly, the database includes anonymised, physiologic and clinical data from patients of various ICUs of a university hospital. The public database is growing. At the time of our downloading of the database, data from 2,769 patients were available. The physiologic data consist of continuous measurements such as invasive radial ABP and ECG waveforms sampled at 125 Hz and time aligned, discrete measurements including thermodilution CO. Each of the available thermodilution measurements was obtained via the pulmonary artery catheter and a single bolus injection (rather than multiple bolus injections). The clinical data constitute wide ranging information including patient characteristics. Our analysis of the database was approved by the Michigan State University IRB (# X05-597). We extracted all 1-min segments of the ra-

dial ABP waveforms that coincided with each reference thermodilution CO measurement in the database and included all of these data pairs in the study. A total of 1,915 pairs of ABP (and ECG) waveform segments and thermodilution CO measurements from 197 patients were available. We then excluded those pairs (a) from patients with only one thermodilution measurement (as relative CO changes within a subject is effectively estimated); (b) from patients on intra-aortic balloon pumps as indicated by the presence of diastolic augmentation in the ABP waveforms (a standard contraindication of pulse contour analysis); and (c) with obvious artifact in the ABP waveform segments as ascertained by visual examination (to evaluate the ability to track CO rather than to detect and suppress artifact). A total of 1,482 data pairs from 169 patients remained for analysis. We applied the LTIA technique to the 1-min radial ABP waveform segments to estimate proportional CO in each patient. Since our data for analysis were not identical to those of Sun et al. (who actually analyzed 1,164 data pairs from 120 patients [103]), we also likewise estimated proportional CO with the benchmark PP·HR/(SP+DP) technique and two other previous techniques of particular relevance, namely PP·HR and MAP. The PP·HR technique, which tracks CO via the product of pulse pressure and heart rate, is perhaps the most widely used pulse contour analysis (e.g., two commercial devices are based on this technique [88]). The MAP technique, which tracks CO via mean ABP, is the most basic pulse contour analysis and therefore serves as a useful reference for comparison [103]. In addition, we similarly explored our technique after the normalization of Liljestrand et al. [57] (LTIA/(SP+DP)). We calibrated each of the five investigational techniques using a single value yielded by thermodilution per patient. We specifically scaled the proportional CO (i.e., $K \cdot CO$) estimates of each technique to have the same mean value as the thermodilution measurements in each patient. Thus, for each patient, K was effectively set to the ratio of the mean value of the $K \cdot CO$ estimates of the technique to the mean value of the thermodilution CO measurements. We assessed the accuracy of each technique through the differences between its calibrated CO estimates and the thermodilution CO measurements. We quantified the magnitude of these CO errors in terms of two metrics drawn from Bland-Altman analysis. One metric is the limits-of-agreement of the absolute errors ($\mu - 1.96 \cdot \sigma / \mu + 1.96 \cdot \sigma$, where μ and σ are respectively the

bias error (i.e., average of all errors) and precision error (i.e., standard deviation of all errors)). Use of this metric allowed comparisons to the investigation of Sun et al. [103]. The other metric is the root-mean-square of the relative errors (RMSE=$\sqrt{\mu^2+\sigma^2}$). Use of this metric, which combines the bias and precision errors into a single number reflecting the total error, permitted comparisons to our previous studies [69, 59]. Further, use of relative errors allowed comparisons to the recommendations of Critchley et al. [28]. We statistically compared the techniques based on the square of their relative errors, which similarly reflect the total error. Since these squared-errors were not normally distributed, we used the Wilcoxon signed-rank test to determine whether the median of the differences between the squared-errors of the published LTIA technique and the squared-errors of another investigational technique was statistically significant. It should be noted that these squared-error differences (i.e., the squared-errors of the LTIA technique minus the corresponding squared-errors of another technique) actually constituted repeated measures rather than truly independent samples with zero correlation.

However, we did not make adjustments for the repeated measures for two reasons. Firstly, the adjustment required would be very complicated and therefore difficult to follow (unlike the basic Wilcoxon signed-rank test). Secondly, and most importantly, we tested these data in terms of the extent of the dependence of samples and found that the samples correlated only little (0.08 to 0.22). Thus, adjustment for repeated measures would not have materially altered the results.

2.3.2 Results

The average characteristics of the 1,482 pairs of 1-min radial ABP waveform segments and reference thermodilution CO measurements from 169 patients for study are as follows. The patients were mostly old (Table 2.1), with two-thirds being male. Three-quarters of the patients had ischemic or other forms of heart disease, whereas the remaining patients had various other conditions. The patients stayed mainly in the cardiac surgery recovery unit (70%) but also in the coronary care unit (19%) and medical or surgical ICUs (11%). Their average SAPS (Simplified Acute Physiology Score) I was 15.5 (4.4 SD) (Table 2.1). On average, 8.8 (6.3) thermodilution CO

Table 2.1: Average characteristics of patients and data.

Characteristic	Units	Mean(SD)	N
Age	year	67.7(13.0)	169
SAPS I		15.5(4.4)	169
Number of CO measurements per patient		8.8(6.3)	169
Duration of CO measurements per patient day		1.1(1.1)	169
CO	L/min	5.3(1.7)	1,482
MAP	mmHg	73.6(10.8)	1,482
HR	bpm	86.2(12.6)	1,482
CO change magnitude (relative to mean CO in patient)	%	12.3(9.9)	1,482

Table 2.2: Overall cardiac output estimation accuracy of the investigational techniques.

Technique	RMSE (%)	Limits-of-Agreement (L/min)	Wilcoxon Signed-Rank Test (p)
LTIA	18.8	-1.96/+1.96	-
MAP	19.8	-1.90/+1.90	0.85
PP·HR	18.4	-1.92/+1.92	0.02
PP·HR/(SP+DP)	14.8	-1.51/+1.51	$<$0.0005
LTIA/(SP+DP)	15.0	-1.56/+1.56	$<$0.0005

measurements made over the course of 1.1 (1.1) days were available from each patient (Table 2.1). The average thermodilution CO was similar to that of a healthy adult population, whereas the average MAP and heart rate (HR) were not (Table 2.1). The average magnitude of the thermodilution CO change relative to the mean thermodilution CO in the patient was 12.3 (9.9) percent (Table 2.1).

Over all the data pairs and patients, the LTIA technique achieved a RMSE of 18.8% and a limits-of-agreement of -1.96/+1.96 L/min (Table 2.2). The MAP and PP·HR techniques attained very similar overall error magnitudes, though the median squared-error difference between the LTIA technique and the latter technique did reach statistical significance (Table 2.2). The normalization of Liljestrand et al. [57] somewhat improved the overall accuracy of both the PP·HR and LTIA techniques. That is, the PP·HR/(SP+DP) and LTIA/(SP+DP) techniques both showed reductions in RMSE by $\sim$3.7% and in the lower and upper limits-of-agreement by $\sim$0.4 L/min (Table 2.2). Further, the median squared-error difference between the original LTIA technique and each of these techniques was statistically significant (Table 2.2).

The CO estimation accuracy of the investigational techniques is indicated as a function of

minimum thermodilution CO change magnitude (Figure 2.2). That is, the data points at Z on the x-axis denote the squared-errors (median $\pm$ quartiles) of each technique only over those data pairs for which the magnitude of the thermodilution CO change relative to the mean thermodilution CO in the patient exceeded Z%. So, for example, 0 on the x-axis would correspond to the results over all the data pairs (which are shown in Table 2.2). The p-values reveal the levels of statistical significance of the median squared-error difference between the pair of techniques with the lowest median squared-errors. (These p-values represent upper bounds on the significance level of the median squared-error difference between the technique with the lowest median squared-error and the remaining techniques in the figure.)

The median squared-error of the LTIA technique increased with the minimum thermodilution CO change magnitude (Figure 2.2). However, the median squared-errors of the PP·HR technique and especially the MAP technique rose at a greater rate (Figure 2.2). As a result, the median squared-error difference between the LTIA technique and each of these basic techniques became greater with minimum thermodilution CO change magnitude and reached statistical significance when the minimum change magnitude was $\geq$30% (Figureřeffig:MIMIC-Result). In particular, the median squared-error differences between the LTIA technique and the PP·HR technique were -45 (-322:69 quartiles), -128 (-704:23), and -862 (-2871:306)$\%^2$ for thermodilution CO change magnitudes exceeding 30, 50, and 70%, respectively. The normalization of Liljestrand et al. [57] was able to yield modest, statistically significant reductions in the median squared-error for both the PP·HR and LTIA techniques when the minimum thermodilution CO change magnitude was 10%, but not any higher (Figure 2.2). In fact, the median squared-errors of these techniques often increased relative to the un-normalized techniques as the minimum thermodilution CO change magnitude grew (Figure 2.2 wherein the results of the normalized LTIA technique are not shown to simplify the figure.)

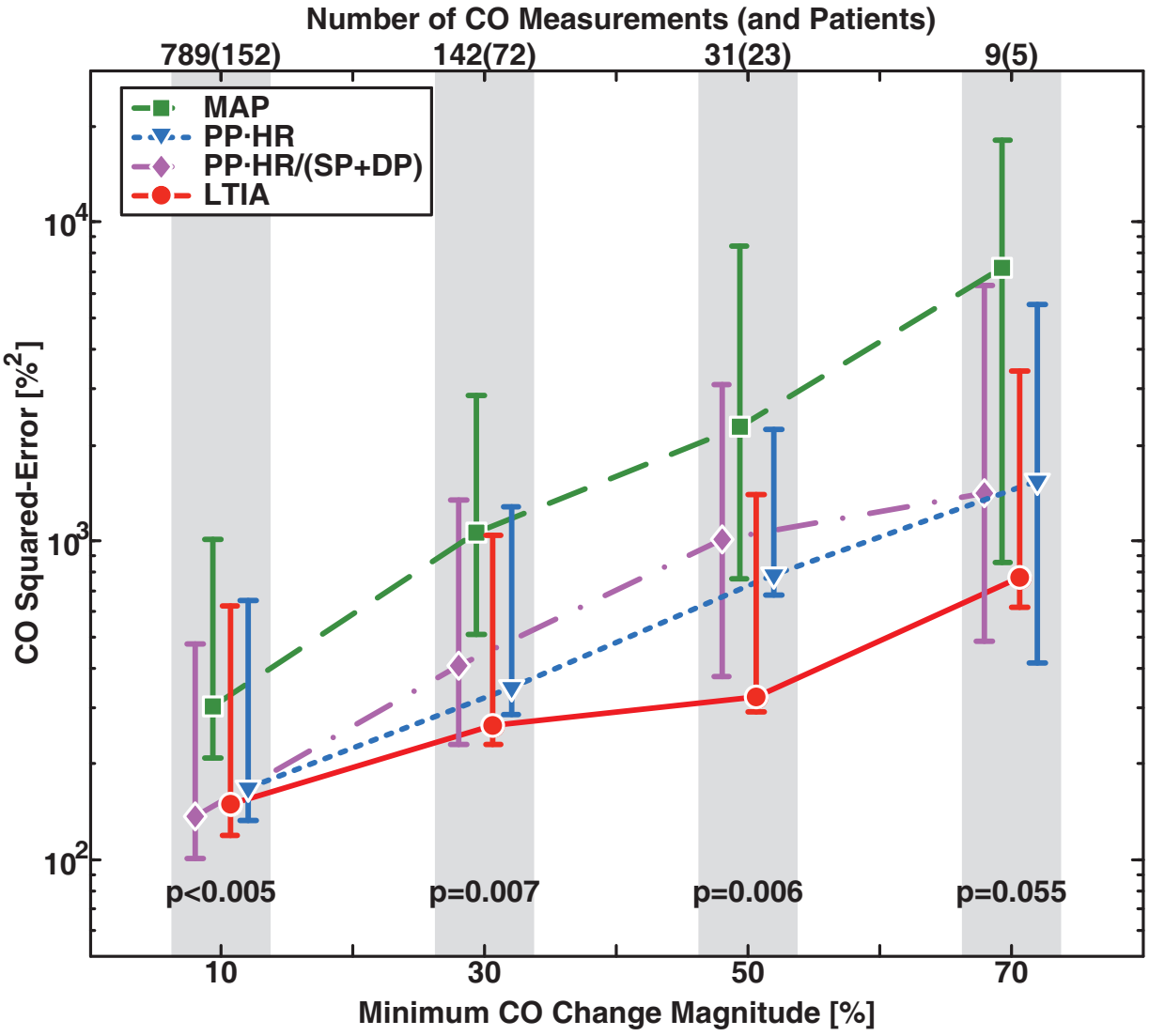

Figure 2.2: CO estimation accuracy of the investigational techniques (on log scale) as a function of the magnitude of the reference CO change.

2.3.3 Discussion

In this study, we assessed our previously developed LTIA technique for uniquely estimating proportional CO from an ABP waveform (Figure 2.1) using the readily and freely available MIMIC II database18. For comparison, we also investigated previous pulse contour analysis techniques of particular relevance. Our results not only provide a first-time indication of the efficacy of the LTIA technique in a significant ICU patient population but also permit future comparisons of it to other techniques.

We specifically studied 1,482 pairs of 1-min radial ABP waveform segments without obvious artifact and reference CO measurements via single bolus injection thermodilution from 169 patients (Table 2.1). The LTIA technique achieved an overall CO error of 18.8% after a single calibration with thermodilution in each patient (Table 2.2). Note that since the precision error of the reference measurements here is known to be $\sim$17% [99, 46, 100], a clinically acceptable level of agreement would be within 19.7% according to the recommendations of Critchley et al. [28].

The overall calibrated CO errors of the PP·HR technique, which has perhaps been the most widely used pulse contour analysis, and the MAP technique, which represents the most basic analysis, were equivalent to that of the LTIA technique (Table 2.1). Further, these much simpler, previous techniques may offer some practical advantages. Importantly, however, the magnitude of the reference CO change was often small in the database. In fact, approximately three-quarters of the thermodilution CO change magnitudes (relative to the mean thermodilution CO in the patient) were less than the precision error of the reference measurements. Without significant changes, any reproducible pulse contour analysis technique, when calibrated, will be able to achieve a reasonable level of CO estimation accuracy.

The MIMIC II database did allow for reasonable comparisons of the techniques only during the appreciable reference CO changes. Indeed, as the magnitude of the thermodilution CO change increased, the accuracy of the LTIA technique became increasingly and statistically superior to the PP·HR and MAP techniques (Figure 2.2).

The normalization with SP+DP suggested by Liljestrand et al. to correct for any ABP-dependent

AC changes [57] did afford some improvement in the overall accuracy of the PP·HR technique as well as the LTIA technique. In particular, the PP·HR /(SP+DP) technique, which was shown to perform best amongst the eight pulse contour analysis techniques studied by Sun et al. using the same database [103], and the LTIA/(SP+DP) technique both achieved overall calibrated CO errors of $\sim$15% (Table 2.2). However, when the magnitude of the thermodilution CO change increased, the normalization was not helpful and even had a tendency to degrade the accuracy of the PP·HR and LTIA techniques (Figure 2.2). Thus, the effectiveness of the normalization here may merely be due to blunting the estimated CO change so as to yield better correspondence to the largely unvarying thermodilution CO measurements rather than actually correcting for changes in AC. Consequently, this normalization may not be generally advisable. However, other types of AC correction factors should not be discounted.

Like the pulse contour analysis study with the MIMIC II database by Sun et al. [103], we assessed all of the investigational techniques using 1-min radial ABP waveform segments for analysis. However, we initially verified the LTIA technique with 6-min ABP waveform segments [69, 59]. We therefore also applied the LTIA technique to ABP waveform segments of 6-min durations here, and its performance did not materially improve (e.g., the overall calibrated CO error was 17.8%). This comparative result indicates that the LTIA technique may be applied to a waveform duration that is comparable to those employed by conventional techniques without any significant sacrifice in accuracy.

In addition to the assessment of the LTIA technique, there were other differences in methodology and materials between this study and that of Sun et al. [103]. Firstly, we had more data for analysis, because the MIMIC II database had grown since their study. Secondly, we excluded $\sim$22% of the available data (1% for only one reference CO measurement from the patient; 15% for patients on intra-aortic balloon pumps; and 6% for obvious waveform artifact), whereas Sun et al. discarded only $\sim$15% mainly due to a greater tolerance of artifact in the ABP waveforms. (Note that, like these investigators, we did not exclude data due to unsteady conditions wherein the thermodilution measurements may be less useful as a CO reference, arterial line damping, or

aortic valve regurgitation, all of which may represent sources of error here.) Thirdly, we calibrated the proportional CO estimates with the mean thermodilution CO in a patient, while Sun et al. employed an optimal calibration likewise involving all thermodilution CO measurements in a patient and a calibration with one thermodilution measurement per patient. Fourthly, we studied the CO estimation accuracy as a function of relative CO change magnitude instead of directional (sign) agreement with the largest reference CO change in each patient as they did. Despite these differences, our results were quite similar to the analogous ones of Sun et al. In particular, the average patient and data characteristics contrasted little. Also, our mean calibration turned out to yield only slightly higher CO errors than their optimal calibration (results not shown). Finally, although the limits-of-agreement here are a bit tighter than those of Sun et al. due to our more stringent requirements on waveform quality, the relative standing of the previous techniques based on this accuracy metric as well as the RMSE metric was maintained over all the data.

The main limitation of this study is the non-trivial error in the reference CO measurements available in the MIMIC II database. (Note that, to somewhat compensate for this error, we performed the calibration using the mean, rather than a single, thermodilution CO in each patient.) Even with this limitation, we felt that it was sensible to test the LTIA technique using the readily and freely available database for two reasons. Firstly, the study would be efficient and without any risk to human subjects. Secondly, and most importantly, the accuracy of the technique relative to other techniques could be fairly revealed, because all technique developers, including vendors offering proprietary techniques, have access to the same data.

In conclusion, we have assessed a continuous and minimally invasive technique for estimating relative CO change by unique LTIA of a radial ABP waveform in a significant ICU patient population using a database that may ultimately develop into a standard for testing pulse contour analysis techniques. The technique achieved a CO estimation error that was overall within recommended clinical limits and became increasingly and significantly smaller than previous techniques as the reference CO change became more meaningful. While the ability to continuously monitor relative CO change would be useful for detecting a hemodynamic event or directing therapy in

ICU patients, future extensions of the LTIA technique to provide absolute CO via a non-invasive calibration and to effectively correct for any AC change are worthwhile.

2.4 Experiment 2: validation in a lower body negative pressure study

2.4.1 Materials and analysis

The ACEMMR Team has developed a safe and reproducible human LBNP protocol that is approved by the Institutional Review Board of the Brooke Army Medical Center (BAMC; Fort Sam Houston, TX). The protocol is documented in detail in several recent publications (e.g., [22, 25, 24]). Briefly, 129 volunteers are recruited from military personnel at the USAISR and BAMC as well as nearby civilian communities. Men and women between 18 and 55 years of age that are nonsmokers and not pregnant, have no cardiovascular abnormalities (e.g., hypotension, neural dysfunction), and meet military fitness and health standards are included in the study after obtaining informed, written consent. Prior to experimentation, the subjects are instructed to abstain from stimulants (e.g., caffeine) and are familiarized with the protocol.

The subject is placed in the supine posture and secured in an LBNP chamber using a neoprene skirt designed to form an airtight seal between the subject and the chamber (Figure 2.3). Instruments for measuring hemodynamic, neural, and metabolic variables are positioned. The physiologic variables are recorded during a five-minute baseline period and following sequential exposure to 15, 30, 45, 60, 70, 90, and 100 mmHg of LBNP for five minutes each. Early termination of LBNP occurs (i.e., return of chamber pressure to 0 mmHg) upon the appearance of cardiovascular collapse defined as follows: (1) precipitous fall in systolic ABP $>$ 15 mmHg and/or precipitous fall in HR $>$ 15 bpm; (2) systolic ABP $<$ 80 mmHg; and/or (3) subject request due to symptoms such as nausea, dizziness, or lightheadedness. After cessation of LBNP and a five-minute transition period to allow the return of fluid sequestered in the lower body, the physiologic variables are recorded for an additional five-minute recovery period. Note that subjects usually reach cardiovascular stability within one to two minutes after termination of the final level of LBNP.

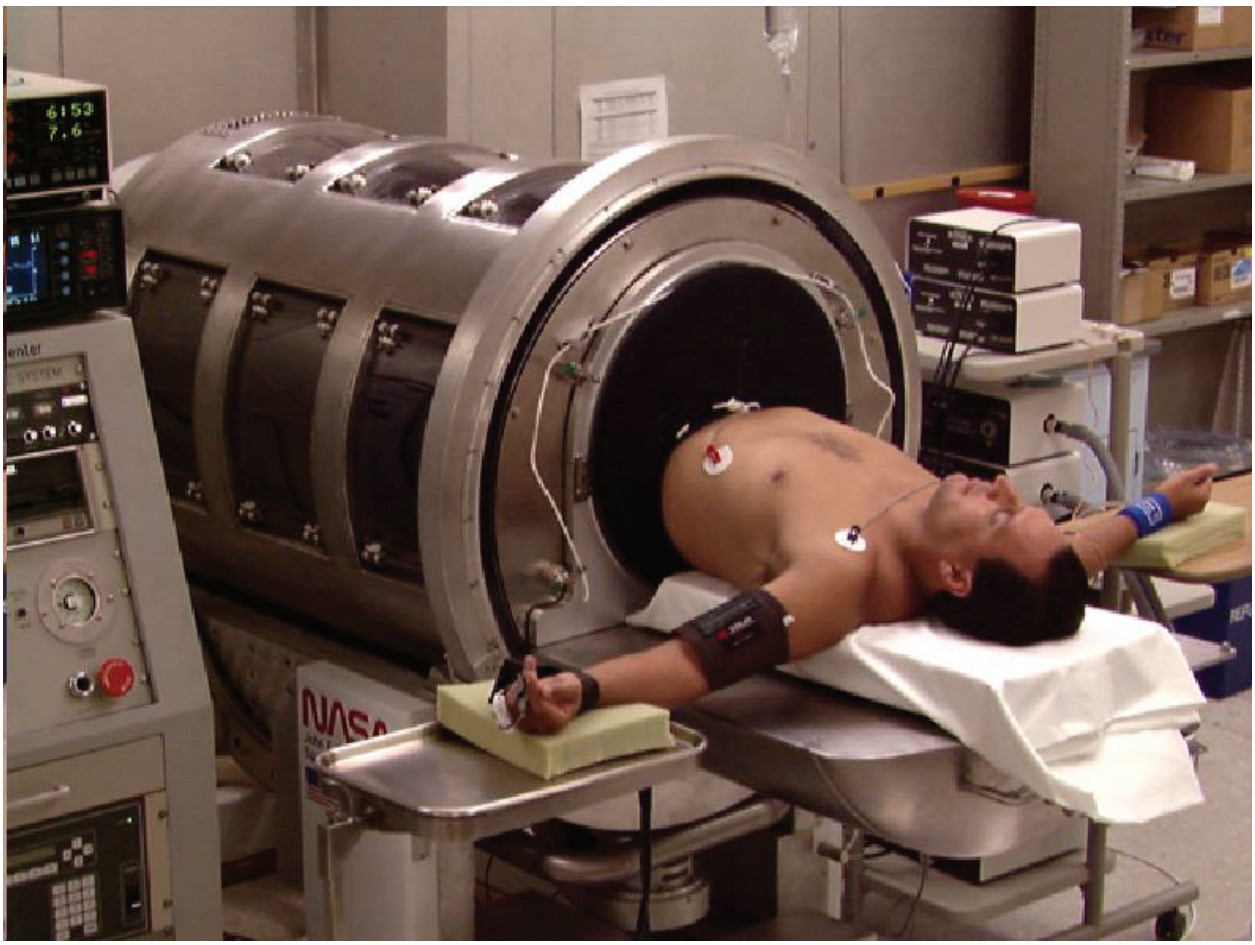

Figure 2.3: One subject in the LBNP experiment.

A non-invasive peripheral ABP waveform is measured with finger-cuff PPG (Finometer, TNO-TPD Biomedical Instrumentation, Amsterdam, The Netherlands). ECG waveforms are measured with a standard four-lead system. CO and beat-to-beat SV are measured non-invasively with E-BI (BioZ Impedance Cardiograph, Cardiodynamics, San Diego, CA). EBI correlates SV changes with the electrical impedance changes in the thorax over each heart beat that are elicited by a low-intensity, high frequency alternating current [27]. Other physiologic variables not directly pertinent to the project are also measured including arterial oxygen saturation via pulse oximetry and, sometimes, tissue (muscle) oxygen saturation and pH via near-infrared spectroscopy. All transducers are interfaced to a personal computer with commercial hardware and software (WINDAQ, Dataq Instruments, Akron, OH). The physiologic variables are recorded at a sampling rate of 500 Hz.

We compared three techniques for the estimation of CO: MAP, PP·HR and LTIA. We again evaluated the accuracy of the individual techniques in terms of the RMSNE.

2.4.2 Results

Figure 2.4 shows the result of LTIA comparing with the reference measurement. As expected, mean ABP was maintained around the baseline level due to compensatory physiologic mechanisms. The PP·HR did not follow the decreasing trend during the LBNP process. Comparing the reference, the Modelflow method overestimated the CO during the LBNP process. The LTIA technique is similar with the Modelflow technique during the LBNP stages. At the recovery stage, however, the LTIA returned to baseline level but Modelflow failed to indicate the return.

2.4.3 Discussion

The human LBNP experiment is considered as a safe simulation of central hypovolemia. In this study, we evaluated the accuracy of five techniques in terms of the capabilities in indicating hemorrhage and recovery. MAP and PP·HR did not indicate the decreasing trend in the LBNP stage. Modelflow and LTIA showed falling during the experiment but the former method failed to return to baseline at the recovery stage. Among all candidate methods, CO estimated by ICG is the most sensitive marker of hypovolemia.

In this study, we assume the AC should be constant. However, AC may be adjusted by varying ABP and vasomotor tone. In the next chapter, we introduced a technique which utilizing PTT to correct the influence of AC.

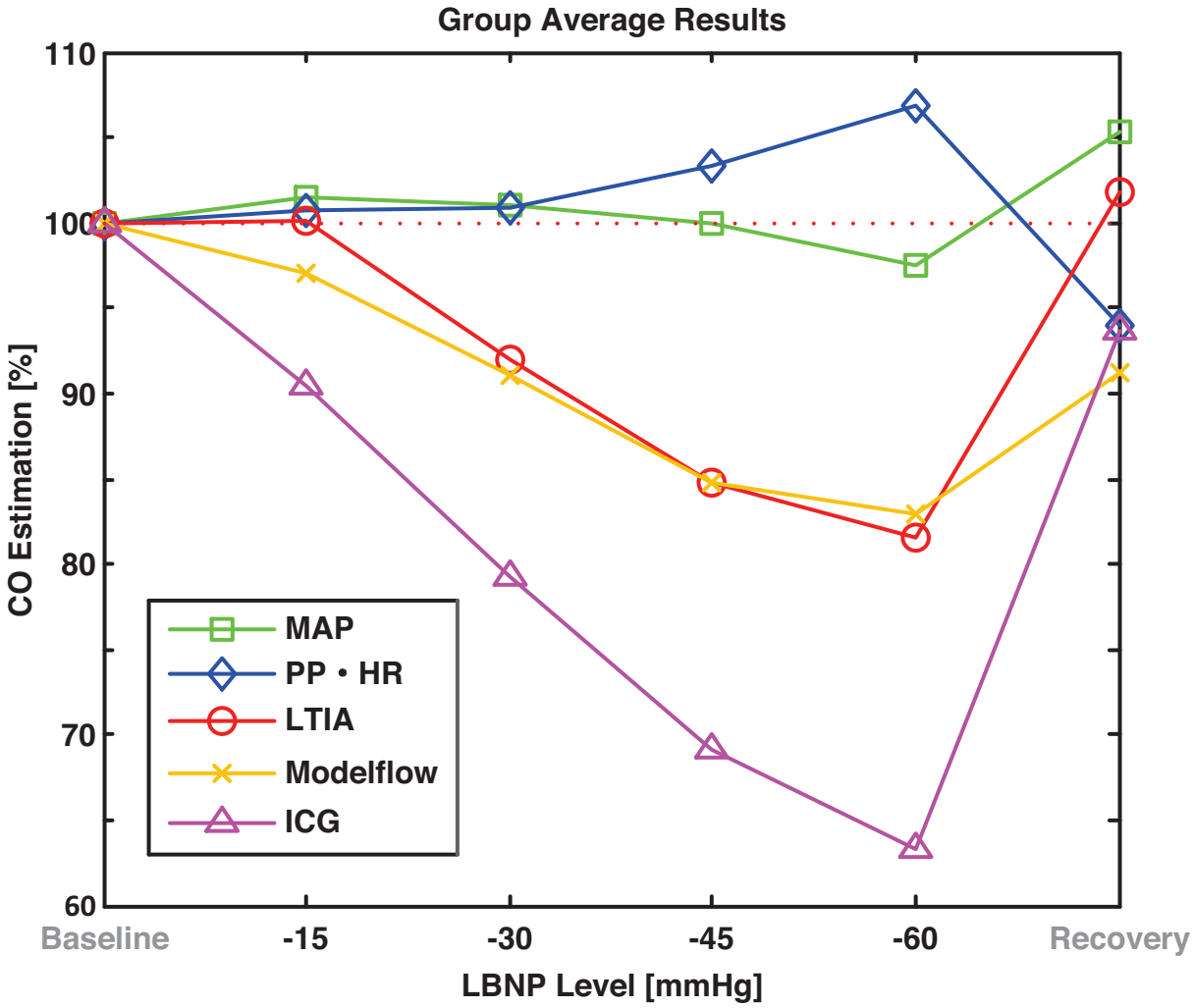

Figure 2.4: Comparison of the candidate techniques for estimating CO.

Chapter 3

PULSE TRANSIT TIME FOR CORRECTING ARTERIAL COMPLIANCE

3.1 Introduction

In the previous chapter, we investigated a technique for estimating CO from peripheral ABP waveform. The technique can overcome the problem of wave contour distortion introduced by wave reflection. The accuracy has been validated in a ICU patient study and a human LBNP study.

However, we also found that the varying AC could be a confounding factor in the estimation. Previous techniques employ empirical curves, in which AC is a averaged function of pressure. This approach ignores the patient-to-patient variation and vasomotor tone. Another potentially feasible approach for correcting AC is the introduction of PTT, which is a direct function of AC. In this study, we will investigate the efficacy of PTT in correcting AC. We first compared the most precise indicator between two transit times in terms of their capabilities in tracking with ABP. Next, we proposed a technique which can robustly estimate PTT. Further, we improved the accuracy of the LTIA in monitoring CO in an animal study and the LBNP study via PTT.

3.2 Pulse arrival time is not an adequate surrogate for pulse transit time as a marker of blood pressure

The tight relationship between pulse transit time (PTT) and arterial blood pressure (ABP) has long been known [5, 12]. The physiologic mechanisms responsible for this relationship are well understood. PTT decreases as the arterial elastic modulus increases according to the Moens-Korteweg equation [73, 83]. The arterial elastic modulus, in turn, increases as ABP increases, because collagen fibers are slack and do not apply tension until the arterial wall is stretched. While changes in vasomotor tone can also modulate the arterial elastic modulus, this effect is less of a factor in the aorta wherein smooth muscle is relatively sparse [16].

PTT can be estimated simply as the foot-to-foot time delay between proximal and distal arterial waveforms. Thus, PTT could conceivably permit continuous, non-invasive, and cuff-less ABP monitoring in the acute setting (after an initial calibration). Indeed, many researchers have pursued PTT as a marker of ABP [83].

Thomas proposed to make the measurement process even simpler by instead using the time delay between the R-wave of an ECG waveform and the distal arterial waveform foot [108]. This pulse arrival time (PAT) has captured great interest recently [1, 37, 70, 113]. PAT is equal to the sum of PTT and the pre-ejection period (PEP). However, PEP, which is determined by the ventricular electro-mechanical delay and isovolumic contraction phase, can vary with contractility and afterload while often constituting a nontrivial fraction of PTT [41, 71, 80, 89]. Thus, PAT, on the contrary, may not be an adequate surrogate for PTT as a marker of ABP.

To our knowledge, only a few researchers have compared PAT to PTT in terms of their ability to predict ABP. Steptoe et al. studied humans and concluded that PAT could be used in lieu of PTT [97]; however, for ethical reasons, the elicited ABP range was too narrow to provide a significant challenge. Ochiai et al. examined animals during several different hemodynamic interventions and drew a similar conclusion [75]; however, the comparisons were made over just a single intervention at a time and were therefore likewise less challenging. Geddes et al. investigated animals over a wide ABP range and concluded that PAT could not be used in place of PTT [39]; however, only a qualitative result from one subject was provided to justify this conclusion. Payne et al. recently performed a complex study in humans and concluded that PAT was an unreliable marker of ABP [78]; however, PTT was similarly ineffective perhaps due to artifact in the non-invasive arterial waveforms that were measured. Thus, continued efforts are needed to determine whether PAT may be used as a surrogate for PTT as a marker of ABP or not.

In this study, we compared PAT and PTT in terms of their ability to predict ABP in animals. Notable aspects of the study include: (a) estimating PAT and PTT through the aorta from high fidelity, invasive arterial waveforms; (b) inducing a wide ABP range via a broad array of hemodynamic interventions; (c) evaluating PAT and PTT across multiple interventions at a time; and (d)

Table 3.1: Subject-by-subject results and interventions.

Subject	Interventions	DBP Range [mmHg]		RMSE [mmHg]	
		MIN	MAX	1/PTT	1/PAT
1	Phenylephrine Nitroglycerin	32	138	5.8	12.4
2	Dobutamine Esmolol	51	77	6.1	6.3
3	Norepinephrine Xylazine	42	117	5.2	6.6
4	Hemorrhage Saline	42	78	3.1	3.8
5	Phenylephrine Nitroglycerin Verapamil High Rate Cardiac Pacing	40	144	5.1	11.4
6	Dobutamine Esmolol Vasopressin Low Rate Cardiac Pacing	29	106	6.5	18.0
Mean±SD	-	39±8	110±29	5.3±1.2	9.8±5.2

providing quantitative results from all subjects.

We studied experimental data collected from six anesthetized dogs under a protocol approved by the MSU All-University Committee on Animal Use and Care. The materials and methods for data collection are described in detail elsewhere [104]. Briefly, the data included ABP waveforms from the ascending aorta and femoral artery via micromanometer-tipped catheters and ECG waveforms, all at sampling rates of 500 Hz. For each subject, the data were obtained during a baseline period and two to four hemodynamic interventions out of a set of 12 different interventions (Table 3.1).

We estimated PAT and PTT using the standard methods [72, 75, 83]. These methods approximate the time delays from the feet of the ABP waveforms wherein wave reflection interference is

minimal. More specifically, first, we automatically detected each foot of the ABP waveforms as the intersection of a line tangent to the initial systolic rise and a horizontal line through the minimum point [20]. This automatic foot detection method was most effective amongst a set of conventional methods (e.g., peak of the derivative) [20]. Then, we visually examined many of the resulting foot detections and, in effect, manually corrected most, if not all, of the misdetections. Finally, we estimated PAT for each beat as the time delay between the ECG R-wave and the subsequent femoral artery ABP foot and PTT for each beat as the time delay between the ascending aortic ABP foot and the ensuing femoral artery ABP foot.

We evaluated the beat-to-beat PAT and PTT estimates in terms of their ability to track beat-to-beat ABP changes. (Note that averaging these quantities over multiple beats did not materially improve the results.) Figure 3.1 illustrates our evaluation procedure per subject. First, we determined diastolic ABP (DBP), mean ABP (MBP), and systolic ABP (SBP) for each beat of the femoral artery ABP waveforms.

Second, we calibrated each of the time delays to each of the ABP parameters using all of the time delay estimates and ABP parameter measurements of the subject. That is, we found the line that best fits these data and then mapped each time delay through the best fit line so as to predict the ABP parameter. Third, we computed the root-mean-squared-error (RMSE = $\sqrt{\mu^2 + \sigma^2}$, where μ and σ are the mean (bias) and standard deviation (precision) of the errors) between the predicted and measured ABP parameters. Then, because velocity often shows better linear correlation to ABP than time delay [39, 96], we repeated this procedure for 1/PAT and 1/PTT. Finally, while we focused on linear correlations, we also explored the effects of fitting curves instead of lines.

We statistically compared the ABP tracking ability of the time delays and their reciprocals. We employed straightforward one-way repeated measures ANOVA to compare the subject average RMSE values after log transformation (for more normally distributed data). When this test yielded $p < 0.05$, we performed multiple pairwise comparisons using the Student-Newman-Keuls post hoc test.

Table 3.2 summarizes the subject average results. The range of each ABP parameter was

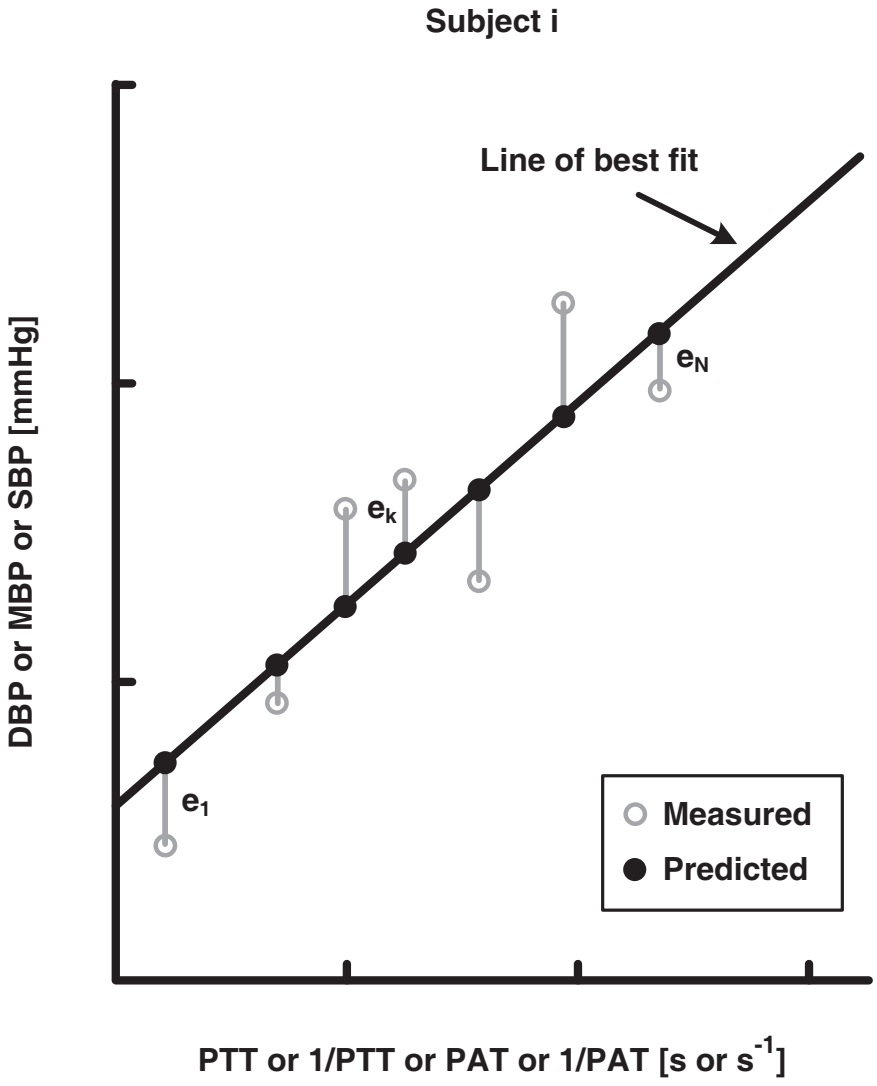

$$\text{RMSE} = \sqrt{\frac{\sum_{k=1}^{N} e_k^2}{N}}$$

Figure 3.1: Procedure for evaluating pulse arrival time (PAT) and pulse transit time (PTT) in terms of their ability to predict arterial blood pressure (ABP) parameters within a subject.

Table 3.2: Subject average results.

	DBP		MBP		SBP	
Range [mmHg]	MIN	MAX	MIN	MAX	MIN	MAX
	39±8	110±29	52±6	138±32	70±9	192±38
RMSE [mmHg]						
PTT	6.5±2.1		6.0±2.3		8.2±2.4++	
1/PTT	5.3±1.2		4.8±1.0		7.5±2.2+	
PAT	10.5±5.4*		1.2±5.7**		13.1±6.1*	
1/PAT	9.8±5.2*		10.4±5.6**		11.9±6.1*	

wide, with SBP varying the most and DBP changing the least. For each ABP parameter, 1/PTT and 1/PAT yielded a lower RMSE value than their non-reciprocal counterparts. However, none of these differences was significant. For PTT and 1/PTT, the DBP and MBP RMSE values were significantly lower than the SBP RMSE value by 1.7 to 2.7 mmHg. For PAT and 1/PAT, the three RMSE values were not significantly different. For each ABP parameter, the RMSE values for PAT and 1/PAT were significantly higher than those for PTT and 1/PTT. The hike in RMSE obtained via PAT over PTT and via 1/PAT over 1/PTT ranged from 4.0 to 5.6 mmHg. The DBP RMSE value for 1/PAT, which was the lowest RMSE value attained via PAT, was 9.8±5.2 mmHg, whereas the corresponding value for 1/PTT was 5.3±1.2 mmHg.

Table 3.1 shows the DBP RMSE values for 1/PTT and 1/PAT as well as the interventions employed for each subject, while Figure 3.7 visually illustrates the correlation between DBP and the reciprocal of the time delays per subject. For each subject, 1/PAT was less effective in tracking DBP changes than 1/PTT. However, the extent of the difference was quite variable because of the intervention disparities. For subject 1, phenylephrine and nitroglycerin were infused. Figure 3.3 illustrates that the vasoconstrictor caused PTT to decrease due to the ABP increase and PEP to increase due to the afterload increase. These opposite direction variations blunted the change in PAT. Thus, the RMSE value for 1/PAT was over twice as large as for 1/PTT. For subjects 5 and 6, twice as many interventions were used compared to the other subjects. PEP was therefore more variable, and, as a result, the RMSE values for 1/PAT were again over twice as large as for 1/PTT. By contrast, for subjects 2 and 4, the DBP ranges were much narrower and thus constituted less of

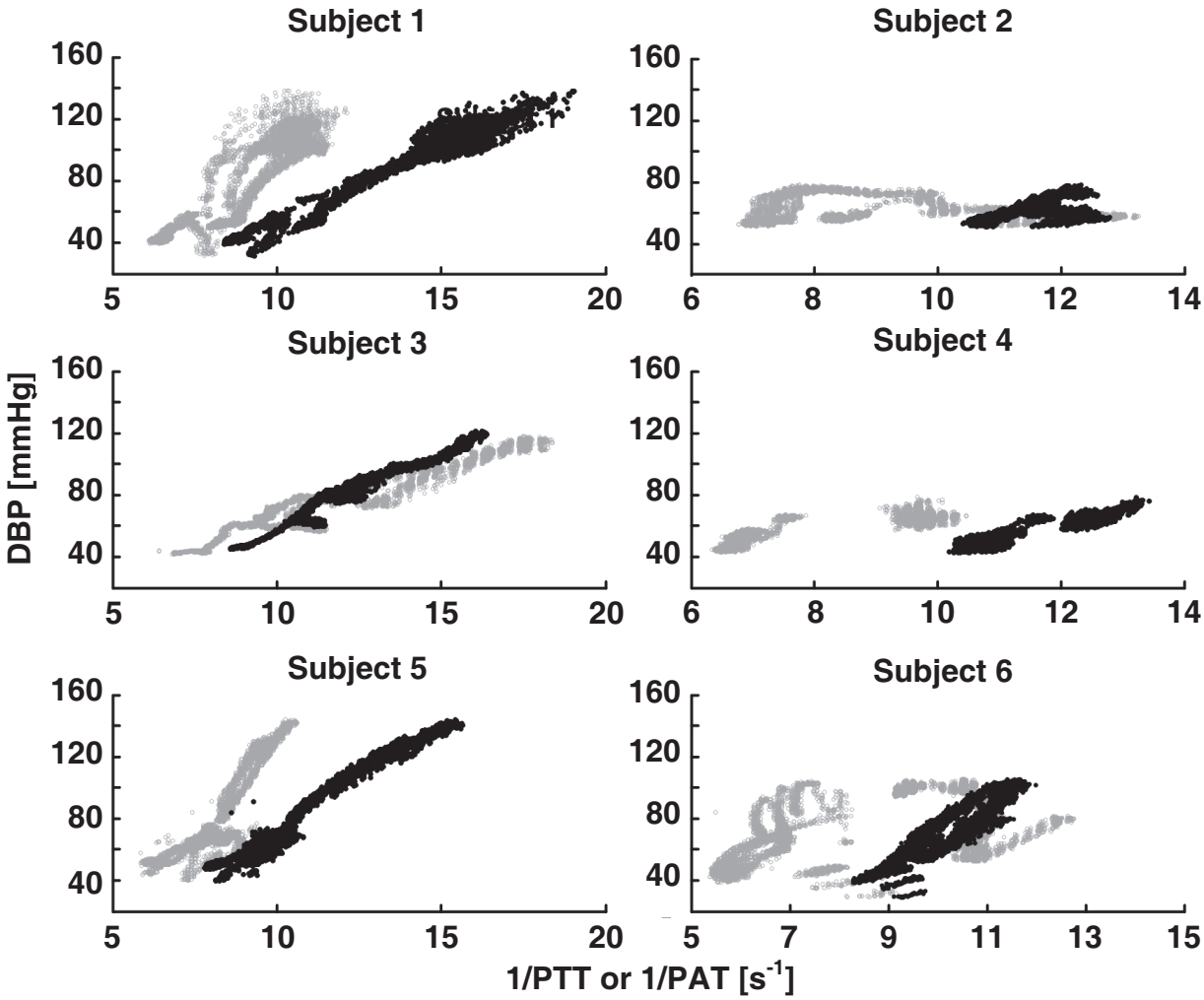

Figure 3.2: Plots of beat-to-beat DBP versus beat-to-beat 1/PTT (black, closed circles) and 1/PAT (gray, open circles) in each subject.

a challenge. Consequently, the RMSE values for 1/PAT were not that much higher than for 1/PTT. For subject 3, norepinephrine and xylazine were infused. These interventions caused PEP and PTT to change in the same direction. For example, norepinephrine caused PTT to decrease because of the increase in ABP and PEP to decrease as the enhancement in cardiac contractility evidently dominated the increase in afterload. Thus, the RMSE value for 1/PAT was again not considerably greater than for 1/PTT.

Figure 3.4 illustrates the trends in DBP, 1/PAT, and 1/PTT from subject 6. In this subject, 1/PAT was far less effective than 1/PTT in tracking the direction of changes in DBP. However, note

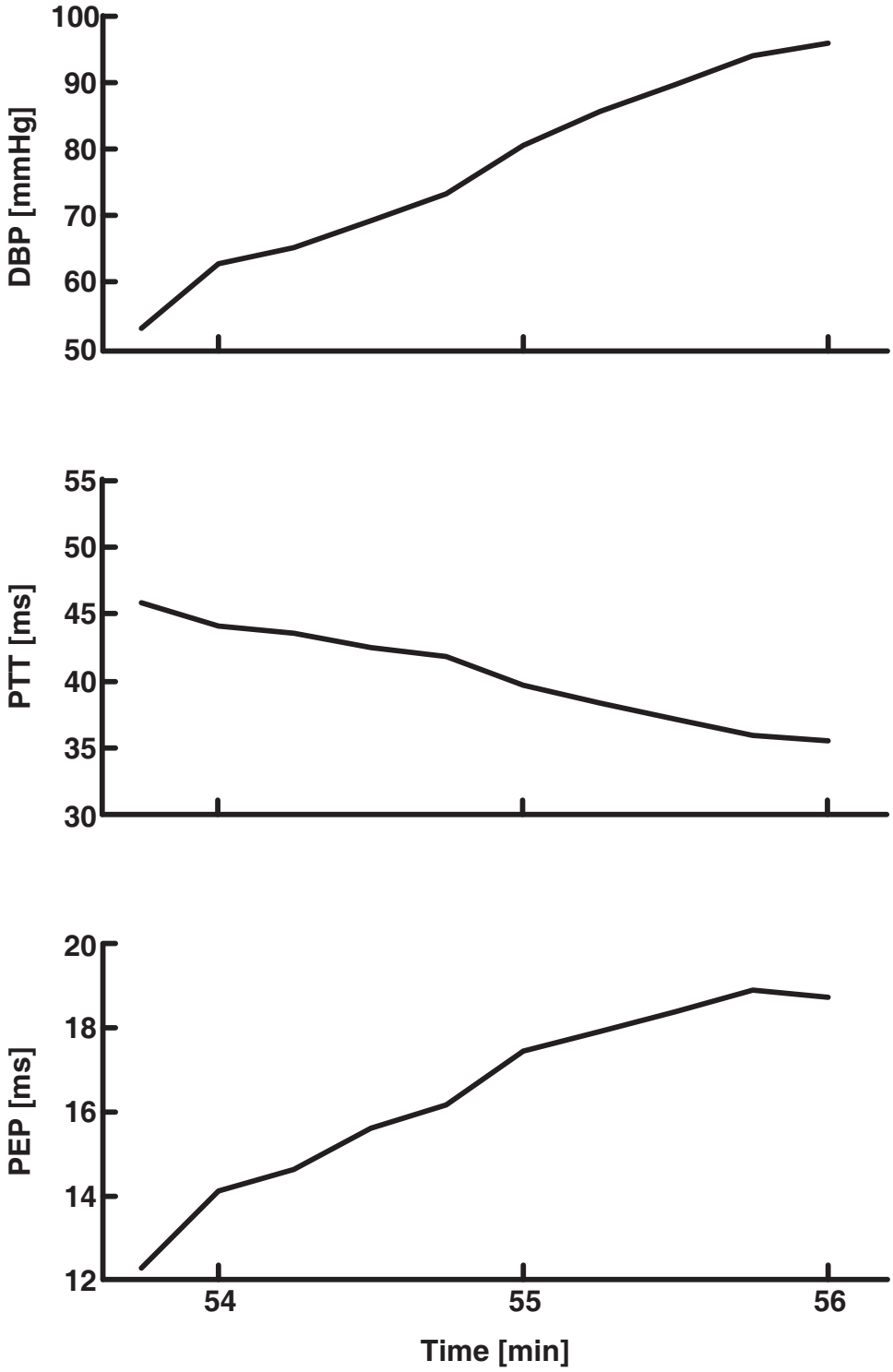

Figure 3.3: Sample trends in DBP, PTT, and the pre-ejection period (PEP) from subject 1 during phenylephrine infusion.

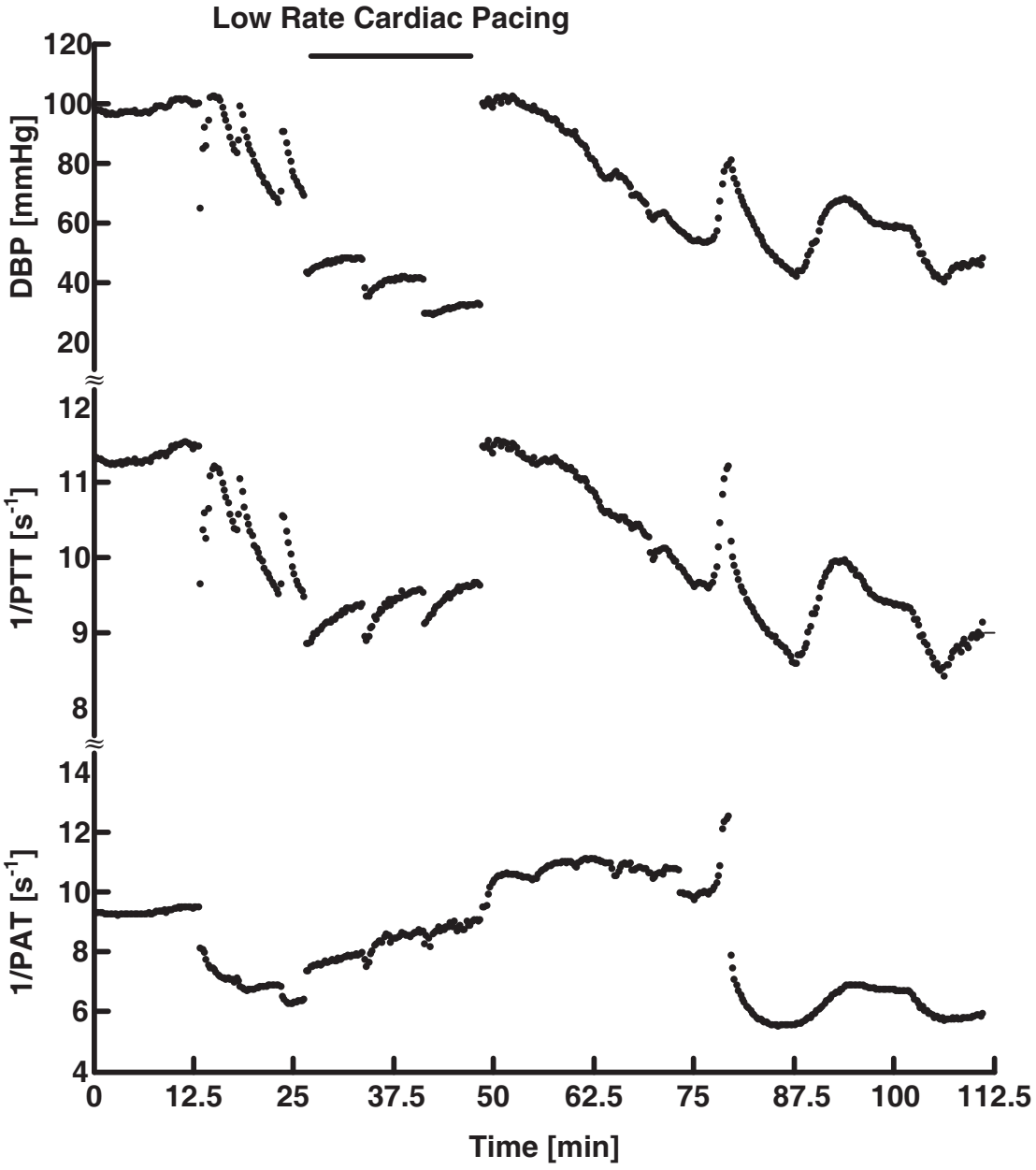

Figure 3.4: Sample trends in DBP, 1/PTT, and 1/PAT from subject 6

that even 1/PTT was ineffective during low rate cardiac pacing. During this intervention, 1/PTT predicted an increase in DBP, but DBP actually fell. In the remaining five subjects, 1/PAT and 1/PTT performed similarly in terms of following directional DBP changes.

In this study, we estimated PAT and PTT through the aorta using high fidelity, invasive arterial waveforms obtained during multiple hemodynamic interventions in each of six animals that induced wide ABP changes on average. We compared these time delays and their reciprocals in terms of their linear correlation with DBP, MBP, and SBP per animal. In contrast to similar studies in the past, our results quantitatively indicate that PAT is not an adequate surrogate for PTT in terms of detecting challenging ABP changes.

Taking the reciprocals of the time delays tended to improve their ability to track ABP. This result is consistent with previous studies that have shown that velocity, rather than time delay, exhibits an excellent linear relationship with ABP over a wide range [39, 96]. To confirm, we employed quadratic and cubic polynomials instead of lines to fit the data [38, 68]. We indeed found that the polynomial fitting tended to reduce the RMSE values much more for the time delays than for their reciprocals. For example, for cubic polynomial fitting, the DBP RMSE values for PTT and 1/PTT were both 4.7 mmHg on average. So, the reciprocals of the time delays were essentially linearly related to the ABP parameters. The use of reciprocals may therefore offer greater simplicity for ABP calibration.

PTT and its reciprocal predicted DBP and MBP significantly better than SBP. These results are consistent with previous experimental studies [74, 114] and theory. That is, PTT should be able predict DBP the best, because it is estimated from the waveform feet. Further, PTT should also be able to predict MBP but not SBP, as only the former generally shows strong correlation with DBP. The difference in the DBP/MBP and SBP RMSE values was 2.2 mmHg on average. This difference can actually be more substantial. For example, we recently showed that the difference in the DBP and SBP RMSE values for 1/PTT was about 4.5 mmHg in conscious humans subjected to lower body negative pressure [114]. On the other hand, PAT and its reciprocal did not predict any of the ABP parameters significantly better than the others. These results are in contrast to theory,

which predicts that PAT should be able to predict DBP and MBP better than SBP for the same reasons as PTT, and previous experimental studies, which have paradoxically shown that PAT is most effective in predicting SBP [73, 96]. Thus, PEP is a confounding factor.

PAT and its reciprocal were significantly inferior to PTT and its reciprocal in tracking all ABP parameters. The RMSE values for PAT and 1/PAT ranged from 9.8 to 13.1 mmHg on average, whereas the corresponding values for PTT and 1/PTT varied from 4.8 to 8.2 mmHg. Further, the RMSE values for PAT and 1/PAT were, on average, $78\pm23\%$ higher than their PTT counterparts. Thus, tracking ABP via PAT was not only markedly worse than via PTT but also unable to meet the FDA bias and precision error limits of 5 and 8 mmHg. These results are congruent with the conclusion of Geddes et al. that PAT cannot be used in place of PTT [39].

For each subject, 1/PAT always tracked DBP less effectively than 1/PTT. However, the extent of the RMSE difference was quite variable and depended on the nature of the ABP changes elicited in the subject. For example, consistent with the results of Steptoe et al. [97], this difference was modest when the ABP range was narrow. In general, the difference increased with the magnitude of ABP change, degree of vasoconstriction, and number of interventions. Thus, in essence, the adequacy of PAT as a surrogate for PTT diminished as the ABP changes became more challenging.

In one subject, 1/PAT was also strikingly less effective than 1/PTT in tracking the direction of the ABP changes. However, in the same subject, even 1/PTT was not useful in this capacity during low rate cardiac pacing. As heart rate fell, 1/PTT increased even though ABP declined. Indeed, the foot-to-foot detection technique can increasingly underestimate PTT with decreasing heart rate, because the extent of constructive interference of the reflected wave with the forward wave increases [73]. Although the FDA only considers the error of ABP measurement devices, the omission of a rigorous assessment of the time delays and their reciprocals in terms of their ability to track dynamic ABP changes does constitute a study limitation.

We were able to accurately locate the waveform feet for PAT and PTT estimation by manual detection of invasive arterial waveforms with little artifact. However, in practice, the time delays would be estimated by automatic detection of the feet of non-invasive arterial waveforms with

nontrivial artifact. Thus, waveform foot misdetections are actually inevitable. Since accurate, automatic detection of the R-wave is feasible even when the ECG waveform is buried in artifact, PAT is less susceptible to misdetections. Thus, as indicated by the results of Payne et al. [78], the difference in tracking ABP via PAT and PTT may be closer in practice. However, ABP tracking via both time delays would obviously become worse with misdetections.

We tested the ABP predicted via PAT and PTT against the same measured ABP that was utilized to calibrate these time delays to ABP. In practice, a ABP calibration curve would first be constructed from simultaneous measurements of the time delays and peripheral ABP during a hemodynamic perturbation and then future peripheral ABP values would be predicted from only measurements of the time delay using the ABP calibration curve. Thus, we effectively employed the optimal ABP calibration curves for both PAT and PTT to reveal (and fairly compare) their best case results. A realistic, sub-optimal ABP calibration curve would certainly further degrade the ABP tracking ability of either time delay in practice.

In this study, PAT yielded ABP errors that were about 80% larger than those of PTT. Further, in contrast to PTT, the ABP errors of PAT exceeded the FDA ABP bias and precision error limits of 5 and 8 mmHg. Thus, PAT was not an adequate surrogate for PTT as a marker of ABP despite the ideal circumstances of this study. Since significant, additional error will result in practice, further pursuit of PAT for continuous, non-invasive, and cuff-less ABP monitoring may not be fruitful. However, further studies comparing PAT to PTT are still needed to draw an irrefutable conclusion. Other useful future research directions include the development of simpler sensors for measuring proximal arterial waveforms, convenient, patient-specific ABP calibration curves, techniques for artifact-robust estimation of the true PTT in the absence of wave reflection, and techniques for more accurately tracking SBP via PTT.

3.3 Improved pulse transit time estimation by system identification analysis of proximal and distal arterial waveforms

3.3.1 Introduction

According to the Moens-Korteweg equation, pulse wave velocity (PWV) increases as the arteries stiffen. Indeed, PWV is the most popular index of arterial stiffness because of the ease of its measurement and its proven independent value in predicting cardiovascular events and mortality in hypertensive patients [8, 53, 60]. In addition, because arterial stiffness increases with arterial blood pressure (ABP), PWV and ABP often show positive correlation, suggesting that PWV could provide a means to achieve continuous, noninvasive, and cuffless ABP monitoring [83].

Conventionally, PWV is determined from the distance and pulse transit time (PTT) between proximal and distal arterial sites [10]. PTT is, in turn, estimated by acquiring arterial waveforms from the two sites and then detecting the foot-to-foot time delay between the waveforms. The premise is that the foot of the proximal waveform represents a time before the return of the reflected wave to its measurement site. However, wave reflection may not always be negligible at the proximal waveform foot. Just as important, it is often difficult to detect the waveform feet reliably because of motion and other artifact [65]. Thus, the foot-to-foot detection technique can yield inaccurate PTT estimates. Compounding matters, ABP changes perturb PWV relatively little [83]. Thus, typical plots of ABP vs. PWV show significant vertical scatter about the line of best fit [83]. This scatter limits the ability of PWV to track ABP.

Several investigators have aimed to improve PTT estimation by more sophisticated analysis of proximal and distal arterial waveforms. Sola et al. [96] applied parametric modeling to the systolic upstrokes of the waveforms to identify their feet more reliably. Pruett et al. [83] computed an average of multiple time delays taken from the early systolic samples of two ABP waveforms to establish PTT estimates that were able to reduce the scatter in ABP vs. PWV plots. While their idea of mitigating PTT error by using more than one pair of samples of the waveforms is interesting, wave reflection becomes a greater factor as the cardiac cycle progresses. This technique is also

restricted to ABP and flow waveforms. Latson et al. applied nonparametric system identification to estimate the impulse response (time domain version of the transfer function) relating a proximal ABP waveform (input) to a distal ABP waveform (output) and then estimated PTT as its time delay [52]. Their intriguing idea was that, since the impulse response represents the distal ABP response to a very narrow pulse applied to proximal ABP at time 0, this PTT estimate should not be corrupted by wave reflection. However, neither Latson et al. nor an ensuing group who reproduced their technique [66] showed that it actually improved PTT estimation. Furthermore, this approach is applicable to arbitrary arterial waveforms (rather than being limited to ABP waveforms) and should afford great robustness to artifact, since PTT is determined from all pairs of waveform samples. However, these latter ideas may have not been noted until now.

We investigated the system identification approach for PTT estimation. We specifically applied a robust parametric system identification technique to an impedance cardiography (ICG) waveform (the proximal input) and a noninvasive peripheral ABP waveform (the distal output) recorded from humans subjected to progressive reductions in central blood volume using a lower-body negative pressure (LBNP) protocol. Because it is difficult to independently measure the true PTT in the absence of wave reflection, we assessed the technique in terms of the ability of its (proportional) PWV estimates to track ABP changes. Our results show that the technique greatly reduced the scatter in ABP vs. PWV plots compared with conventional foot-to-foot detection techniques. A preliminary version of this study has been reported in abbreviated form [115].

3.3.2 Materials and methods

3.3.2.1 Physiological data

Existing, de-identified physiological data from humans subjected to a LBNP protocol were analyzed. The data collection procedures were approved by the Institutional Review Board of the Brooke Army Medical Center (Fort Sam Houston, TX) and are described in detail in several recent publications [23, 87]. Briefly, fit and typically young subjects that showed no signs of cardiovascu-

lar abnormalities (e.g., hypertension, hypotension, autonomic nervous dysfunction) and were not pregnant or taking any medications known to alter autonomic nervous function were studied.

The subjects were instrumented for measurement of various physiological data, including noninvasive stroke volume estimates via ICG, a noninvasive peripheral ABP waveform via finger-cuff photoplethysmography, and an ECG waveform. Subjects were positioned supine in a LBNP chamber. The data were then recorded at a sampling rate of 500 Hz during 1) a 5-min baseline period; 2) 5-min chamber decompression at -15, -30, -45, and -60 mmHg each; 3) additional increments of -10 mmHg for 5 min until the onset of hemodynamic decompensation [as indicated by presyncopal symptoms, sudden fall in ABP or heart rate (HR), systolic pressure (SP) < 80 mmHg, or at the subject's request]; and 4) a 10-min recovery period.

For this study, 15-s steady segments of data during the baseline period, each distinct LBNP period, and the recovery period were extracted. Because PWV estimates would be assessed in terms of their ability to track ABP changes, appreciable changes in ABP within a subject were needed for the assessment to be challenging and useful. Thus, data from subjects with more modest diastolic pressure (DP) changes (maximum average DP over the periods minus the minimum average DP over the periods < 20 mmHg) were excluded. Data from 15 of 66 available subjects (nine males and six females; age 31 $\pm$ 8 yr; height 173 $\pm$ 12 cm; weight 76 $\pm$ 15 kg) remained for analysis.

3.3.2.2 PTT estimation

PTT was estimated by applying conventional foot-to-foot detection techniques to the simultaneous pairs of the 15-s segments of the differentiated ICG waveform (a proximal arterial waveform that is specifically related to thoracic flow) or the ECG waveform (a commonly proposed surrogate for the proximal arterial waveform) and the peripheral ABP waveform (a distal arterial waveform). PTT was then estimated by applying a parametric system identification technique to the same pairs of ICG and peripheral ABP waveform segments.

3.3.2.3 Conventional foot-to-foot detection techniques

Figure 3.5 shows the conventional foot-to-foot detection techniques. First, the waveform feet were detected as the R waves for the ECG waveform, the standard B points for the ICG waveform (i.e., the time of zero derivative before the peak), and the minima for the peripheral ABP waveform (i.e., DP). These foot detection techniques yielded the best results among a set of conventional techniques [20] and are thus referred to as optimized henceforth. Next, the time delays between each R wave and subsequent DP (T_{d1}) and between each B point and ensuing DP (T_{d2}) were determined. Finally, the time delays were averaged over the 15-s waveform segments to reduce noise in the PTT estimates.

3.3.2.4 Parametric system identification technique

Figure 3.6 shows the parametric system identification technique. The differentiated ICG waveform was considered to be the input $x(t)$ to a system while the peripheral ABP waveform $y(t)$ was regarded as the resulting output. The system was identified by finding its impulse response $h(t)$, which when convolved with $x(t)$, optimally fitted $y(t)$. The time delay of $h(t)$ (T_{d3}) was then detected as the estimate of PTT. This estimate may be viewed as the time delay for a very narrow pulse of thoracic flow to reach the peripheral ABP measurement site or the time delay between the entire ICG and peripheral ABP waveforms after equalizing their shapes. Mathematical details are provided immediately below.

The impulse response $h(t)$ was estimated as per the following autoregressive exogenous input structure:

$$y(t) = \sum_{k=1}^{n} a_k y(t-k) + \sum_{k=0}^{m} b_k x(t-k) + e(t). \tag{3.1}$$

where a_k and b_k are sets of unknown parameters that define $h(t)$, n and m denote the number of parameters in the sets, and $e(t)$ is the unmeasured residual error [58]. The term n had little effect on the results and was arbitrarily fixed to five, whereas the term m should scale with PTT

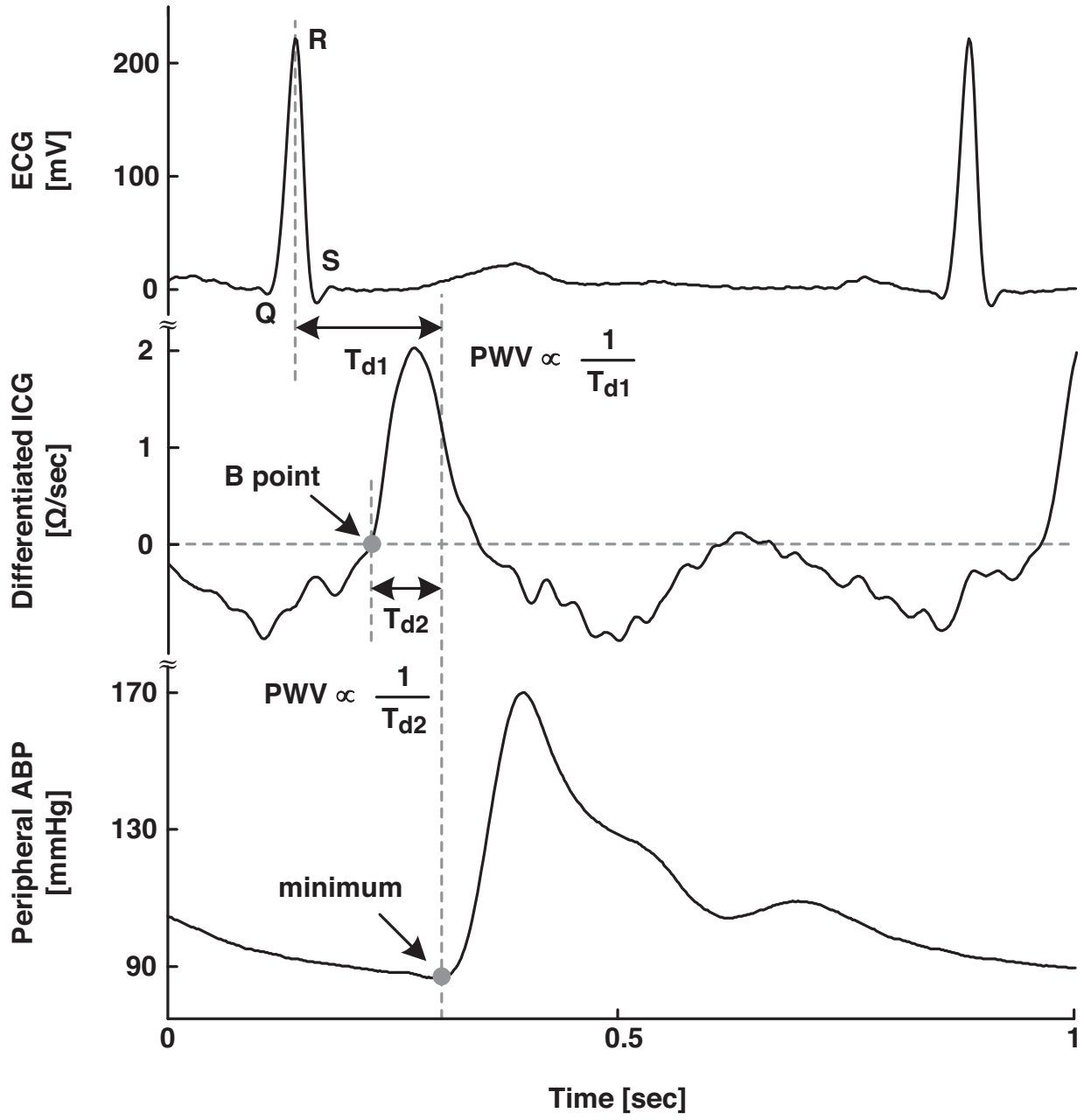

Figure 3.5: Optimized conventional foot-to-foot detection techniques for estimating pulse transit time (PTT) from either an ECG or impedance cardiography (ICG) waveform (a proximal waveform) and a simultaneous noninvasive peripheral arterial blood pressure (ABP) waveform (a distal waveform) [the time delays between each R wave and subsequent DP (T_{d1}) and between each B point and ensuing DP (T_{d2})].

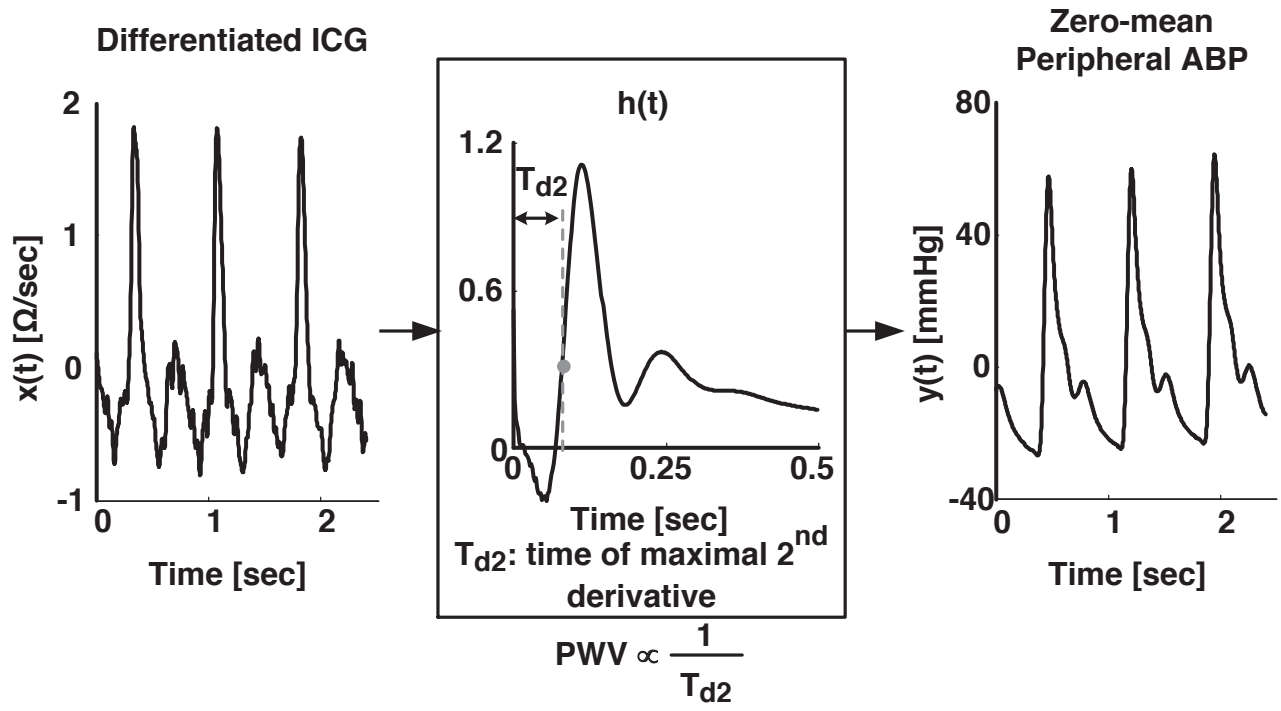

Figure 3.6: Parametric system identification technique for estimating PTT from simultaneous ICG and noninvasive peripheral ABP waveforms.

and was simply set to T_{d2} times the sampling rate. The parameters were then estimated from the 15-s segments of $x(t)$ and zero-mean $y(t)$ by linear least-squares minimization of $e(t)$ [58]. The time delay T_{d3} was thereafter determined as the time of the maximal second derivative of $h(t)$ between its first zero-crossover with positive derivative and its peak. This time, which denotes when the slope of $h(t)$ is changing most during its rise to the peak, provided a good marker of the foot location of $h(t)$ [20]. [Determining T_{d3} as the first zero-crossover with positive derivative, which indicates when $h(t)$ first becomes positive as it rises to the peak, yielded similar results.]

3.3.2.5 PTT assessment and comparison

The PTT estimates of each technique were assessed based on their ability to track the average DP of the analyzed peripheral ABP waveform segments in each subject. Figure 3.1 shows the PTT assessment procedure. First, since PWV generally shows better linear correlation to DP than PTT, the reciprocals of the PTT estimates were first taken to arrive at proportional PWV estimates per

subject. (Note that the proportionality constant, which represents the distance between the proximal and distal arterial sites, was not needed here.) Next, two quantitative metrics were computed. One metric was the standard correlation coefficient (r) between the proportional PWV estimates and measured DP. The other metric was the root mean squared error (RMSE) between the DP predicted by mapping the proportional PWV estimates through the line of best fit established from the correlation analysis and the measured DP.

The PTT estimates of the techniques were then statistically compared. Straightforward one-way repeated-measures ANOVA was specifically employed to compare the subject average r values and log-transformed RMSE values of the three techniques. Because both of these tests revealed $P < 0.05$, multiple pairwise comparisons between all techniques were then performed using the Student-Newman-Keuls post hoc test.

3.3.3 Results

Figure 3.7 shows sample plots of measured DP vs. the proportional PWV estimated by each technique from subjects 15 and 12. In subject 15, the parametric system identification technique noticeably reduced the scatter about the line of best fit compared with the conventional foot-to-foot detection techniques, especially with the ECG waveform substituted for the ICG waveform. In subject 12, the conventional techniques produced proportional PWV estimates that showed non-physiological, negative correlation with DP, whereas the system identification technique yielded estimates that revealed the expected positive correlation.

Figure 3.8 shows plots of the DP predicted by each technique vs. measured DP from all 15 subjects and the corresponding overall RMSE values (i.e., the root mean square of the errors pooled together from all of the subjects). The system identification technique showed better predictions than both of the conventional techniques. Table 3.3 shows the DP range and r and RMSE values of each technique per subject. The average r and RMSE values of the system identification technique were 0.81 ± 0.16 and 4.3 ± 1.3 mmHg. For comparison, the corresponding values were 0.59 ± 0.37 ($P < 0.05$) and 5.9 ± 2.5 ($P < 0.01$) mmHg for the conventional technique applied to the same

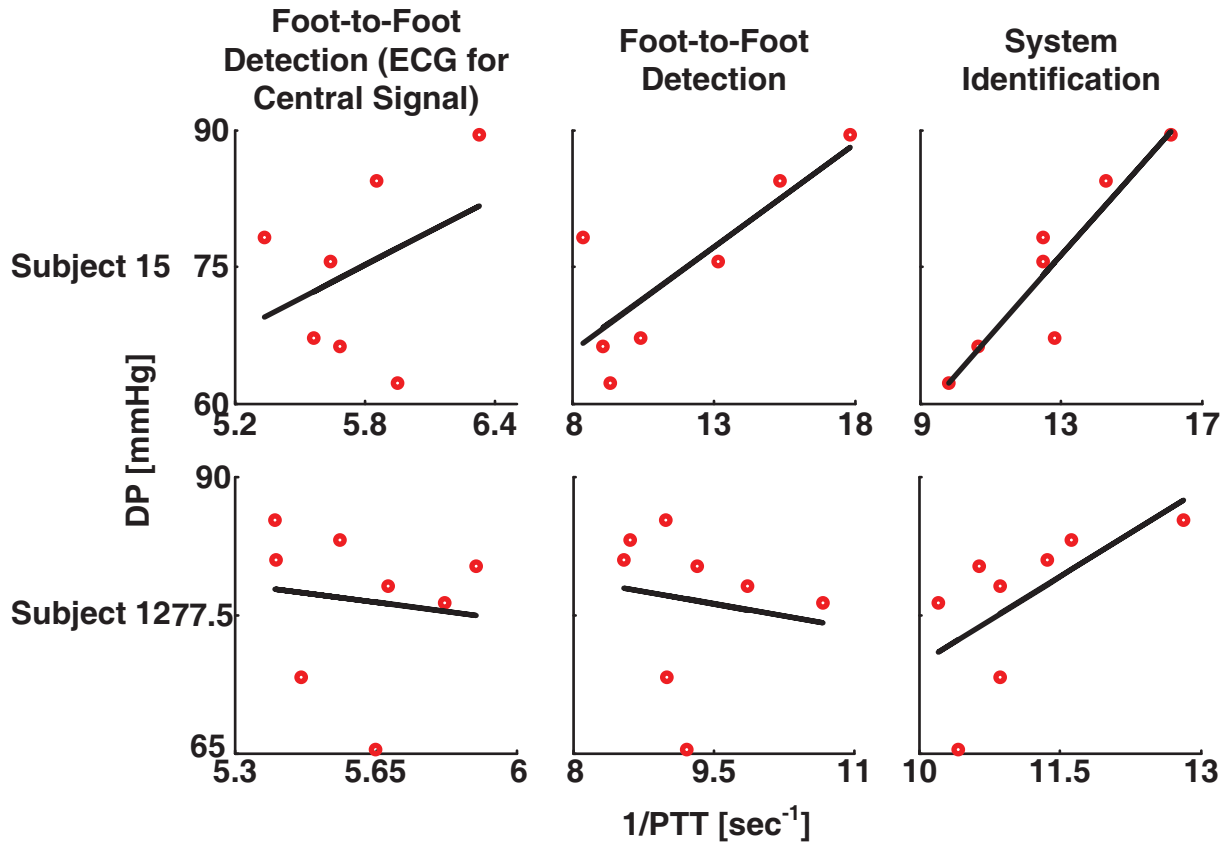

Figure 3.7: Plots of measured DP vs. the proportional PWV estimated by each technique from subjects 15 and 12.

waveforms and 0.28 $\pm$ 0.40 (P < 0.001) and 7.2 $\pm$ 1.8 (P < 0.001) mmHg for the conventional technique with the ECG waveform substituted for the ICG waveform. [Although not indicated in Table 1, the r and RMSE values of the two conventional techniques were also statistically different (P < 0.05).] Furthermore, of the 15 *r* values corresponding to each subject, only 3 were < 0.80 for the system identification technique compared with 8 and 15 for the conventional techniques.

3.3.4 Discussion

In summary, PWV is a useful marker of arterial stiffness and may permit continuous, noninvasive, and cuffless ABP monitoring. Conventionally, PWV is determined as the ratio of the distance and PTT between proximal and distal arterial sites. PTT is, in turn, estimated by detecting the foot-to-foot time delay between waveforms measured at the two arterial sites of interest. However, this

Table 3.3: Results of each pulse transit time estimation technique per subject.

Subject	DP Range	System Identification (PTT = T_{d3})		Conventional Detection (PTT = T_{d2})		Conventional Detection (PTT = T_{d1})	
		r	RMSE	r	RMSE	r	RMSE
1	75-101	0.55	6.8	0.39	7.5	0.33	7.7
2	97-121	0.96	2.7	0.91	3.8	0.53	7.8
3	71-99	0.85	4.2	0.86	4.2	0.63	6.3
4	95-116	0.85	4.0	0.88	3.6	0.46	6.8
5	88-130	0.95	4.8	0.66	11.8	0.76	10.1
6	64-86	0.92	2.4	0.86	3.1	0.47	5.3
7	69-100	0.84	5.9	0.18	10.8	0.20	10.7
8	54-75	0.83	3.6	0.81	3.8	0.36	6.1
9	64-85	0.38	6.5	0.61	5.6	-0.89	3.2
10	65-91	0.85	4.5	0.85	4.5	0.29	8.2
11	72-95	0.91	3.3	0.71	5.4	0.35	7.2
12	65-86	0.63	5.0	-0.15	6.4	-0.13	6.4
13	50-71	0.82	3.9	-0.23	6.6	-0.12	6.8
14	62-83	0.91	3.4	0.69	5.9	0.49	7.1
15	62-89	0.92	3.7	0.81	5.5	0.39	8.6
Average	70-95	0.81 ± 0.16	4.3 ± 1.3	0.59 ± 0.37	5.9 ± 2.5	0.28 ± 0.40	7.2 ± 1.8

technique can provide inaccurate PTT estimates because of wave reflection interference and wave-

Fig. 2. Parametric system identification technique for estimating PTT from simultaneous ICG and noninvasive peripheral ABP waveforms. First, the former waveform is regarded as an input $x(t)$ to a system while the latter waveform is considered to be the resulting output $y(t)$. Next, the system is identified by finding a parametric impulse response $h(t)$ (see equation in MATERIALS AND METHODS) that, when convolved with x(t), optimally fits y(t). Finally, the time delay (T_{d3}) of $h(t)$ is detected as the time of its maximal second derivative so as to yield as an estimate of PTT. Fig. 3. Procedure for evaluating the PTT estimates of the techniques in terms of their ability to track diastolic pressure (DP) within a subject. Note that 1/PTT here is simply proportional to pulse wave velocity (PWV). RMSE is the root mean squared error. form artifact. The system identification approach for estimating PTT potentially provides a means to overcome both of these limitations while being applicable to arbitrary types of arterial waveforms. We applied a parametric system

identification technique to noninvasive ICG and peripheral (finger) ABP waveforms measured from healthy humans during progressive LBNP. The resulting PTT estimates correlated with ABP much better than those of optimized conventional techniques. To our knowledge, these results are the first to demonstrate that the system identification approach can indeed improve PTT estimation.

3.3.4.1 System identification approach for PTT estimation

The system identification approach for PTT estimation is employed as follows. First, proximal and distal arterial waveforms are measured and respectively regarded as the input and output of a system. Next, the system impulse response is identified from the measured input and output. Finally, the time delay of the impulse response is detected as an estimate of PTT. This approach is similar in concept to previous techniques for estimating PTT that have experimentally eliminated the reflected wave by applying a transient perturbation to a proximal arterial site and then measuring the time delay for the response to occur at a distal arterial site [2, 50]. However, the obvious advantage of the system identification approach is that no experimental perturbation is needed. The system identification approach should also afford significant advantages over conventional foot-to-foot detection techniques and other previous techniques for estimating PTT without a perturbation. First, this approach effectively determines PTT from all pairs of samples of the waveforms, rather than just one pair or a few pairs, by mathematically eliminating the reflected wave or, more generally, equalizing the waveform shapes. In this way, the approach should be robust to waveform artifact while revealing the true PTT in the absence of wave reflection. The approach is therefore intended to improve the accuracy of PTT estimation rather than to make the PTT measurement process more convenient as others have proposed via an ECG or otherwise [85]. Second, the system identification approach is applicable to arbitrary types of arterial waveforms, including those indicative of ABP, flow, and volume, instead of being restricted to certain types of waveforms [83]. For example, the waveforms could be acquired with tonometry, ultrasound, ballistocardiography (proximal only), electrical impedance, pulse oximetry, and even noncontact laser Doppler vibrometry [29]. The disadvantage of the approach is that it may not be able to estimate PTT on a beat-to-beat basis,

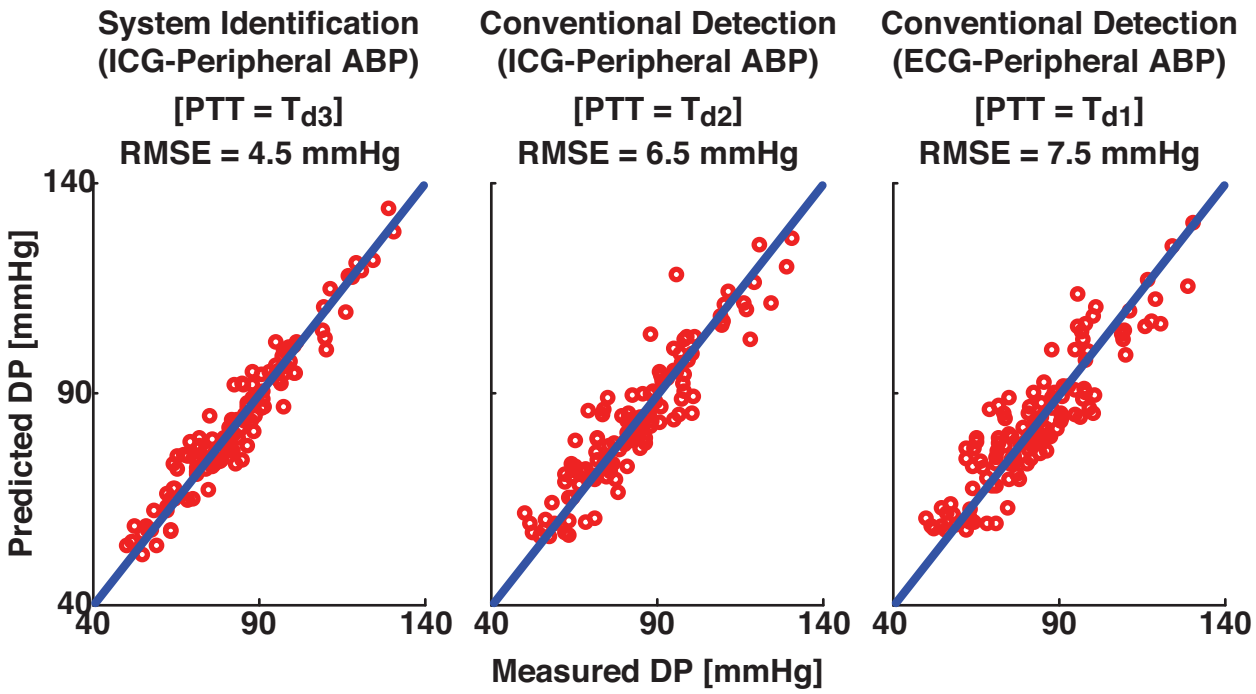

Figure 3.8: Plots of the DP predicted from the proportional PWV estimates of each technique vs. measured DP from all 15 subjects.

since longer waveform segments are typically needed to reliably identify the impulse response.

3.3.4.2 Evaluation approach and limitations

Ideally, we would have evaluated the parametric system identification technique against reference measurements of PTT. However, these measurements are not simple to make. We therefore evaluated the technique in terms of the ability of its proportional PWV estimates to track changes in ABP induced by progressive LBNP. Note that the approach of evaluating PWV estimates in terms of their ability to track ABP changes is not new and originates from many studies that have shown a tight, acute relationship between PWV and ABP [39, 83].

However, we acknowledge that ABP was likely not the only significant determinant of the true PWV in this study. Indeed, vasomotor tone changes (e.g., vasoconstriction occurred during LBNP as a compensatory response), which may have altered PWV without appreciably influencing ABP, constitute the major study limitation. If PWV were estimated through the aorta, which is relatively

sparse in smooth muscle [63], rather than to a finger, such changes may have been less of a factor. On the other hand, HR and cardiac output were probably not significant determinants of PWV in this study for the following reasons. First, PWV in large arteries is essentially constant across frequencies because of negligible viscous effects [65]. Thus, since we investigated PWV through largely nonviscous arteries, PWV here should have been mostly independent of HR. Second, PWV characterizes the properties of the arteries only. Therefore, cardiac output could have only impacted PWV via alterations in ABP.

Although the relationship between ABP and PWV generally follows an exponential [83], it could be well approximated here as linear because of the relatively narrow ABP range elicited by the LBNP. Thus, we quantitatively evaluated the ability of the technique to track ABP changes in terms of the linear correlation between its PWV estimates and ABP.

3.3.4.3 Tracking DP

In 15 subjects, DP was perturbed appreciably (20 mmHg) by the LBNP. In these subjects, the parametric system identification technique achieved an average r value between its proportional PWV estimates and measured DP of 0.81 ± 0.16 and an average RMSE value between the DP predicted from these estimates and measured DP of 4.3 ± 1.3 mmHg. These averages were $\sim$30% better than those of an optimized version of the conventional foot-to-foot detection technique applied to the same waveforms. Furthermore, in two subjects, the system identification technique was able to profoundly "correct" the PWV estimates of the conventional technique to show appropriate positive, rather than negative, correlation with DP.

We also assessed the conventional foot-to-foot detection technique with the ECG waveform substituted for the ICG waveform. This commonly proposed technique actually estimates the sum of PTT and the preejection period (PEP). Because PEP generally changed in the opposite direction of PTT with progressive LBNP (results not shown), the technique performed poorly in tracking DP. Note that the RMSE values of this technique should be interpreted with caution. For example, in subject 9, the technique showed a strong, nonphysiological negative correlation between its PWV

estimates and DP and consequently a small RMSE value.

3.3.4.4 Tracking other ABP parameters

The proportional PWV estimates of the parametric system identification technique may correlate best with mean ABP, as they arise from all waveform samples. However, because LBNP perturbed DP much more than mean ABP, we focused on DP tracking. Note that the PWV estimates of the conventional techniques are designed to track DP by virtue of being derived from the waveform feet. Nevertheless, the PWV estimates of the system identification technique were able to follow DP better than those of the conventional techniques. The likely reason is that DP correlated well with mean ABP here, which is generally the case. On the other hand, SP can show less correlation to DP and mean ABP. Indeed, for those subjects whose SP changed by >20 mmHg (n = 12), none of techniques yielded proportional PWV estimates that were able to track SP (average r and RMSE values ranged from 0.11 $\pm$ 0.50 to 0.29 $\pm$ 0.45 and from 8.6 $\pm$ 3.6 to 9.0 $\pm$ 4.3 mmHg; P = not significant). These results are not an indictment against the system identification technique or the conventional technique applied to the same waveforms, since their PWV estimates correlated significantly better with DP. However, because the PWV estimates of the conventional technique applied to the ECG waveforms showed poor tracking of all ABP parameters, we conclude that it is not suitable during progressive central hypovolemia.

3.3.4.5 Reproducibility

In addition to accuracy, reproducibility across time in the same subjects would be another necessary attribute for the parametric system identification technique. In subjects 1 and 4, repeated measurements were available on a second day. We therefore conducted preliminary reproducibility testing of the technique. The overall RMSE of the PTT estimates on the second day relative to the first day was just 4.9%. Thus, the technique was highly reproducible. Furthermore, the first and second day r values between the proportional PWV estimates and measured DP were 0.55 and 0.51 in one of the subjects and 0.85 and 0.80 in the other subject. Thus, the evaluation results of

the technique were also reproducible. For the conventional techniques, the corresponding reproducibility results were generally not as strong. For example, the overall RMSE values of their PTT estimates between the two days were $\sim$13% each.

3.3.4.6 Future directions and potential clinical applications

Further investigation of the system identification approach for PTT estimation is warranted. First and foremost, testing of the approach in patients recommended for PWV monitoring (e.g., elderly, hypertensives) is a must. Thorough reproducibility testing also remains to be performed. In addition, refinements to the specific technique described herein via other system identification and time-delay estimation techniques are also needed to reduce or even eliminate instances of poor performance (i.e., subject 9).

With successful future efforts, the system identification approach for PTT estimation may be employed for improved arterial stiffness monitoring in hypertension patients. For example, consistent with common practice [60], this approach could be applied to noninvasive carotid and femoral ABP waveforms obtained with tonometry in these patients for more accurate PWV estimation and thus potentially superior prognostic information (although nontrivial PWV error may still be present because of transit distance measurement inaccuracy). The approach could also be applied to arterial waveforms acquired with simple sensors (e.g., carotid artery and toe pulse oximeters) for potentially accurate, continuous, noninvasive, and cuffless ABP monitoring. However, other problems, including convenient construction of patient-specific calibration curves relating DP and mean ABP to PWV as well as SP estimation, must be solved before it could be used for such convenient ABP monitoring.

3.4 Cardiac output monitoring techniques with pulse transit time correction

3.4.1 Introduction

Cardiac output (CO) is perhaps the most important hemodynamic variable to be able to monitor in critically ill patients. It can provide timely indication of a hemodynamic event, aid in diagnosis [82], and direct therapy so as to improve patient outcomes [64, 81]. Even so, the pulmonary artery catheter, which has been the standard CO monitoring device, is declining in use due to the frequent complications that result from its invasiveness [112].

A potential approach for minimally invasive CO monitoring is to mathematically analyze the radial arterial blood pressure (ABP) waveform that is already being measured in many patients. Indeed, various "pulse contour analysis" techniques have been proposed [69]. For example, the most popular technique assumes that the pulse pressure (PP) is proportional to stroke volume in order to estimate relative CO changes via the product of PP and heart rate (HR) [34]. However, these techniques have generally been unable to track CO during hemodynamic instability, when monitoring is of greatest need (see, e.g., [18, 55, 84] and references therein). As a result, they have not been widely adopted in clinical practice.

Pulse contour analysis has proven challenging, because the shape of the radial ABP waveform not only changes with CO but also with wave reflection and total arterial compliance (AC). More specifically, this waveform arises as the sum of forward and backward traveling waves that are in-phase, and the magnitude of the backward wave relative to the forward wave (i.e., the reflection index) increases with peripheral resistance and may likewise be sensitive to other arterial parameters [102, 104]. So, for example, increases in the reflection index induced by vasoconstriction can cause PP to rise despite no change, or even a decrease, in stroke volume. Yet, most techniques assume that each beat of the radial ABP waveform can be represented with a simple lumped model such as a Windkessel and thus ignore this phenomenon [69]. AC decreases with increasing ABP due to slack collagen fibers and may be modulated by vasomotor tone. While such changes in AC, which is mainly determined by the aorta, may often be small compared to CO changes due in part

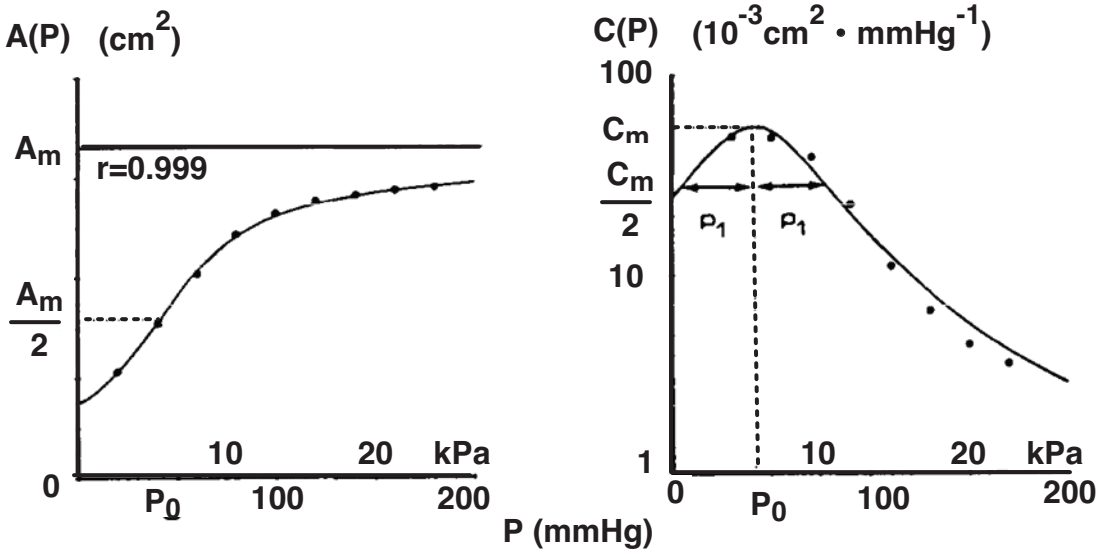

Figure 3.9: Conventional techniques employing empirical curves for correcting AC.

to relatively sparse aortic smooth muscle [16], they likely become significant near the limits of the ABP range. So, for example, decreases in AC induced by severe hypertension can cause PP to escalate independent of stroke volume. Many techniques do incorporate corrections for AC changes. Most notably, current techniques employ nomograms derived from in vitro experiments that allow AC to be estimated from ABP such as the one shown in figure 3.9 [51, 88, 111]. However, the AC to ABP relationship surely varies amongst subjects and in vivo, and vasomotor tone-induced AC changes may become appreciable.

In sum, a pulse contour analysis technique is needed that can overcome the challenges posed by both confounding wave reflection and AC changes. In this way, CO may be tracked accurately and minimally invasively during the crucial periods of hemodynamic instability.

We previously proposed a technique for estimating relative CO changes by long time interval analysis of a radial ABP waveform [69]. The idea is to circumvent the confounding wave reflection by analyzing the slow, beat-to-beat variations in the waveform wherein such phenomenon is no longer a major factor. We showed that this technique can track CO fairly well during several physiologic conditions [69, 87]. However, the technique assumes constant AC.

In this study, we aimed to (1) correct the CO estimates of the long time interval analysis technique for any AC changes using pulse transit time (PTT), a well-known marker of AC that can be non-invasively measured, and (2) demonstrate proof of concept via comparison of the corrected and original techniques using invasive hemodynamic waveforms.

3.4.2 The technique

The original technique is shown in Figure 3.10 and is described in detail elsewhere [69, 59]. Briefly, first, a cardiac contractions signal $x(t)$ is formed through an impulse train in which each impulse is located at the foot of the radial ABP waveform $y(t)$ and is scaled by the ensuing PP. Then, an impulse response $h(t)$ is identified, which when convolved with $x(t)$, optimally fits $y(t)$. By definition, $h(t)$ represents the ABP response to a single cardiac contraction. Next, the slow Windkessel time constant τ, which is equal to the product of the total peripheral resistance (TPR) and AC, is determined by fitting an exponential to the tail end of $h(t)$ once the faster wave reflections have vanished. In principle, τ is reliably determined by virtue of accurate coupling of the slow, beat-to-beat variations in $x(t)$ to $y(t)$. Finally, mean ABP (MAP) is divided by τ to determine CO to within a scale factor equal to $1/AC$. This scale factor is assumed to be constant so as to permit estimation of relative CO changes in a subject over a monitoring period.

The assumption of constant AC is not satisfactory in situations like major blood pressure changes. To correct this technique for any AC changes, PTT is introduced through simultaneous measurements from central and peripheral sites in the aorta, where dominantly determines AC. According to the Bramwell-Hill equation, the PTT and AC are approximately related as follows:

$$PTT = \sqrt{\frac{\rho l}{A} AC} \tag{3.2}$$

where ρ is the blood density, d is distance between the two measurement sites, and A is the average arterial cross-sectional area [11]. Thus, the original technique can be corrected for AC changes precisely as follows:

$$CO \propto PTT^2 \frac{MAP}{\tau} \tag{3.3}$$

The scale factor is now $\rho d/A$. While ρ and d are constant per subject, A could change with ABP. However, A is controlled by the product of AC and ABP, which are two inversely related terms. So, as shown in figure 3.9, A should change significantly smaller comparing with AC [51]. In this way, the PTT correction may support improved estimation of relative CO changes.

To robustly estimate PTT, a system identification technique is applied to the central and peripheral arterial waveforms. This technique is described in detail in the previous section. Briefly, a rational system is built which convolves the central arterial waveform to optimally fit the peripheral arterial waveform. Second, the impulse response of the system is excited. Third, PTT is determined as the time delay of the impulse response. Thus, PTT is effectively determined from both of the entire waveforms, rather than just their feet, after mathematically eliminating the reflected wave by virtue of equalizing their shapes. In this way, the technique will be robust to artifact while revealing the true PTT in the absence of wave reflection.

The corrected technique is summarized in figure 3.10. First, τ is estimated by long time interval radial ABP waveform analysis. Then, PTT is estimated by system identification analysis of central and peripheral arterial waveforms. Finally, proportional CO is computed from τ and PTT so as to monitor relative CO changes in a subject.

3.4.3 Technique evaluation in an animal study

Our technique was first validated in an animal study. Our experimental data were collected from five anesthetized Yorkshire swine under a protocol approved by the MIT Committee on Animal Care. Details of the materials and methods for data collection are described elsewhere [69]. Specifically, blood pressure waveforms from the thoracic aorta and femoral artery were collected via micromanometer-tipped catheters. An additional radial ABP was obtained via a 23- or 25-gauge angiocatheter which was placed as distal as possible to the brachial artery. The reference CO was measured via an ultrasonic flow probe around the aortic root. All data were recorded at a sampling

1) Estimate $\tau = TPR \cdot AC$

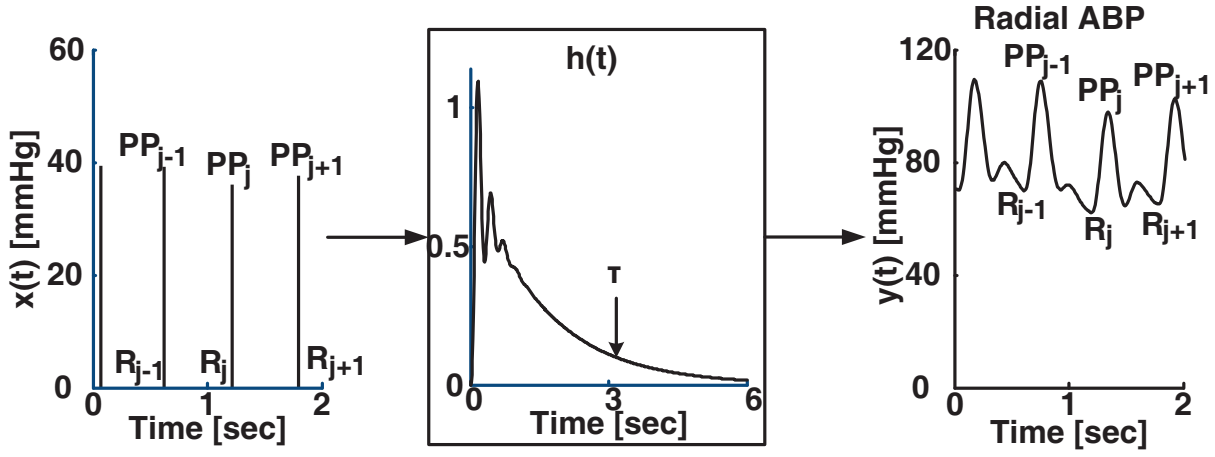

2) Estimate $PTT = \sqrt{\frac{\rho l}{A} AC}$

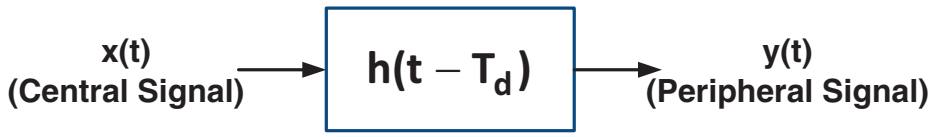

$$PTT = T_d$$

3) Compute proportional CO

$$CO \propto PTT^2 \frac{\overline{ABP}}{\tau}$$

Figure 3.10: LTIA with PTT correction for estimating CO.

frequency of 250 Hz. For each subject, a 75-150 min experiment was performed to change CO and other hemodynamic parameters, with a subset of following interventions: infusions of volume, phenylephrine, dobutamine, isoproterenol, esmolol, nitroglycerine, and progressive hemorrhage. Different infusion rates were implemented followed by brief recovery periods.

Off-line analysis was first applied to the measured waveforms which were resampled to 90 Hz. Second, the proportional CO trends were estimated from the femoral ABP by the long time interval analysis. Third, two PTTs were estimated by the system identification technique for comparison: one is determined from the aorta-radial pair (rPTT) and the other is identified from the aorta-femoral pair (fPTT). In order to acquire high resolution time delay, we estimated PTTs using data at their original sampling frequency (250Hz). Last, the corresponding reference CO was established by averaging the flow probe trend over the identical time interval.

For the original technique, the proportional CO trend was first scaled to the reference CO trend by equalizing their mean values for each individual animal over the entire experiment. Then, the root-mean-squared-normalized-error (RMSNE) of the scaled CO estimates was computed as a metric. For the corrected technique, the proportional CO trend is divided by PTT^2 (from both rPTT and fPTT separately), followed by scaling based on the mean value of the reference CO signal. The RMSNE was also computed for comparison. Next, log-transformation was utilized to the RMSNE values for improving uniformity, followed by paired t-test to determine the statistical significance level between the original technique and the corrected technique. In addition, in order to evaluate the benefits of the introduction of PTT, the value of calibrated new CO was determined in situation where there were huge changes in ABP.

3.4.3.1 Results

Table 3.4 lists the characteristics of segments and compares results of original and corrected techniques for every individual subject. The ABP range was wide, with the average of 77.4 $\pm$ 16.9 mmHg. Without PTT correction, the average RMSNE of the original technique was 14.9 $\pm$ 4.3 %. Comparing with the original technique, the estimation error with fPTT correction was reduced

Table 3.4: Characteristics of ABP and RMSNE values of original and corrected techniques for every individual subject.

Animal	ABP [mmHg]	CO RMSNE [%]		
	Mean ± Std	Original Technique	Corrected Technique	
			fPTT	rPTT
1	57.2 ± 16.9	20.9	16.6	17.9
2	76.4 ± 19.0	12.6	13.2	14.8
3	88.6 ± 13.5	16.0	14.0	12.6
4	87.3 ± 17.6	9.3	7.6	9.2
5	77.6 ± 17.5	15.7	13.8	10.5
Average	77.4 ± 16.9	14.9 ± 4.3	13.0 ± 3.3 (p = 0.055)	13.0 ± 3.5 (p = 0.25)

Table 3.5: RMSNE values of original and corrected techniques for segments at two extremes in every individual subject.

Animal	Max $\overline{ABP}$-Min $\overline{ABP}$ [mmHg]	CO RMSNE [%]		
		Original Technique	Corrected Technique	
			fPTT	rPTT
1	71.2	81.0	52.1	29.4
2	73.4	34.6	6.1	21.0
3	50.5	60.2	9.1	19.3
4	53.1	16.8	16.0	15.5
5	56.2	36.7	11.5	2.2
Average	60.8 ± 10.6	45.9 ± 25.0	19.0 ± 18.9 (p = 0.042)	17.5 ± 9.9 (p = 0.076)

to 13.0 ± 3.3 % (p=0.055). On the other hand, the estimation error with rPTT correction was decreased to 13.0 ± 3.5 %. But the difference was not significant (p=0.25).

Table 3.5 compares results of original and corrected techniques for segments with greatest ABP change in every individual subject. To evaluate the estimation, we picked the segment with either largest or smallest ABP in one subject. The average range of ABP change was 60.8 ± 10.6 mmHg. The RMSNE of the uncorrected technique was 45.9 ± 25.0 %. The error was reduced to 19.0 ± 18.9 % (p = 0.042) with fPTT correction and 17.5 ± 9.9 % (p = 0.076) with rPTT correction, respectively.

Figure 3.11 illustrates trends in CO values of the measured reference (solid), uncorrected estimation (dashed) and fPTT corrected estimation (dot dashed). Note during the intervention of

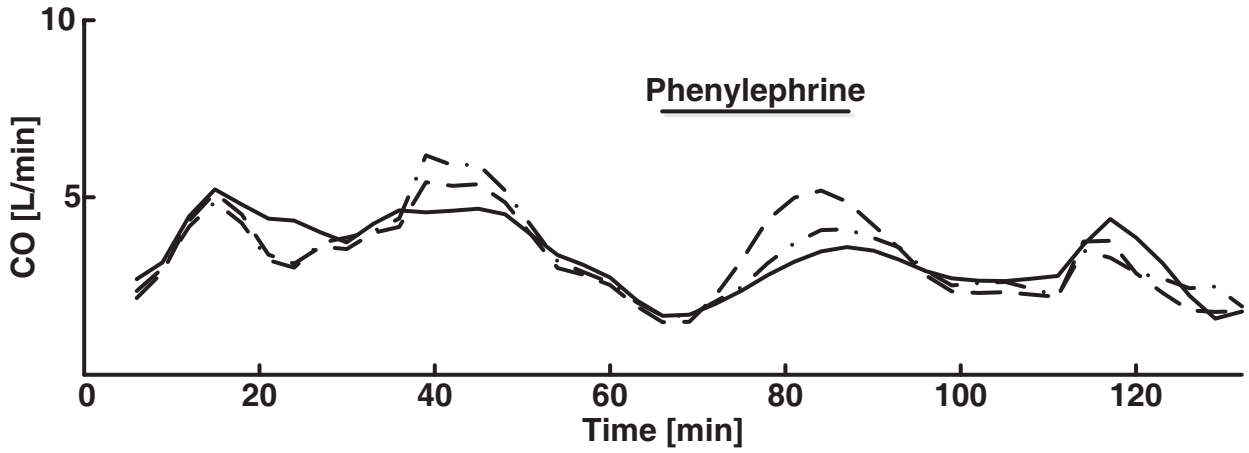

Figure 3.11: CO trends of the measured reference (solid), uncorrected estimation (dashed) and fPTT corrected estimation (dot dashed).

phenylephrine, the corrected method is apparently closer to the uncorrected method.

3.4.3.2 Discussion

In summary, we employed PTT measurements in an attempt to correct the relative CO change estimates of our long time interval radial ABP waveform analysis technique for any AC change. We tested this corrected technique using previously collected data from swine during various drug and volume interventions. Our results showed that the technique was able to reduce the calibrated CO estimation error by 18% relative to the uncorrected technique.

Our available data included only invasive PTT measurements. Thus, the results here demonstrate proof-of-concept. In practice, PTT could be measured non-invasively using, for example, arterial tonometry or pulse oximetry. Further, the average standard deviation of MAP over all the animals was $\sim$15 mmHg. We suspect that the corrected technique will afford greater improvements in CO estimation accuracy during more severe changes to MAP and other modes of hemodynamic instability. Future testing to address both of these issues would be worthwhile.

3.4.4 Technique evaluation in a human lbnp study

We proposed another investigation of the new physiologic waveform analysis techniques for early detection of hemorrhage during transport and higher echelon medical care of combat casualties. The materials and data analysis have been described in previous chapters. Briefly, 129 subjects were secured in a sealed chamber with progressively negative pressure. Blood was sucked into the lower body in order to simulate central hypovolemia. ECG, ABP and ICG were recorded for analysis. The algorithm of LTIA was performed identically as previously described. We estimated PTT from a black-box model system with input of zero-mean ICG and output of zero-mean ABP. The PTT was determined as the maximal 2^{nd} derivative of the impulse response of the system.

3.4.4.1 Results

Figure 3.12 shows the results of original and corrected techniques of LTIA comparing with the reference measurement. The introduction of PTT greatly decreased the CO estimation during LBNP. Therefore, the corrected LTIA is a more sensitive marker of the simulated hemorrhage.

3.4.5 Discussion

During the experiment of LBNP, a decrease of MAP would result in an increase of PTT, whereas the increasing resistance due to hemorrhage would reduce the PTT. From results in our experiment, the resistance should be the dominant factor in determining PTT.

In this chapter, we demonstrated preliminary results of two techniques with PTT correction. With PTT correction, the accuracy of the techniques was found qualitatively enhanced. However, the preliminary results need further evaluations in the following areas: (a) Statistical tests for significance level should be performed; and (b) Quantitative metrics should be evaluated, such as RMSE, or ROC AUC analysis. In sum, PTT is verified as an indicator for reflecting AC variation and it can be used to eliminate the estimation errors of pulse contour analysis techniques.

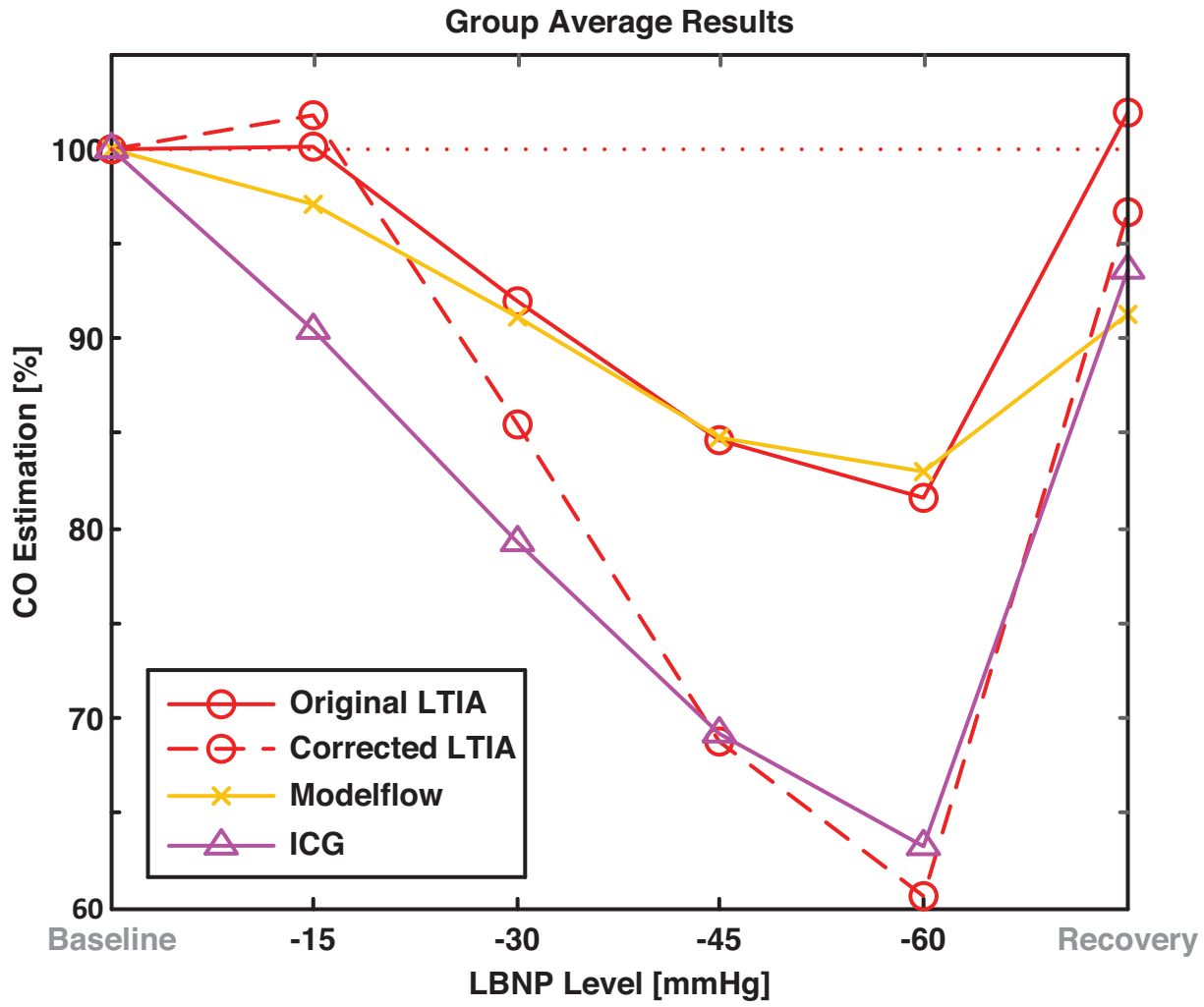

Figure 3.12: Comparison of the candidate techniques for estimating CO. LTIA was corrected with PTT for the changing AC.

Chapter 4

CARDIAC OUTPUT MONITORING FROM PERIPHERAL ARTERIAL BLOOD PRESSURE BY SHORT TIME INTERVAL ANALYSIS

4.1 Introduction

Techniques described in previous chapters require the measurement of waveform over multiple heart beat cycles. Empirically, the length of the waveform should be longer than 1 minute. In this chapter, we will introduce a method which permits to estimate CO beat by beat. The method develops a tube-load model with an adaptive transfer function, which can reconstruct the central arterial blood pressure waveform from a peripheral arterial blood pressure waveform.

4.2 The technique

To estimate CO from a peripheral ABP waveform, we introduced a previously developed tube-load model. The principle of the model has been described in Chapter 1. Briefly, we first reconstructed the central ABP waveform from a peripheral ABP waveform. Then we applied the Windkessel model to he reconstructed central ABP to get an estimate of CO. The accuracy was even improved with PTT for correcting AC.

4.2.1 Central blood and flow waveform reconstruction from a peripheral arterial blood pressure waveform

The idea of the technique is to define the transfer function relating peripheral ABP to central ABP with a distributed model, which accounts for confounding wave reflections, and to then estimate the unknown model parameters by exploiting pre-knowledge of aortic flow. Like all of the new techniques here, the technique is adaptive by virtue of updating the parameters of the transfer function each time a new segment of the peripheral ABP waveform becomes available for analysis.

More specifically, the arterial tree is modeled as a parallel arrangement of m distributed, uniform tubes terminated by lumped parameter loads. By building the peripheral ABP to central ABP transfer function, the central ABP is reconstructed, which is less affected by wave reflection. Then, the time constant τ is estimated in the Windkessel model by fitting the diastolic decay of the reconstructed central ABP. The SV can be derived and the corresponding CO is achieved by SV·HR.

Our adaptive transfer function technique is illustrated in figure 4.1. Briefly, the arterial tree is modeled as m parallel, uniform, and frictionless tubes with terminal loads. The i^{th} tube represents the wave travel path between the central aorta and the i^{th} peripheral artery. Each tube has constant characteristic impedance (Z_{ci}) and allows waves to travel along the entire tube with constant time delay (T_{di}). The i^{th} terminal load represents the arterial bed distal to the i^{th} peripheral artery. Each terminal load has frequency-dependent impedance characterized by peripheral resistance (R_i), peripheral compliance (C_i), and Z_{ci}. According to this model, a peripheral ABP waveform ($p_{pi}(t)$) is related to the central ABP waveform ($p_c(t)$) through a transfer function defined in terms of T_{di}, R_iC_i, and $Z_{ci}C_i$.

The three unknown parameters are estimated from $p_{pi}(t)$ by exploiting the fact that central aortic blood flow (ABF) is negligible during diastole. Thus, the flow at each tube entrance in the model (central ABF component ($q_{ci}(t)$)) may likewise be small during this time interval. That is, according to the model, $p_{pi}(t)$ is related to $q_{ci}(t)$ through a transfer function also defined in terms of T_{di}, R_iC_i, and $Z_{ci}C_i$ (see peripheral ABP central ABF transfer function in Fig. 2). These common parameters are estimated by finding the peripheral ABP central ABF transfer function, which when applied to $p_{pi}(t)$, optimally fits $q_{ci}(t)$ (scaled by Z_{ci}) to zero over its diastolic intervals. This optimization is achieved via a nonlinear least squares search over a physiologic range of the parameters. The optimization is facilitated with an initial measurement of T_{di} (i.e., pulse transit time between the central aorta and peripheral artery measurement site), which sets the search range for this key parameter.

Finally, the peripheral ABP central ABP transfer function with the estimates of T_{di}, R_iC_i, and

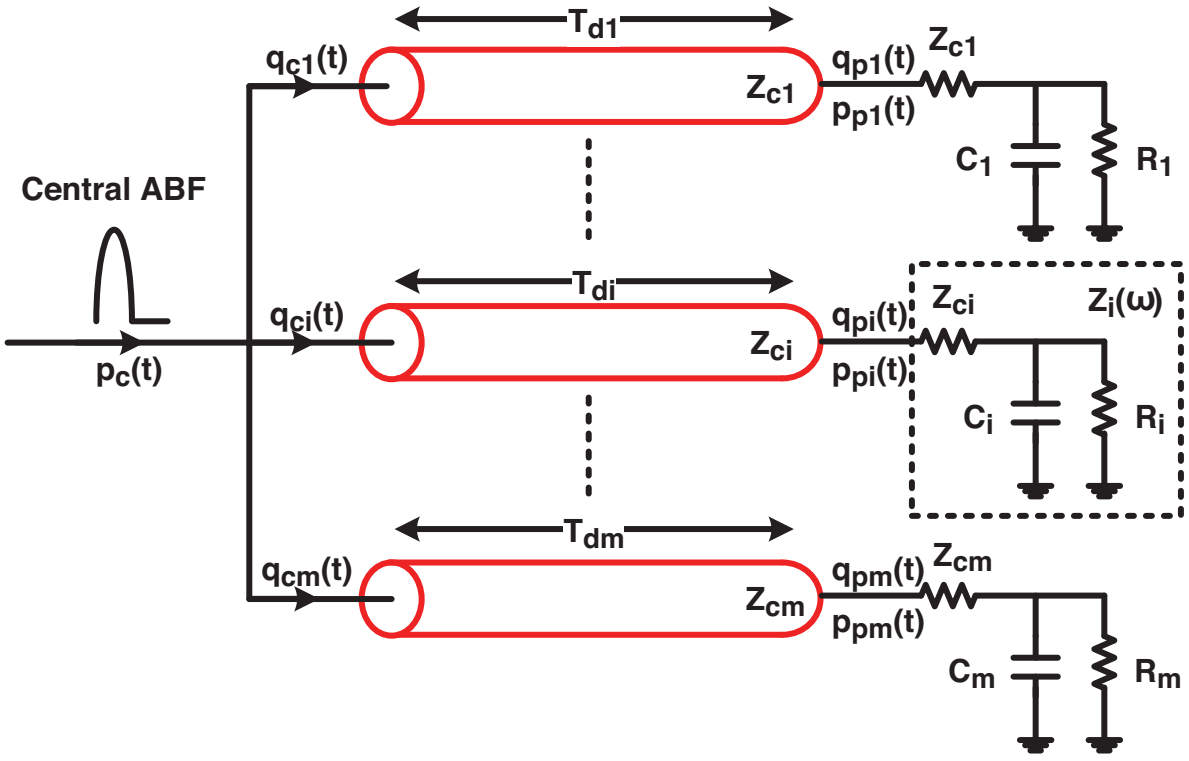

Peripheral ABP→Central ABP

$$p_{pi}(t) \rightarrow \frac{\left(\frac{1}{R_iC_i}+\frac{1}{2Z_{Ci}C_i}+j\omega\right)e^{j\omega Tdi}+\frac{1}{2Z_{Ci}C_i}e^{-j\omega Tdi}}{\frac{1}{R_iC_i}+\frac{1}{Z_{Ci}C_i}+j\omega} \rightarrow p_c(t)$$

Peripheral ABP→Central ABF

$$p_{pi}(t) \rightarrow \frac{\left(\frac{1}{R_iC_i}+\frac{1}{2Z_{Ci}C_i}+j\omega\right)e^{j\omega Tdi}-\frac{1}{2Z_{Ci}C_i}e^{-j\omega Tdi}}{\frac{1}{R_iC_i}+\frac{1}{Z_{Ci}C_i}+j\omega} \rightarrow Z_{ci}q_{ci}(t)$$

$= 0$ during diastole

Figure 4.1: Structure of the tube-load model and the model transfer functions.

$Z_{ci}C_i$ is applied to $p_{pi}(t)$ so as to derive $p_c(t)$.

4.2.2 Stroke volume estimation from a central blood pressure waveform

The reconstructed central ABP was then applied to a Windkessel model for an estimation of SV. Amongst techniques estimating SV from pressure waveforms, perhaps Bourgeois et al. performed the most compelling study. They developed a more intricate technique which had no assumption about the cardiac ejection time [9]. They introduced the Windkessel model for the representation of the arterial tree, which can account for the lumped compliance of the large arteries and the total peripheral resistance of the small arteries. According to this model, central ABP should decay like a pure exponential during each diastolic interval with a time constant (τ) equal to the product of TPR and AC. The technique is able to provide an estimation of proportional SV for each beat via the governing Windkessel model equation:

$$SV \propto p_a(t_{ee}) - p_a(t_{be}) + \frac{\int_{t_{be}}^{tee} p_a(t)dt}{\tau}. \tag{4.1}$$

4.3 Materials and analysis

4.3.1 Experimental data

De-identified physiologic data from humans subjected to a well-established LBNP protocol to simulate hemorrhage and resuscitation were studied [87]. The data collection procedures were approved by the Institutional Review Board of the Brooke Army Medical Center. The procedures pertinent to this particular study are briefly described as follows. 129 young, healthy humans in the supine posture were secured in an LBNP chamber. Instruments were positioned for measurement of various physiologic variables including a non-invasive impedance cardiography (ICG) waveform and a non-invasive finger ABP waveform (Finometer, TNO-TPD Biomedical Instrumentation, Amsterdam, The Netherlands). For comparison, The physiologic variables were recorded at a sampling frequency of 500 Hz during a five-minute baseline period and following sequential exposure

to increasing levels of LBNP up to at least 60 mmHg for five minutes each. After termination of LBNP and a five-minute equilibration period, the physiologic variables were recorded for an additional five-minute recovery period.

In this study, we also introduced PTT for correction the varying AC. The algorithm has been described in the previous chapter. Briefly, we developed a black-box whose transfer function can be characterized as a standard form of ARX system. The input and the output of the system are zero-mean differentiated impedance cardiography and zero-mean peripheral arterial pressure, respectively. The PTT can be determined as the maximal 2^{nd} derivative of the impulse response of the system.

4.3.2 Data analysis

The adaptive transfer function technique was applied to the peripheral ABP waveforms during the baseline period, each LBNP level, and the recovery period. Central and peripheral PP were then respectively determined from the derived and measured ABP waveforms. SV was also estimated from the derived central ABP from the Bourgeois' technique.

4.4 Results

Figure 4.2 illustrates a sample of the derived central and measured peripheral ABP waveforms. Consistent with known physiology, central PP was appreciably smaller than peripheral PP. Figure 4.3 illustrates the group average results. When central PP and peripheral PP were multiplied with HR to obtain CO surrogates, only CO derived from central PP demonstrated a decline with progressive LBNP. Hence, central PP provided a considerably more accurate and sensitive indication of reduced SV than peripheral PP.

The estimated CO derived with Bourgeois' algorithm was consistently lower than the estimated central PP·HR during the LBNP. The result was as expected since the algorithm had no assumption of the cardiac ejection time. Therefore, it yielded more accurate estimation of CO. Further, when

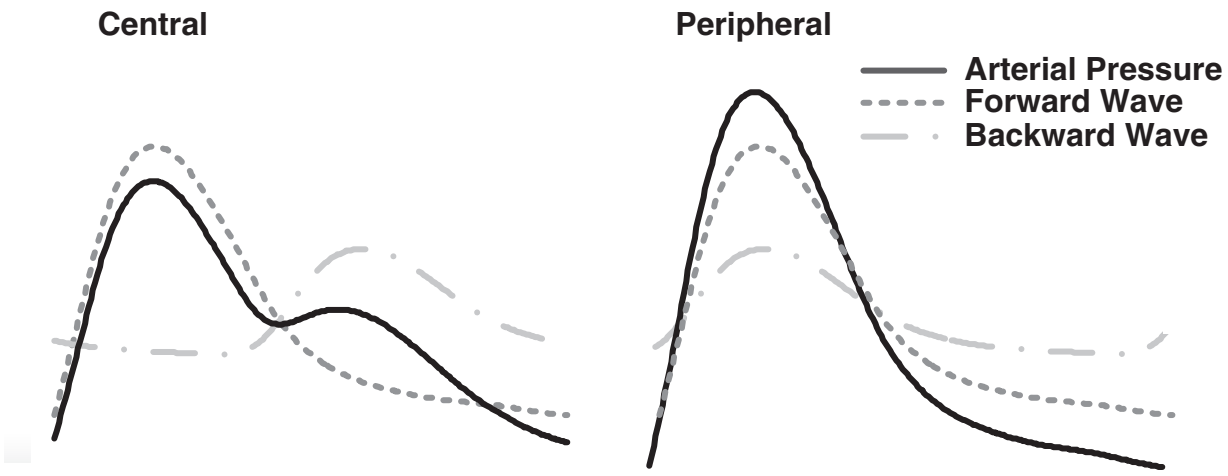

Figure 4.2: Sample plot of measured arterial blood pressure (solid) and computed forward (short dash) and backward (dash dot) waves in the central aorta and a peripheral artery.

the PTT was introduced for correcting AC, the corrected CO was significantly reduced and thus it was an earlier indicator of simulated hemorrhage.

4.5 Discussion

In summary, there is a profound need for early and convenient detection of hemorrhage in both civilian and military medicine. Central PP - as a surrogate of SV - can provide an early marker of blood loss, but only peripheral PP is convenient to measure.

We tested our previously developed adaptive transfer function technique for deriving the central ABP waveform from a peripheral ABP waveform in healthy humans subjected to a LBNP protocol. In this laboratory procedure, negative pressure is applied to the abdomen and lower extremities through a pressure chamber with an airtight seal so as to cause blood to pool in the lower body. A chamber pressure of -40 mmHg causes about a one liter shift of blood from the upper body to lower body [25]. As a result, similar to early hemorrhage, CO declines markedly even though mean ABP is maintained [49]. Our results showed that the derived central PP provided an earlier and more sensitive marker of LBNP and a far more accurate measure of reduced SV than measured peripheral PP. As predicted by wave reflection theory, the drop in peripheral PP due to a declining SV was

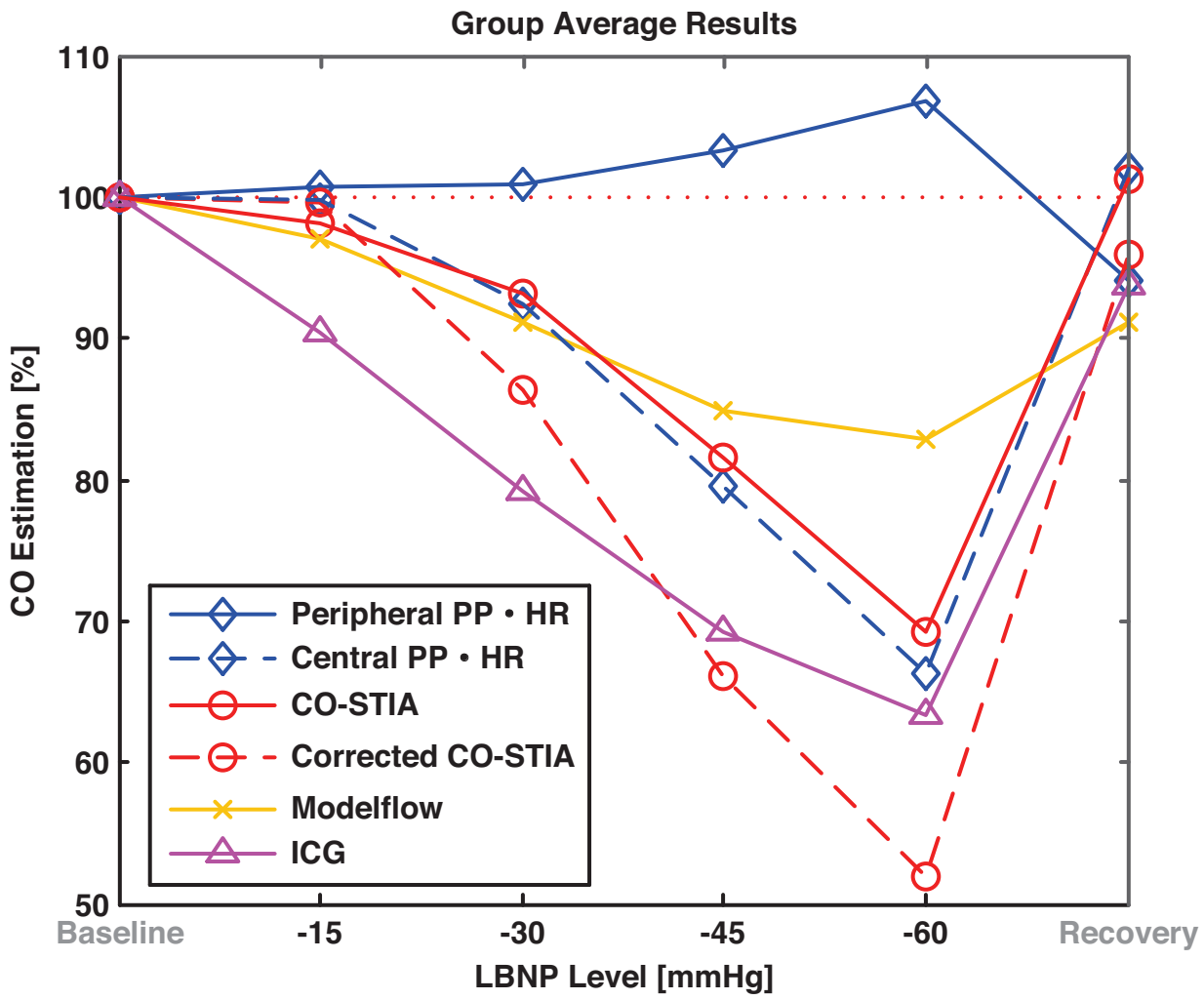

Figure 4.3: Group average results of reconstructed central pulse pressure vs. measured peripheral pulse pressure.

buffered by the compensatory vasoconstriction that occurred during LBNP. However, central PP was much less impacted by the rise in total peripheral resistance, presumably due to the significant time delay between the forward and backward waves in the central aorta.

This study improves upon our previous efforts to estimate SV and CO by long time interval analysis of a peripheral ABP waveform [87]. In particular, that technique estimates average CO over approximately 30-60 sec intervals. The technique described in the current study can potentially estimate beat-to-beat SV and could therefore detect rapid changes during hemorrhage and other physiologic conditions.

The assumption of PP to be a surrogate of SV is instantaneous cardiac ejection. In practice, it occurs over finite time for the heart to eject blood from the central aorta to the periphery. Therefore, we tried to circumvent this assumption by estimating the Windkessel time constant via fitting an exponential to the diastolic decay of the derived central ABP waveform, which is less complicated by wave reflection than a peripheral ABP waveform. The SV estimated by Bourgeois' method showed earlier indication of hemorrhage than the estimated central PP.

The group average of PTT was progressively decreasing during the LBNP experiment. In principle, decreasing ABP should lead to an increase of PTT. On the other hand, increasing resistance due to hemorrhage will change PTT to the other direction. From the result in our experiment, the decreasing PTT indicated that the resistance is the dominant factor.

In future, we will quantitatively evaluate the techniques with statistical analysis, such as ROC AUC. The discrimination between the low-tolerant and high-tolerant subjects will be investigated as well.

Chapter 5

CARDIAC OUTPUT MONITORING FROM PULMONARY ARTERIAL PRESSURE BY LONG TIME INTERVAL ANALYSIS

5.1 Introduction

Cardiac output (CO), which represents the total blood flow rate in the circulation, can also be monitored from a measurement of pulmonary arterial pressure waveform. Meanwhile, left atrial pressure (LAP), which generally indicates the blood pressure attained in the left ventricle during the cardiac filling phase, can be simultaneously tracked with the pulmonary arterial pressure waveform. As two of the most important quantities, the information of CO and LAP collected from critically ill patients can facilitate the diagnosis, monitoring, and treatment of various disease processes such as left ventricular failure, mitral valve disease, and shock of any cause. For example, patients with left ventricular failure often have symptom of a decrease in CO and an increase in LAP, whereas a decrease in CO while LAP is falling may indicate that the patient is going into hypovolemic shock.

So far, the use of the balloon-tipped, flow-directed pulmonary artery catheter is the gold standard method for measuring CO and LAP in critically ill patients [61, 106]. As previously discussed, CO is specifically estimated according to the thermodilution method. This method involves injecting a bolus of cold saline in the right atrium, measuring temperature downstream in the pulmonary artery, and computing the average CO based on conservation laws. LAP is estimated through the pulmonary capillary wedge pressure (PCWP) method. This method involves advancing the catheter into a branch of the pulmonary artery, inflating the balloon, and measuring the resulting steady-state PCWP. In theory, PCWP should nearly equal LAP, since flow has ceased through the branch.

A major limitation of the catheterization method is that it requires an operator, which therefore does not permit continuous monitoring. Moreover, risks exist in the implementation such as partial

wedging and balloon over-inflation [54, 67]. Indeed, the developers of the PCWP method and the pulmonary artery catheter each reported that they could properly measure PCWP only about 75% of the time [106]. Similar technical problems can also be encountered in implementing the thermodilution method. Perhaps, as a result of these shortcomings, the clinical benefit of the pulmonary artery catheter is still controversial [93].

On the other hand, continuous monitoring of pulmonary artery pressure (PAP) is available with the invention of the pulmonary artery catheter. Since CO and LAP are both known to be significant determinants of PAP, it should, in principle, be possible to continuously monitor these two critical hemodynamic variables by mathematical analysis of a PAP waveform. Such an approach could be utilized in critically ill patients to, for example, assess the effects of interventions in real-time, provide an early indicator of deleterious hemodynamic events, save precious time in the busy intensive care unit (ICU), as well as circumvent the aforementioned technical problems in implementing the standard measurement methods.

To our knowledge, only four papers are found in the literature for monitoring CO by PAP waveform analysis [21, 32, 107, 116]. These papers described techniques that analyzed intra-beat PAP variations in which highly complex wave and inertial effects are prominent [73]. On the other hand, there is substantial literature on estimating LAP through the end-diastolic PAP (e.g., [61, 45]). However, this simple analysis is not as accurate as PCWP [45] and is known to be unreliable during pulmonary hypertension [61]. One paper in the literature was found which involves training a neural network to predict PCWP from a PAP waveform [30]. However, the accuracy of technique was limited by its training group. Thus, no advanced technique has been introduced in the literature which can both monitor LAP and CO by mathematical analysis of a PAP waveform.

In this chapter, we evaluate a technique for continuous monitoring of both CO and LAP by mathematical analysis of a PAP waveform over time scales greater than a cardiac cycle in which the confounding effects of wave and inertial phenomena are attenuated [73]. The technique has been proposed in a previous animal study. In this study, we evaluated the technique with respect to

pulmonary artery catheterization data from 180 critically ill patients.

5.2 The technique

Our technique for monitoring CO and LAP from a PAP waveform is extended from a technique we previously developed for estimating CO from an arterial blood pressure waveform by long time interval analysis [59, 69]. The method can be briefly described as follows:

The novel technique is based on the Windkessel modeling of the pulmonary system in Figure 5.1(a). The pulmonary system consists of a resistor, a capacitor and a constant voltage source. The resistor represents the pulmonary arterial resistance (PAR), and the capacitor stands for the pulmonary arterial compliance (PAC). The constant voltage source describes the left atrial pressure. According to the circuit theory, during each diastolic interval, the PAP should exponentially decay to the average LAP, rather than zero pressure. The time constant τ of the decay should be the product of PAR and PAC. By fitting an exponential function to the PAP waveform, both τ and LAP can be determined. Then CO can be subsequently derived with a scale factor of 1/PAC by subtracting LAP from mean PAP (MPAP) and dividing the difference by τ.

However, pure exponential diastolic decay is often obscure to observe in experimental PAP waveforms (Figure 5.1(b)) [107] due to complex wave reflections and inertial effects in the pulmonary circulation [73]. On the other hand, our previous study has indicated that the confounding wave and inertial effects may be faster than the exponential Windkessel dynamics. This concept implies that if pulsatile activity abruptly ceased, then PAP would eventually decay like a pure exponential and ultimately equilibrate to LAP once the faster wave and inertial dynamics vanished. Thus, the Windkessel model of Figure 5.1(a) is a more valid representation of the long time scale or beat-to-beat variations in the PAP waveform.

Our technique therefore analyzes the PAP waveform over long time intervals (seconds to minutes) in order to determine the pure exponential decay and equilibrium pressure that would eventually result if pulsatile activity suddenly ceased. More specifically, average LAP and the response of PAP minus average LAP to a single, solitary cardiac contraction ($h(t)$ in Figure 5.2) are simulta-

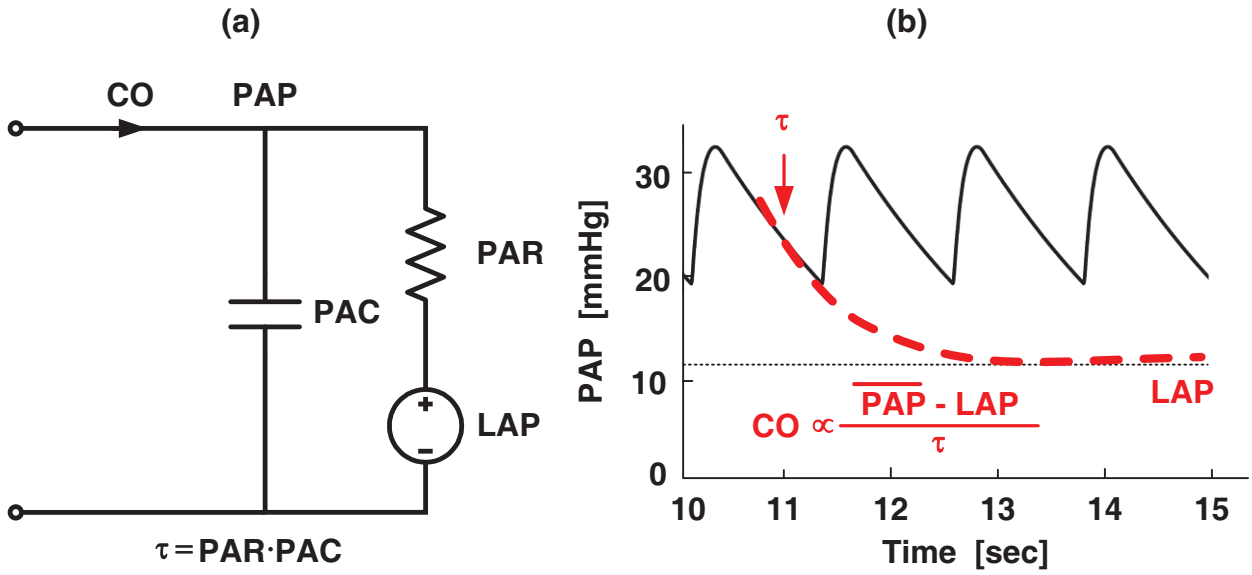

Figure 5.1: (a) Windkessel model of the pulmonary artery pressure (PAP) waveform. (b) Experimental PAP waveform and diastolic decay fitting.

neously estimated by optimal fitting or prediction of ∼6 min contiguous segments of a PAP waveform. Then, the Windkessel time constant τ is determined by fitting a mono-exponential function to the tail end of $h(t)$ once the faster wave and inertial effects have vanished (Figure 5.2). Finally, proportional CO is computed via Ohm's law (Figure 5.2). The technique, which is illustrated in Figure 5.2, is specifically implemented in four mathematical steps.

First, a cardiac contractions signal is constructed by formation of an impulse train. Each impulse is located at the R-wave of a simultaneous surface electrocardiogram (ECG) measurement and has unity area. Second, the PAP waveform segment ($y(t)$) is fitted according to the sum of an unknown constant term and the convolution between an unknown impulse response ($h(t)$) and the constructed cardiac contractions signal ($x(t)$). That is, the constant term and $h(t)$ are estimated so as to permit the best fit or prediction of $y(t)$ in the least squares sense. The estimated constant term represents the average LAP, while the estimated $h(t)$ is defined to represent the PAP-LAP response to a single cardiac contraction. The impulse response $h(t)$ and average LAP are specifically estimated with the following autoregressive exogenous input equation with constant term c:

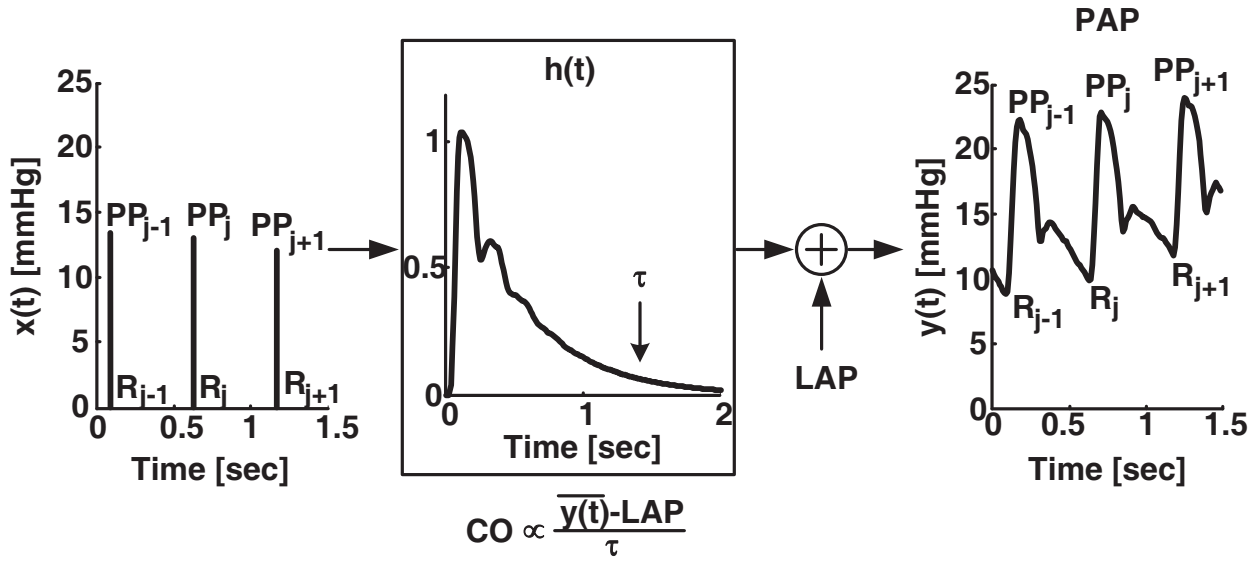

Figure 5.2: Illustration of how the mathematical analysis technique determines the time constant τ of the Windkessel model in Figure 5.1, average left atrial pressure (LAP), and proportional cardiac output (CO) from a pulmonary artery pressure (PAP) waveform.

$$y(t) = c + \sum_{k=1}^{m} a_k y(t-k) + \sum_{k=l}^{n} b_k x(t-k) + e(t). \tag{5.1}$$

where $e(t)$ is the unmeasured residual error, a_k, b_k are unknown parameters, and m and n limit the number of these parameters (model order) [58]. For a fixed model order, the parameters including c are estimated from $x(t)$ and $y(t)$ through the least-squares minimization of $e(t)$, which has a closed-form solution [58]. With the estimated parameters, average LAP and $h(t)$ are computed as follows:

$$LAP = \hat{c}/(1 - \sum_{k=1}^{m} \hat{a_k}). \tag{5.2}$$

$$h(t) = \sum_{k=1}^{m} \hat{a_k} h(t-k) + \sum_{k=l}^{n} \hat{b_k} \delta(t-k). \tag{5.3}$$

where ^ indicates estimates and $\delta(t)$ is the impulse function.

Next, τ is determined over the interval of the estimated $h(t)$ ranging from one to two seconds following the time of its maximum value based on the exponential equation:

$$h(t) = Ae^{-t/\tau} + w(t). \tag{5.4}$$

The parameters A and τ are estimated through the least squares minimization of the unmeasured residual error $w(t)$, which has a closed-form solution after log transformation of $h(t)$. In principle, accurate determination of τ as well as average LAP is achieved by virtue of $h(t)$ reliably coupling the long time scale variations in $x(t)$ to $y(t)$-LAP.

Finally, proportional CO is computed by dividing MPAP-LAP with τ. Note that the continuous proportional CO provided by the technique may be conveniently calibrated to continuous absolute CO with a single thermodilution measurement.

5.3 Materials and analysis

5.3.1 Pulmonary artery catheterization data

The pulmonary artery catheterization data utilized here for the mathematical analysis were obtained from the MIMIC II (Multi-parameter Intelligent Monitoring for Intensive Care II) database, which is described in detail elsewhere and freely available on the web. Briefly, this database includes 247 critically ill patient records that were archived from patient monitors in ICUs of the hospital formerly known as the Beth Israel Hospital, Boston, MA. Each of these records consists of continuous waveforms sampled at 125 Hz such as PAP and surface ECG leads as well as one-minute trends such as thermodilution CO, PCWP, and heart rate (HR). 180 of the 247 patient records were applicable for technique evaluation, as they included a PAP waveform and more than one reference thermodilution CO measurement (as the technique estimates changes in CO) and/or at least one PCWP measurement. Within each of these records, CO as well as PCWP were naturally changing due to disease progression and therapy.

Based on these 247 MIMIC patient records, we created a data set for technique evaluation as follows. First, we downloaded from these records all of the distinct, one-minute thermodilution CO and PCWP measurements and corresponding three-minute segments of the PAP waveforms.

Then, we visually examined each of the PAP waveform segments and extracted the artifact-free records. A total of 87 pairs of artifact-free PAP waveform segments and reference PCWP from 27 patient records and a total of 1211 pairs of artifact-free PAP waveform segments and reference thermodilution CO from 180 patient records remained for the subsequent evaluation of our technique.

5.3.2 Data analysis

After applying the technique to all 1211 PAP waveform segments, the resulting proportional CO and absolute LAP estimates were quantitatively compared with their respective reference thermodilution CO and PCWP measurements as follows. First, the proportional CO estimates were scaled to have the same mean as the reference thermodilution CO within each patient record. Then, the root-mean-squared-normalized-errors (RMSNEs) between the calibrated CO and their respective reference measurements were computed. For comparison, the RMSNE between MPAP, PP·HR and the reference CO were also computed.

On the other hand, the root-mean-squared-errors (RMSE) between the absolute LAP estimates and the reference PCWP were calculated. For comparison, the RMSE between the mean end-diastolic PAP (EDPAP) and their reference PCWP measurements was also computed.

In our previous study, we found that our technique was more robust to challenging physiologic conditions than conventional techniques. We also performed similar analysis in this study. To be more specific, for the CO estimates, we investigated the CO estimation accuracy of the investigational techniques as a function of minimum thermodilution CO change magnitude. The magnitude was increased from baseline up to 40%.

5.4 Results

Table 5.1 summarizes the results of the evaluation of the technique with respect to the MIMIC II database. This table shows that the technique achieved an overall CO RMSNE of 17.6% (after a

Table 5.1: Overall cardiac output estimation accuracy of the investigational techniques.

Technique	RMSE (%)	Limits-of-Agreement (L/min)	Wilcoxon Signed-Rank Test (p)
LTIA	17.60	-1.84/+1.84	-
MPAP	22.48	-2.19/+2.19	<0.001
PP·HR	19.67	-1.94/+1.94	0.30

Table 5.2: Overall left atrial pressure estimation accuracy of the investigational techniques.

Technique	RMSE (mmHg)	Limits-of-Agreement (mmHg)	Paired t-Test (p)
LTIA	4.9	-8.58/+10.57	-
EDPAP	5.9	-3.83/+12.31	<0.001

single calibration), whereas the errors of MPAP and PP·HR were 22.48% and 19.67%, respectively. Figure 5.3 shows the results with increasing CO magnitude. The LTIA technique was least affected by the change. The overall LAP RMSE has the error of 4.9 mmHg, which is significantly better than the conventional EDPAP technique with the error of 5.9 mmHg, as illustrated in Table 5.2.

5.5 Discussion

The technique was validated in our previous study. We now evaluated the technique with respect to the MIMIC II database, which includes fully annotated hemodynamic records from thousands of ICU patients. The analysis was performed from 180 critically ill patients and have compared the resulting CO and LAP estimates with standard operator-dependent thermodilution CO and PCWP measurements, respectively. Comparing with conventional techniques, our technique is more accurate in estimating CO and LAP. When the patient condition becomes more challenging, the advantage between our technique and other conventional techniques is more significant.

One potential limitation of our technique is the assumption of constant PAC. In future, the accuracy might be improved with the measurement PTT. With future successful testing, the technique may ultimately be employed in critically ill patients so as to effectively automate the pulmonary artery catheter.

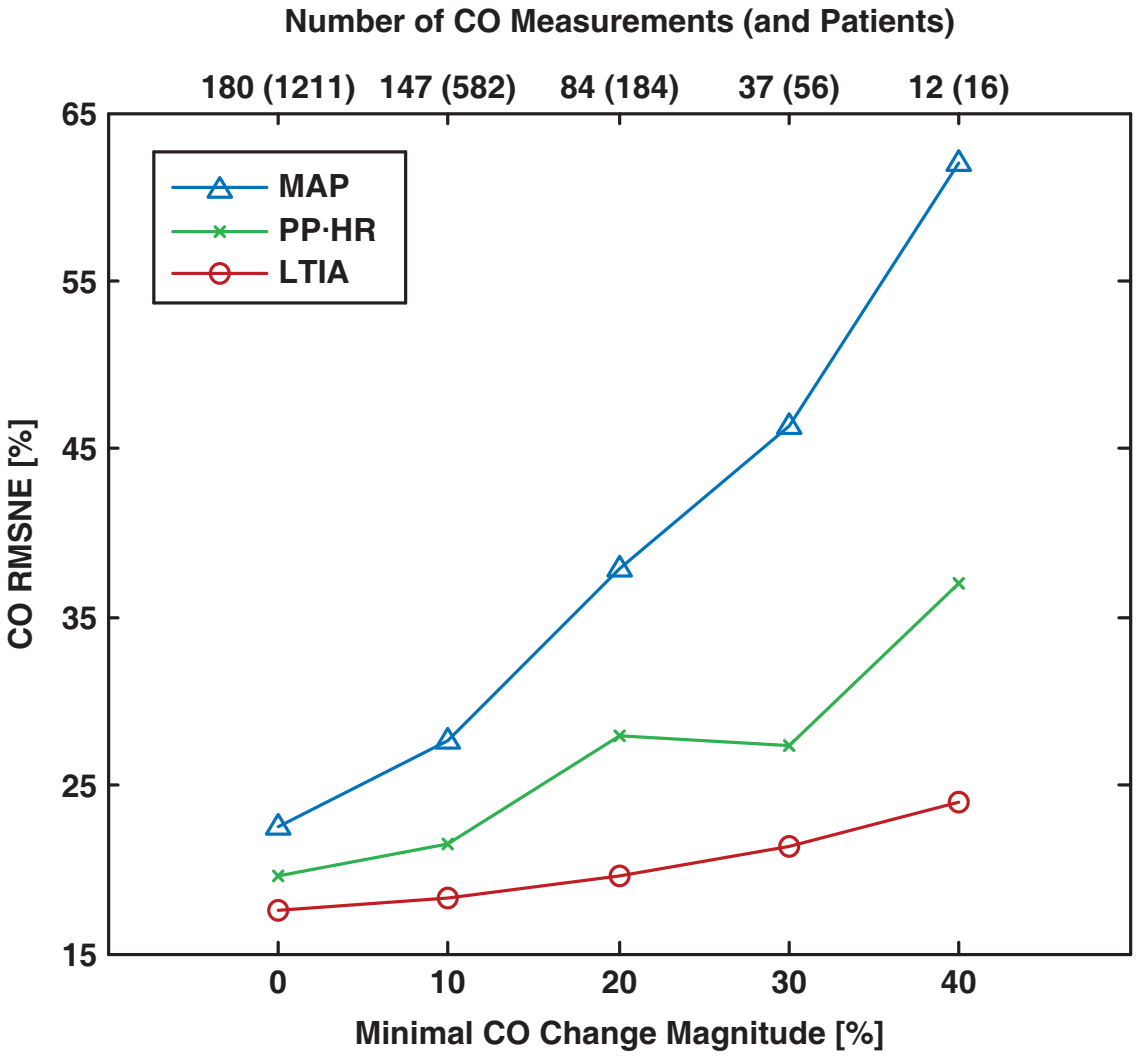

Figure 5.3: Illustration of how the mathematical analysis technique determines the time constant τ of the Windkessel model in Figure 5.1, average left atrial pressure (LAP), and proportional cardiac output (CO) from a pulmonary artery pressure (PAP) waveform.

Chapter 6

CONCLUSIONS

6.1 Summary

In this report, we proposed several novel physiologic waveform analysis techniques, which will prove both reliable and superior to previous techniques, for monitoring cardiac output. The long time interval analysis can remove the reflection confounding issue by estimating the cardiac output over multiple beats. The technique was evaluated on a large, medical/surgical ICU patient dataset. Our proposed technique was comparative with other traditional methods at the baseline level and the technique became increasingly superior to others with more challenging cardiac output changes. We also introduced pulse transit time to overcome the estimation error by varying arterial compliance. With the pulse transit time correction, we validated our technique in an animal study and a human lower body negative pressure experiment. The decreasing pulse transit time excellently compensated the arterial compliance variation, the corrected techniques overlapped with the reference method, while other methods all overestimated the cardiac output during the LBNP process. In addition, we compared the effects of pulse transit time and pulse arrival time, in terms of their capabilities in tracking blood pressure. We implemented high-fidelity, invasive measurements over wide hemodynamic conditions. From our results, we concluded that the pulse arrival time is not an adequate surrogate for pulse transit time and we only recommended future research should focus on pulse transit time.

In addition, we employed the tube-load model with adaptive transfer function to estimate CO from a peripheral ABP waveform. In order to identify unknown parameters of the model, we exploited the fact that central flow should be negligible during diastole. This technique permits beat-by-beat estimation and thus it can facilitate the real-time CO monitoring. The PTT was also introduced to overcome the influence of AC.

Further, we adapted our LTIA model to estimate CO from a pulmonary artery pressure. The Windkessel model was modified with an additional constant term. This novel technique is able to simultaneously estimate CO and left atrial pressure, which are two important physiologic variables.

6.2 Future work

In future, an extension can be performed to the tube-load technique. The extended model can estimate relative change in end-diastolic volume (EDV) from the central ABP waveform, which may be derived from a peripheral ABP waveform with the preceding adaptive transfer function technique. EDV is considered as an earlier marker of hypovolemia than SV. The idea of the technique is to build upon the Windkessel technique by modeling the left ventricle in addition to the arterial tree so as to split an SV estimate into its cardiac end-systolic volume (ESV) and EDV components. The basic steps are to (1) represent both the ejection and diastolic intervals of the central ABP waveform with a lumped parameter model; (2) estimate the lumped model parameters to with a constant AC scale factor by fitting the model to each beat of the waveform; and (3) use the proportional parameter estimates for each beat to compute beat-to-beat EDV and ESV to within the same scale factor.

More specifically, first, the entire central ABP waveform is represented with a modified Windkessel model of the left ventricle and arterial tree (see electrical analog in Figure 6.1). In the model, the left ventricle is characterized by the well-known variable elastance (reciprocal of compliance) model whose elastance (ventricular elastance, VE) is time-varying ($E(t)$) [101, 92]. Assuming absence of valve disease, the aortic valve is modeled by an ideal diode. The arterial tree is represented with the Windkessel model as justified above. In addition to compliance, the left ventricle (and large arteries) is parameterized with an unstressed volume (ventricular unstressed volume, VUV). Then, the model parameters can be derived from the following discretized governing equation:

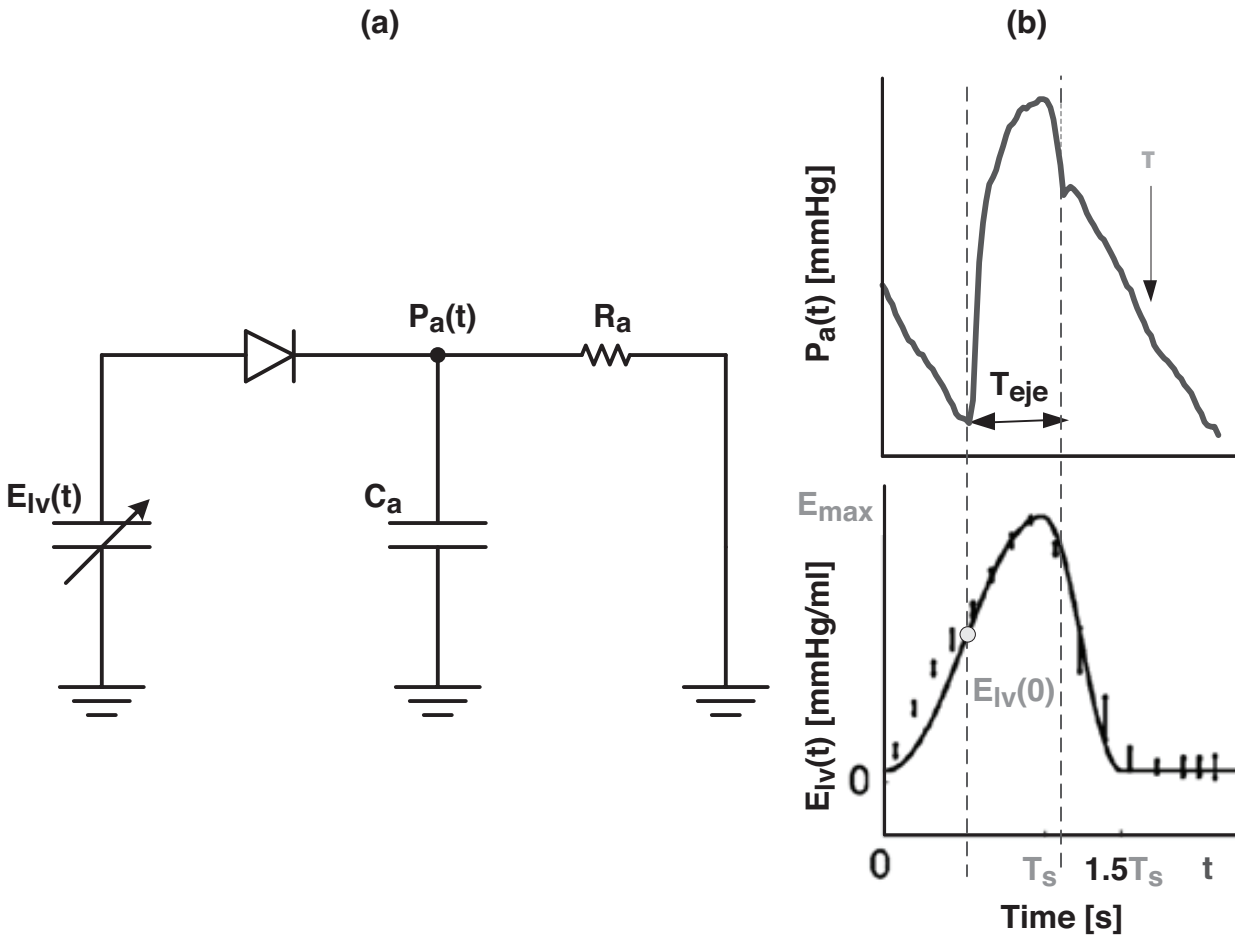

Figure 6.1: New technique for monitoring EDV by analysis of the central ABP waveform, which may be derived from a peripheral ABP waveform. (a) Lumped parameter model of the left ventricle and arterial tree upon which the technique is based. (b) The unknown model parameters (in gray) are estimated by fitting the model to the ejection and diastolic intervals of each beat of the ABP waveform so as to compute relative change in beat-to-beat EDV.

$$\frac{p_a(t_{be})}{AC \cdot E(t_{be})} - \frac{p_a(t)}{AC \cdot E(t)} = p_a(t) - p_a(t_{be}) + \frac{T}{2\tau} \sum_{k=t_{be}+1}^{t} [p_a(k) + p_a(k-1)], \quad t_{be} \le t \le t_{ee}, \quad (6.1)$$

where T is the sampling period, and t_{be} and t_{ee} are the beginning and end times of the ejection interval. Both T and $p_a(t)$ for t_{be} and t_{ee} are known, while the proportional model parameters, τ = TPR· AC and AC· E(t) for $t_{be} \le t \le t_{ee}$, need to be determined. Equation 6.1 represents an under-determined set of equations with N equations and $N+2$ unknowns, so it does not provide a basis for uniquely determining these parameters. In order to find solutions to the equations,

a parametric function is assumed to succinctly characterize the time-varying VE as justified by previous studies. In particular, Senzaki et al. showed that experimental VE functions, normalized in both amplitude and time, were remarkably consistent in 87 patients despite wide variations in their ventricular states (see discrete values in the lower panel of Figure 6.1) [94]. Heldt et al. then showed that these normalized VE data could be well fitted, especially during the relevant ejection interval (i.e., the higher elastance range), by a parametric raised cosine function (Figure 6.1) [42]. Substituting this parametric function into (6.1) reduces the number of unknowns to four, namely τ, $AC \cdot E_{max}$, $AC \cdot E(t_{be})$, and T_s (Figure 6.1). These four parameters then can be estimated for each beat in two steps. First, τ is estimated by fitting an exponential to the diastolic interval of $p_a(t)$ (see Figure 6.1). Second, the estimated τ is substituted into (6.1), and AC·E_{max}, AC·$E(t_{be})$, and T_s are estimated from $p_a(t)$ over the ejection interval by optimally fitting both sides of this equation to each other. This optimization is achieved via a nonlinear least squares search over a physiologic range of the three parameters.

Finally, the beat-to-beat proportional EDV can be derived from the estimated proportional VE function over the ejection interval, AC·E(t) for $t_{be} \leq t \leq t_{ee}$, and the central ABP waveform $p_a(t)$, via the following governing equation:

$$EDV \propto \frac{p_a(t_{be})}{AC \cdot E(t_{be})} + \frac{VUV}{AC} \tag{6.2}$$

VUV/AC is much smaller than EDV in normal subjects such as soldiers [47], so VUV/AC may be neglected or set to a nominal value (e.g., 15 mmHg in dogs [9, 101]), rather than estimated. This value can be measured for patients with dilated hearts by obtaining EF via imaging and finding the value of VUV/AC. In this case, the EF estimated from the ABP waveform should equal to the independent EF measurement.

Given the available reconstructed central ABP, EDV and EF can be estimated by this approach. We expect that EDV would be a more acute marker of hemorrhage than SV. The technique will be evaluated with the data in the LBNP study.

BIBLIOGRAPHY

BIBLIOGRAPHY

[1] C. Ahlstrom, A. Johansson, F. Uhlin, T. Länne, and P. Ask. Noninvasive investigation of blood pressure changes using the pulse wave transit time: a novel approach in the monitoring of hemodialysis patients. *Journal of Artificial Organs*, 8(3):192–7, January 2005.

[2] M. Anliker, M. B. Histand, and E. Ogden. Dispersion and attenuation of small artificial pressure waves in the canine aorta. *Circulation Research*, 23(4):539–51, October 1968.

[3] A. P. Avolio. Multi-branched model of the human arterial system. *Medical & Biological Engineering & Computing*, 18(6):709–18, November 1980.

[4] K. Azer and C. S. Peskin. A one-dimensional model of blood flow in arteries with friction and convection based on the Womersley velocity profile. *Cardiovascular Engineering*, 7(2):51–73, June 2007.

[5] H. C. Bazett and N. B. Dreyer. Measurements of pulse wave velocity. *American Journal of Physiology*, 63:94–116, 1922.

[6] F. J. Belda, G. Aguilar, J. L. Teboul, D. Pestaña, F. J. Redondo, M. Malbrain, J. C. Luis, F. Ramasco, A. Umgelter, J. Wendon, M. Kirov, and E. Fernández-Mondéjar. Complications related to less-invasive haemodynamic monitoring. *British Journal of Anaesthesia*, 106(4):482–6, April 2011.

[7] G. Biancofiore, L. A. H. Critchley, A. Lee, L. Bindi, M. Bisà, M. Esposito, L. Meacci, R. Mozzo, P. DeSimone, L. Urbani, and F. Filipponi. Evaluation of an uncalibrated arterial pulse contour cardiac output monitoring system in cirrhotic patients undergoing liver surgery. *British Journal of Anaesthesia*, 102(1):47–54, 2009.

[8] J. Blacher, R. Asmar, S. Djane, G. M. London, and M. E. Safar. Aortic pulse wave velocity as a marker of cardiovascular risk in hypertensive patients. *Hypertension*, 33(5):1111–7, May 1999.

[9] M. J. Bourgeois, B. K. Gilbert, G. Von Bernuth, and E. H. Wood. Continuous determination of beat to beat stroke volume from aortic pressure pulses in the dog. *Circulation Research*, 39(1):15–24, July 1976.

[10] P. Boutouyrie, S. Laurent, and M. Briet. Importance of arterial stiffness as cardiovascular risk factor for future development of new type of drugs. *Fundamental & Clinical Pharmacology*, 22(3):241–6, June 2008.

[11] J. C. Bramwell. The velocity of the pulse wave in man. *Proceedings of the Royal Society of London Series B-Containing Papers of a Biological Character*, 93(652):298–306, 1922.

[12] J. C. Bramwell, A. C. Downing, and A. V. Hill. The effect of blood pressure on the extensibility of the human artery. *Heart*, 10(4):289–300, 1923.

[13] R. Burattini and K. B. Campbell. Modified asymmetric T-tube model to infer arterial wave reflection at the aortic root. *IEEE Transactions on Bio-medical Engineering*, 36(8):805–14, August 1989.

[14] R. Burattini and K. B. Campbell. Effective distributed compliance of the canine descending aorta estimated by modified T-tube model. *The American Journal of Physiology*, 264(6 Pt 2):H1977–87, June 1993.

[15] R. Burattini and K. B. Campbell. Physiological relevance of uniform elastic tube-models to infer descending aortic wave reflection: a problem of identifiability. *Annals of Biomedical Engineering*, 28(5):512–523, 2000.

[16] A. C. Burton. Relation of structure to function of the tissues of the wall of blood vessels. *Physiological Reviews*, 34(4):619–42, October 1954.

[17] K. B. Campbell, R. Burattini, D. L. Bell, R. D. Kirkpatrick, and G. G. Knowlen. Time-domain formulation of asymmetric T-tube model of arterial system. *American Journal of Physiology*, 258(6 Pt 2):H1761–H1774, 1990.

[18] L. Camporota and R. Beale. Pitfalls in haemodynamic monitoring based on the arterial pressure waveform. *Critical Care*, 14(2):124, January 2010.

[19] M. Chikhani and I. K. Moppett. Minimally invasive cardiac output monitoring: what evidence do we need? *British Journal of Anaesthesia*, 106(4):451–453, 2011.

[20] Y. C. Chiu, P. W. Arand, S. G. Shroff, T. Feldman, and J. D. Carroll. Determination of pulse wave velocities with computerized algorithms. *American Heart Journal*, 121(5):1460–70, May 1991.

[21] A. A. Cibulski, P. H. Lehan, and H. K. Hellems. Pressure methods for estimating right and left ventricular stroke volumes. *The American Journal of Physiology*, 225(6):1460–6, December 1973.

[22] V. A. Convertino, W. H. Cooke, and J. B. Holcomb. Arterial pulse pressure and its association with reduced stroke volume during progressive central hypovolemia. *The Journal of Trauma*, 61(3):629–34, September 2006.

[23] V. A. Convertino, K. L. Ryan, C. A. Rickards, J. Salinas, J. G. McManus, W. H. Cooke, and J. B. Holcomb. Physiological and medical monitoring for en route care of combat casualties. *The Journal of Trauma*, 64(4 Suppl):S342–53, April 2008.

[24] W. H. Cooke and M. M. Dowlyn. Power spectral analysis imperfectly informs changes in sympathetic traffic during acute simulated microgravity. *Aviation, Space, and Environmental Medicine*, 71(12):1232–8, December 2000.

[25] W. H. Cooke, K. L. Ryan, and V. A. Convertino. Lower body negative pressure as a model to study progression to acute hemorrhagic shock in humans. *Journal of Applied Physiology*, 96(4):1249–61, April 2004.

[26] E. S. Cooper and W. W. Muir. Continuous cardiac output monitoring via arterial pressure waveform analysis following severe hemorrhagic shock in dogs. *Critical Care Medicine*, 35(7):1724–1729, 2007.

[27] L. A. Critchley. Impedance cardiography. The impact of new technology. *Anaesthesia*, 53(7):677–84, July 1998.

[28] L. A. H. Critchley and J. A. J. H. Critchley. A meta-analysis of studies using bias and precision statistics to compare cardiac output measurement techniques. *Journal of Clinical Monitoring and Computing*, 15(2):85–91, 1999.

[29] M. De Melis, U. Morbiducci, L. Scalise, E. P. Tomasini, D. Delbeke, R. Baets, L. M. Van Bortel, and P. Segers. A noncontact approach for the evaluation of large artery stiffness: a preliminary study. *American Journal of Hypertension*, 21(12):1280–3, December 2008.

[30] B. P. DeBoisblanc, A. Pellett, R. Johnson, M. Champagne, E. McClarty, G. Dhillon, and M. Levitzky. Estimation of pulmonary artery occlusion pressure by an artificial neural network. *Critical Care Medicine*, 31(1):261–6, January 2003.

[31] G. Della Rocca, M. Cecconi, and M. G. Costa. Mini invasive hemodynamic monitoring: from arterial pressure to cardiac output. *Signa Vitae*, 3:7–9, 2008.

[32] A. F. DeLoskey, W. W. Nichols, C. R. Conti, and C. J. Pepine. Estimation of beat-to-beat stroke volume from the pulmonary arterial pressure contour in man. *Medical & Biological Engineering & Computing*, 16(6):707–14, November 1978.

[33] R. A. Dyer, J. L. Piercy, A. R. Reed, G. W. Strathie, C. J. Lombard, J. A. Anthony, and M. F. James. Comparison between pulse waveform analysis and thermodilution cardiac output determination in patients with severe pre-eclampsia. *British Journal of Anaesthesia*, 106(1):77–81, January 2011.

[34] J. Erlanger. An experimental study of blood pressure and of pulse-pressure in man. *Johns Hopkins Hosp Rep*, 12(145-378), 1904.

[35] K. C. Fleming, J. M. Evans, and D. S. Chutka. Caregiver and clinician shortages in an aging nation. In *Mayo Clinic Proceedings*, volume 78, pages 1026–1040, 2003.

[36] R. Fogliardi, R. Burattini, and K. B. Campbell. Identification and physiological relevance of an exponentially tapered tube model of canine descending aortic circulation. *Medical Engineering & Physics*, 19(3):201–211, 1997.

[37] J. Y. A. Foo, C. S. Lim, S. J. Wilson, G. R. Williams, M. A. Harris, and D. M. Cooper. Pulse transit time ratio as a potential marker for paediatric crural and brachial blood pressure index. *Journal of Human Hypertension*, 21(5):415–7, May 2007.

[38] P. Fung, G. Dumont, C. Ries, C. Mott, and M. Ansermino. Continuous noninvasive blood pressure measurement by pulse transit time. In *Conference proceedings : 26th Annual International Conference of the IEEE Engineering in Medicine and Biology Society. IEEE Engineering in Medicine and Biology Society. Conference*, volume 1, pages 738–41, January 2004.

[39] L. A. Geddes, M. H. Voelz, C. F. Babbs, J. D. Bourland, and W. A. Tacker. Pulse transit-time as an indicator of arterial blood-pressure. *Psychophysiology*, 18(1):71–74, 1981.

[40] J.-O. Hahn, A. T. Reisner, and H.H Asada. Modeling and 2-sensor blind identification of human cardiovascular system. *Control Engineering Practice*, 17(11):1318–1328, November 2009.

[41] W. S. Harris, C. D. Schoenfeld, and A. M. Weissler. Effects of adrenergic receptor activation and blockade on the systolic preejection period, heart rate, and arterial pressure in man. *The Journal of Clinical Investigation*, 46(11):1704–14, November 1967.

[42] T. Heldt, E. B. Shim, R. D. Kamm, and R. G. Mark. Computational modeling of cardiovascular response to orthostatic stress. *Journal of Applied Physiology*, 92(3):1239–54, March 2002.

[43] K. Hirata, M. Kawakami, and M. F. O'Rourke. Pulse wave analysis and pulse wave velocity: a review of blood pressure interpretation 100 years after Korotkov. *Circulation Journal*, 70(10):1231–1239, 2006.

[44] W. Huberts, E. M. H. Bosboom, and F. N. van de Vosse. A lumped model for blood flow and pressure in the systemic arteries based on an approximate velocity profile function. *Mathematical Biosciences and Engineering*, 6(1):27–40, January 2009.

[45] C. B. Humphrey, J. A. Gibbons, T. L. Folkerth, A. R. Shapiro, and R. G. Fosburg. An analysis of direct and indirect measurements of left atrial filling pressure. *The Journal of Thoracic and Cardiovascular Surgery*, 71(5):643–7, May 1976.

[46] J. R. C. Jansen, J. J. Schreuder, J. P. Mulier, N. T. Smith, J. J. Settels, and K. H. Wesseling. A comparison of cardiac output derived from the arterial pressure wave against thermodilution in cardiac surgery patients. *British Journal of Anaesthesia*, 87(2):212–222, 2001.

[47] D. A. Kass, M. Midei, W. Graves, J. A. Brinker, and W. L. Maughan. Use of a conductance (volume) catheter and transient inferior vena caval occlusion for rapid determination of pressure-volume relationships in man. *Catheterization and Cardiovascular Diagnosis*, 15(3):192–202, January 1988.

[48] J. S. Kim, Y. J. Chee, J. W. Park, J. W. Choi, and K. S. Park. A new approach for non-intrusive monitoring of blood pressure on a toilet seat. *Physiological Measurement*, 27(2):203–11, February 2006.

[49] D. S. Kimmerly and J. K. Shoemaker. Hypovolemia and neurovascular control during orthostatic stress. *American Journal of Physiology. Heart and Circulatory Physiology*, 282(2):H645–55, February 2002.

[50] M. Landowne. A method using induced waves to study pressure propagation in human arteries. *Circulation Research*, 5(6):594–601, November 1957.

[51] G. J. Langewouters, K. H. Wesseling, and W. J. A. Goedhard. The static elastic properties of 45 human thoracic and 20 abdominal aortas in-vitro and the parameters of a new model. *Journal of Biomechanics*, 17(6):425–435, 1984.

[52] T. W. Latson, W. C. Hunter, N. Katoh, and K. Sagawa. Effect of nitroglycerin on aortic impedance, diameter, and pulse-wave velocity. *Circulation Research*, 62(5):884–90, May 1988.

[53] S. Laurent, P. Boutouyrie, R. Asmar, I. Gautier, B. Laloux, L. Guize, P. Ducimetiere, and A. Benetos. Aortic stiffness is an independent predictor of all-cause and cardiovascular mortality in hypertensive patients. *Hypertension*, 37(5):1236–41, May 2001.

[54] J. W. Leatherman and R. S. Shapiro. Overestimation of pulmonary artery occlusion pressure in pulmonary hypertension due to partial occlusion. *Critical Care Medicine*, 31(1):93–7, January 2003.

[55] A. J. Lee, J. H. Cohn, and J. S. Ranasinghe. Cardiac output assessed by invasive and minimally invasive techniques. *Anesthesiology Research and Practice*, 2011:475151, January 2011.

[56] H.-Y. Lee and B.-H. Oh. Aging and arterial stiffness. *Circulation Journal*, 74(11):2257–2262, 2010.

[57] Z. E. Liljestrand. Vergleichen die bestimmungen des minutenvolumens des herzens beim menschen mittels der stichoxydulmethodeund durch blutdruckmessung. *Ztschr Ges Exper Med*, 59:105–122, 1928.

[58] L. Ljung. *System Identification: Theory for the User, Second Edition*. Prentice Hall PTR, 2nd edition, 1999.

[59] Z. Lu and R. Mukkamala. Continuous cardiac output monitoring in humans by invasive and noninvasive peripheral blood pressure waveform analysis. *Journal of Applied Physiology*, 101(2):598–608, 2006.

[60] G. Mancia, G. De Backer, A. Dominiczak, R. Cifkova, R. Fagard, G. Germano, G. Grassi, A. M. Heagerty, S. E. Kjeldsen, S. Laurent, K. Narkiewicz, L. Ruilope, A. Rynkiewicz, R. E. Schmieder, H. A. J. S. Boudier, A. Zanchetti, A. Vahanian, J. Camm, R. De Caterina, V. Dean, K. Dickstein, G. Filippatos, C. Funck-Brentano, I. Hellemans, S. D. Kristensen, K. McGregor, U. Sechtem, S. Silber, M. Tendera, P. Widimsky, J. Luis Zamorano, S. Erdine, W. Kiowski, E. Agabiti-Rosei, E. Ambrosioni, L. H. Lindholm, M. Viigimaa, S. Adamopoulos, V. Bertomeu, D. Clement, C. Farsang, D. Gaita, G. Lip, J.-M. Mallion, A. J. Manolis, P. M. Nilsson, E. O'Brien, P. Ponikowski, J. Redon, F. Ruschitzka, J. Tamargo, P. van Zwieten, B. Waeber, and B. Williams. 2007 guidelines for the management of arterial hypertension: the task force for the management of arterial hypertension of the european society of hypertension (ESH) and of the european society of cardiology (ESC). *Journal of Hypertension*, 25(6):1105–87, June 2007.

[61] P. L. Marino. *The ICU Book*. Williams & Wilkins, 2 edition, 1998.

[62] M. Masè, W. Mattei, R. Cucino, L. Faes, and G. Nollo. Feasibility of cuff-free measurement of systolic and diastolic arterial blood pressure. *Journal of Electrocardiology*, 44(2):201–7, 2011.

[63] D. A. Mcdonald. Regional Pulse-Wave Velocity in Arterial Tree. *Journal of Applied Physiology*, 24(1):73–&, 1968.

[64] M. McKendry, H. McGloin, D. Saberi, L. Caudwell, A. R. Brady, and M. Singer. Randomised controlled trial assessing the impact of a nurse delivered, flow monitored protocol for optimisation of circulatory status after cardiac surgery. *British Medical Journal*, 329(7460):258–261, 2004.

[65] W. Milnor. *Hemodynamics*. Williams & Wilkins, 2nd edition, 1989.

[66] G. F. Mitchell, J. M. Pfeffer, and M. A. Pfeffer. The heart and conduit vessels in hypertension. *The Medical Clinics of North America*, 81(6):1247–1271, 1997.

[67] A. H. Morris, R. H. Chapman, and R. M. Gardner. Frequency of technical problems encountered in the measurement of pulmonary artery wedge pressure. *Critical Care Medicine*, 12(3):164–70, March 1984.

[68] J. Muehlsteff, X. L. Aubert, and M. Schuett. Cuffless estimation of systolic blood pressure for short effort bicycle tests: the prominent role of the pre-ejection period. In *Conference proceedings : 28th Annual International Conference of the IEEE Engineering in Medicine and Biology Society. IEEE Engineering in Medicine and Biology Society. Conference*, volume 1, pages 5088–92, January 2006.

[69] R. Mukkamala, A. T. Reisner, H. M. Hojman, R. G. Mark, and R. J. Cohen. Continuous cardiac output monitoring by peripheral blood pressure waveform analysis. *IEEE Transactions on Bio-medical Engineering*, 53(3):459–67, March 2006.

[70] J. E. Naschitz, S. Bezobchuk, R. Mussafia-Priselac, S. Sundick, D. Dreyfuss, I. Khorshidi, A. Karidis, H. Manor, M. Nagar, E. R. Peck, S. Peck, S. Storch, I. Rosner, and L. Gaitini. pulse transit time by R-wave-gated infrared photoplethysmography: review of the literature and personal experience. *Journal of Clinical Monitoring and Computing*, 18(5-6):333–342, December 2004.

[71] D. B. Newlin and R. W. Levenson. Pre-Ejection Period - Measuring Beta-Adrenergic Influences Upon the Heart. *Psychophysiology*, 16(6):546–553, 1979.

[72] W. W. Nichols and M. F. O'Rourke. *McDonald's Blood Flow in Arteries: Theoretical, Experimental and Clinical Principles*. Number 6341. A Hodder Arnold Publication, 5th edition, 2005.

[73] A. Noordergraaf. *Circulatory System Dynamics*. Academic Press, 1978.

[74] J. Nürnberger, S. Dammer, A. Opazo Saez, T. Philipp, and R. F. Schäfers. Diastolic blood pressure is an important determinant of augmentation index and pulse wave velocity in young, healthy males. *Journal of Human Hypertension*, 17(3):153–8, March 2003.

[75] R. Ochiai, J. Takeda, H. Hosaka, Y. Sugo, R. Tanaka, and T. Soma. The relationship between modified pulse wave transit time and cardiovascular changes in isoflurane anesthetized dogs. *Journal of Clinical Monitoring and Computing*, 15(7-8):493–501, 1999.

[76] H. Paarmann, H. V. Groesdonk, B. Sedemund-Adib, T. Hanke, H. Heinze, M. Heringlake, and J. Schön. Lack of agreement between pulmonary arterial thermodilution cardiac output and the pressure recording analytical method in postoperative cardiac surgery patients. *British Journal of Anaesthesia*, 106(4):475–81, April 2011.

[77] A. J. Pappano, W. G. Wier, M. T. Nelson, and M. N. Levy. *Cardiovascular Physiology*. Mosby, 9th edition, 2006.

[78] R. A. Payne, C. N. Symeonides, D. J. Webb, and S. R. J. Maxwell. Pulse transit time measured from the ECG: an unreliable marker of beat-to-beat blood pressure. *Journal of Applied Physiology*, 100(1):136–141, 2006.

[79] P. J. Peyton and S. W. Chong. Minimally invasive measurement of cardiac output during surgery and critical care: a meta-analysis of accuracy and precision. *Anesthesiology*, 113(5):1220–1235, 2010.

[80] V. M. Pigott, D. H. Spodick, E. H. Rectra, and A. H. Khan. Cardiocirculatory responses to exercise: physiologic study by noninvasive techniques. *American Heart Journal*, 82(5):632–41, November 1971.

[81] M. R. Pinsky. Hemodynamic evaluation and monitoring in the ICU. *Chest*, 132(6):2020–2029, 2007.

[82] M. R. Pinsky and J.-L. Vincent. Let us use the pulmonary artery catheter correctly and only when we need it. *Critical Care Medicine*, 33(5):1119–22, May 2005.

[83] J. D. Pruett, J. D. Bourland, and L. A. Geddes. Measurement of pulse-wave velocity using a beat-sampling technique. *Annals of Biomedical Engineering*, 16(4):341–347, 1988.

[84] J. Pugsley and A. B. Lerner. Cardiac output monitoring: is there a gold standard and how do the newer technologies compare? *Seminars in Cardiothoracic and Vascular Anesthesia*, 14(4):274–82, December 2010.

[85] A. Qasem and A. Avolio. Determination of aortic pulse wave velocity from waveform decomposition of the central aortic pressure pulse. *Hypertension*, 51(2):188–195, February 2008.

[86] J. K. Raines, M. Y. Jaffrin, and A. H. Shapiro. A computer simulation of arterial dynamics in the human leg. *Journal of Biomechanics*, 7(1):77–91, January 1974.

[87] A. T. Reisner, D. Xu, K. L. Ryan, V. A. Convertino, C. A. Rickards, and R. Mukkamala. Monitoring non-invasive cardiac output and stroke volume during experimental human hypovolaemia and resuscitation. *British Journal of Anaesthesia*, 106(1):23–30, January 2011.

[88] A. Rhodes and R. Sunderland. Arterial Pulse Power Analysis: The LiDCO plus System. *Functional Hemodynamic Monitoring*, 42(Table 1):183–192, 2005.

[89] J. Ross and B. E. Sobel. Regulation of cardiac contraction. *Annual Review of Physiology*, 34:47–90, January 1972.

[90] M. Saeed, M. Villarroel, A. T. Reisner, G. Clifford, L. W. Lehman, G. Moody, T. Heldt, T. H. Kyaw, B. Moody, and R. G. Mark. Multiparameter intelligent monitoring in intensive care II: a public-access intensive care unit database. *Critical Care Medicine*, 39(5):952–60, May 2011.

[91] K. Sagawa, R. K. Lie, and J. Schaefer. Translation of Otto Frank's paper "Die Grundform des Arteriellen Pulses" Zeitschrift für Biologie 37: 483-526 (1899). *Journal of Molecular and Cellular Cardiology*, 22(3):253–4, March 1990.

[92] K. Sagawa, H. Suga, A. A. Shoukas, and K. M. Bakalar. End-systolic pressure/volume ratio: a new index of ventricular contractility. *The American Journal of Cardiology*, 40(5):748–53, November 1977.

[93] J. D. Sandham, R. D. Hull, R. F. Brant, L. Knox, G. F. Pineo, C. J. Doig, D. P. Laporta, S. Viner, L. Passerini, H. Devitt, A. Kirby, and M. Jacka. A randomized, controlled trial of the use of pulmonary-artery catheters in high-risk surgical patients. *The New England Journal of Medicine*, 348(1):5–14, January 2003.

[94] H. Senzaki, C. H. Chen, and D. A. Kass. Single-beat estimation of end-systolic pressure-volume relation in humans. A new method with the potential for noninvasive application. *Circulation*, 94(10):2497–506, November 1996.

[95] S. J. Sherwin, V. Franke, J. Peiró, and K. Parker. One-dimensional modelling of a vascular network in space-time variables. *Journal of Engineering Mathematics*, 47(3/4):217–250, 2003.

[96] J. M. Solà, S. F. Rimoldi, and Y. Allemann. Ambulatory Monitoring of the Cardiovascular System: the Role of Pulse Wave Velocity. In Domenico Campolo, editor, *New Developments in Biomedical Engineering*, page 714. InTech, 2010.

[97] A. Steptoe, H. Smulyan, and B. Gribbin. Pulse-wave velocity and blood-pressure change - calibration and applications. *Psychophysiology*, 13(5):488–493, 1976.

[98] N. Stergiopulos, B. E. Westerhof, and N. Westerhof. Total arterial inertance as the fourth element of the windkessel model. *American Journal of Physiology*, 276(1 Pt 2):H81–8, 1999.

[99] C. W. Stetz, R. G. Miller, G. E. Kelly, and T. A. Raffin. Reliability of the thermodilution method in the determination of cardiac output in clinical practice. *The American Review of Respiratory Disease*, 126(6):1001–4, December 1982.

[100] J. H. Stevens, T. A. Raffin, F. G. Mihm, M. H. Rosenthal, and C. W. Stetz. Thermodilution cardiac-output measurement - effects of the respiratory cycle on Its reproducibility. *JAMA*, 253(15):2240–2242, 1985.

[101] H. Suga and K. Sagawa. Instantaneous pressure-volume relationships and their ratio in the excised, supported canine left ventricle. *Circulation Research*, 35(1):117–26, July 1974.

[102] M. Sugimachi, T. Shishido, K. Miyatake, and K. Sunagawa. A new model-based method of reconstructing central aortic pressure from peripheral arterial pressure. *The Japanese Journal of Physiology*, 51(2):217–222, April 2001.

[103] J. X. Sun, A. T. Reisner, M. Saeed, T. Heldt, and R. G. Mark. The cardiac output from blood pressure algorithms trial. *Critical Care Medicine*, 37(1):72–80, 2009.

[104] G. Swamy, N. B. Olivier, and R. Mukkamala. Calculation of forward and backward arterial waves by analysis of two pressure waveforms. *IEEE Transactions on Biomedical Engineering*, 57(12):2833–2839, 2010.

[105] G. Swamy, D. Xu, N. B. Olivier, and R. Mukkamala. An adaptive transfer function for deriving the aortic pressure waveform from a peripheral artery pressure waveform. *American Journal of Physiology Heart and Circulatory Physiology*, 297(5):H1956–H1963, 2009.

[106] H. J. Swan, W. Ganz, J. Forrester, H. Marcus, G. Diamond, and D. Chonette. Catheterization of the heart in man with use of a flow-directed balloon-tipped catheter. *The New England Journal of Medicine*, 283(9):447–51, August 1970.

[107] T. Tajimi, K. Sunagawa, A. Yamada, Y. Nose, A. Takeshita, Y. Kikuchi, and M. Nakamura. Evaluation of pulse contour methods in calculating stroke volume from pulmonary artery pressure curve (comparison with aortic pressure curve). *European Heart Journal*, 4(7):502–11, July 1983.

[108] J. G. Thomas. A method for continuously indicating blood pressure. *The Journal of Physiology*, 129(3):75–6P, September 1955.

[109] C. Vlachopoulos, K. Aznaouridis, and C. Stefanadis. Prediction of cardiovascular events and all-cause mortality with arterial stiffness: a systematic review and meta-analysis. *Journal of the American College of Cardiology*, 55(13):1318–27, March 2010.

[110] J. Wan, B. Steele, S. A. Spicer, S. Strohband, G. R. Feijóo, T. J. R. Hughes, and C. A. Taylor. A one-dimensional finite element method for simulation-based medical planning for cardiovascular disease. *Computer Methods in Biomechanics and Biomedical Engineering*, 5(3):195–206, 2002.

[111] K. H. Wesseling, J. R. Jansen, J. J. Settels, and J. J. Schreuder. Computation of aortic flow from pressure in humans using a nonlinear, three-element model. *Journal of Applied Physiology*, 74(5):2566–73, May 1993.

[112] R. S. Wiener and H. G. Welch. Trends in the use of the pulmonary artery catheter in the United States, 1993-2004. *JAMA*, 298(4):423–429, 2007.

[113] M. Y Wong, C. Poon, and Y.-T. Zhang. An evaluation of the cuffless blood pressure estimation based on pulse transit time technique: a half year study on normotensive subjects. *Cardiovascular Engineering*, 9(1):32–8, March 2009.

[114] D. Xu, K. L. Ryan, C. A. Rickards, G. Zhang, V. A. Convertino, and R. Mukkamala. Improved pulse transit time estimation by system identification analysis of proximal and distal arterial waveforms. *American Journal of Physiology. Heart and Circulatory Physiology*, 301(4):H1389–95, October 2011.

[115] D. Xu, G. Zhang, N. B. Olivier, and R. Mukkamala. Monitoring aortic stiffness in the presence of measurement artifact based on an arterial tube model. In *Conference proceedings : 32nd Annual International Conference of the IEEE Engineering in Medicine and Biology Society. IEEE Engineering in Medicine and Biology Society. Conference*, volume 2010, pages 3453–3456, January 2010.

[116] A. A. Zacharoulis, C. J. Mills, I. T. Gabe, and J. P. Shillingford. Estimation of stroke volume from the pulmonary artery pressure record. *Cardiovascular Research*, 8(4):506–16, July 1974.

[117] M. Zagzoule and J. P. Marc-Vergnes. A global mathematical model of the cerebral circulation in man. *Journal of Biomechanics*, 19(12):1015–1022, 1986.